UNIVERSITY OF SOUTHAMPTON

FACULTY OF PHYSICAL AND APPLIED SCIENCES

Physics and Astronomy

Large Hadron Collider Phenomenology of Vector-like Quarks beyond the Narrow Width Approximation

by

Dermot O'Brien

Thesis for the degree of Doctor of Philosophy

November 2018

UNIVERSITY OF SOUTHAMPTON

ABSTRACT

FACULTY OF PHYSICAL AND APPLIED SCIENCES
Physics and Astronomy

Doctor of Philosophy

LARGE HADRON COLLIDER PHENOMENOLOGY OF VECTOR-LIKE QUARKS BEYOND THE NARROW WIDTH APPROXIMATION

by Dermot O'Brien

The topic of this thesis is the phenomenology of Vector-Like Quarks (VLQs) at the Large Hadron Collider (LHC), with a focus on understanding the difference between the commonly adopted experimental VLQ search strategies that use the Narrow Width Approximation (NWA) in comparison to search strategies aimed at exploring signals arising from the production and propagation of VLQs at large width (LW). The effects on the cross sections are found to be non-negligible, with particularly important contributions from the topologies where the VLQ is coupled to the light generation Standard Model (SM) quarks. These off-shell effects are studied in a model-independent way for final states compatible with processes of pair production of VLQs, compared to the on-shell topologies in the NWA with the same final state. An analogous analysis has been performed for VLQs interacting with bosonic Dark Matter (DM) candidates and SM quarks to explore at the same time the potential to characterise VLQs with LW and the discrimination of scalar or vector DM states. A study is also performed for processes of single VLQ production, where a model-independent interpretation of the results has been obtained by exploiting a suitable factorisation of the VLQ couplings. The topologies considered where those containing the production of a single VLQ decaying into a three particle final state This analysis found similar results compared to the two previously mentioned studies. The model-independent parametrisation for the interpretation of results of VLQ single production is currently being used in experimental searches by CMS, and as such I have been included as an author of a CMS analysis for single production of a Vector-Like (VL) top partner.

Table of Contents

Declaration of Authorship xvii

Acknowledgements xix

Nomenclature xxi

1 Introduction 1
- 1.1 The Large Hadron Collider . . . 2
- 1.2 The Standard Model . . . 5
  - 1.2.1 Gauge symmetry . . . 5
  - 1.2.2 Fermion matter content . . . 5
  - 1.2.3 Spontaneous symmetry breaking . . . 6
  - 1.2.4 Coupling of fermion matter states to Higgs doublet . . . 7
- 1.3 Phenomena the SM cannot account for . . . 9
  - Dark matter: . . . 9
  - Massive neutrinos . . . 12
  - The matter anti-matter asymmetry . . . 12
  - The strong CP problem . . . 13
  - Gravity: . . . 13
  - Dark energy: . . . 13
  - The hierarchy problem: . . . 14
  - Patterns that appear in the SM . . . 14
- 1.4 New quarks as a probe of physics beyond the SM . . . 15
- 1.5 Model framework of VLQs . . . 16
  - 1.5.1 Symmetries, interactions and representations . . . 17
    - 1.5.1.1 Interaction terms . . . 17
    - 1.5.1.2 Mass terms . . . 18
    - 1.5.1.3 Summary of allowed representations . . . 19
    - 1.5.1.4 Mixing of allowed representations and modified couplings 19
    - 1.5.1.5 Coupling to the Higgs boson . . . 22
  - 1.5.2 The Lagrangian term for VLQs . . . 22
- 1.6 The Narrow Width Approximation (NWA) . . . 25
- 1.7 Pair and single production of VLQs . . . 26
  - 1.7.1 Pair production . . . 27
  - 1.7.2 Single production . . . 27
- 1.8 Current state of experimental VLQ searches at the LHC . . . 29
  - 1.8.1 Pair and single production searches for VLQs at ATLAS . . . 29

1.8.1.1 Combined decays of $T \to Wb, Zt, Ht$ or $B \to Wt, Zb, Hb$ VLQ analysis . . . 29
1.8.1.2 Search for VLQ involving a decay $T, B \to Zq$ analysis . . . 31
1.8.2 Pair and single production searches for VLQs at CMS . . . 33
1.8.2.1 Combined decays of $T \to Wb, Zt, Ht$ or $B \to Wt, Zb, Hb$ VLQ analysis . . . 33
1.8.2.2 Search for VLQ involving a decay of $T \to Zt$ analysis . . . 34

2 Production of extra quarks at the LHC beyond the NWA 37
2.1 Introduction . . . 37
2.2 Setup . . . 38
2.2.1 Definitions . . . 38
2.2.2 Tools and validation . . . 40
2.3 Benchmarks and constraints . . . 41
2.3.1 How large can the width be? . . . 43
2.4 Extra T quark mixing with third generation SM quarks . . . 44
2.4.1 Large width effects on the signal at parton level . . . 44
2.4.2 Interference with SM background . . . 47
2.4.3 Results at detector level . . . 49
2.5 Extra T quark mixing with first generation SM quarks . . . 51
2.5.1 Large width effects on the signal at parton level . . . 51
2.5.2 Interference with SM background . . . 52
2.5.3 Results at detector level . . . 53
2.6 Conclusions . . . 55

3 Production of XQs decaying to DM beyond the NWA at the LHC 57
3.1 Introduction . . . 57
3.2 Model and conventions . . . 58
3.2.1 Lagrangian terms . . . 58
3.2.2 Observables and conventions . . . 60
3.2.3 Channels . . . 61
3.3 Analysis tools and experimental searches . . . 62
3.4 Extra T quark interacting with Dark Matter and the SM top quark . . . 63
3.4.1 Large width effects at parton level . . . 63
3.4.2 Large width effects at detector level . . . 65
3.4.3 Dependence on the chirality of the couplings . . . 68
3.5 Extra T quark interacting with Dark Matter and the SM up quark . . . 69
3.5.1 Large width effects at parton level . . . 69
3.5.2 Large width effects at detector level . . . 71
3.5.3 Dependence on the chirality of the couplings . . . 72
3.6 Exclusion limits in the $M_T - M_{DM}$ plane . . . 74
3.7 Conclusions . . . 75

4 Single production of VLQs with large width at the LHC 79
4.1 Introduction . . . 79
4.2 Model-independent parameterisation of the cross-section . . . 80
4.3 Phenomenological analysis . . . 83
4.3.1 Benchmarks . . . 84

4.3.2 Recasting and reinterpretation of experimental data 86
4.3.3 Reinterpretation through the reduced cross-section $\hat{\sigma}$ 89
4.3.3.1 Including interference terms for $pp \to Wbj$ via T 90
4.4 Conclusions 93

5 Conclusions **95**

References **99**

List of Figures

1.1 Amount of collected integrated luminosity (fb^{-1}) recorded at CMS for the years that the LHC was running and collecting data, at proton-proton beam energies 7, 8 and 13 TeV [21]. The values for ATLAS are similar to that shown from CMS. . . . 3

1.2 Exotica summary plots for resonances, extra dimensions, etc. from CMS, presented at ICHEP 2016 [22]. . . . 4

1.3 Comparison of rotation curves for M31 and the Galaxy as a function from the centre. Solid line: rotation curve for M31, dashed line: rotation curve from Schmidt model of the galaxy, Filled circles, observed rational velocities [33]. . . . 10

1.4 This figure and caption is from Ref. [41]. Shown above in the top panel is a colour image from the Magellan images of the merging cluster 1E0657−558, with the white bar indicating 200 kpc at the distance of the cluster. In the bottom panel is a 500 ks Chandra image of the cluster. Shown in green contours in both panels are the weak lensing κ reconstruction with the outer contour level at $\kappa = 0.16$ and increasing in steps of 0.07. The white contours show the errors on the positions of the κ peaks and correspond to 68.3%, 95.5%, and 99.7% confidence levels. The blue +s show the location of the centers used to measure the masses of the plasma clouds. . . . 11

1.5 This figure and caption is from Ref. [42], this analysis was provided the image courtesy of Chandra X-ray Observatory [43]. False colour image of Bullet Cluster 1E0657-558. The surface density $\sum$-map reconstructed from X-ray imaging observations is shown in red and the convergence κ-map as reconstructed from strong and weak gravitational lensing observations is shown in blue. . . . 11

1.6 Complete list of the generic topologies for final states compatible with single VLQ production in the 5FS. Topologies on the left column can be described in both the NWA and LW regimes while topologies on the right column are neglected in the NWA approximation. Here, V represents the W and Z bosons of the SM. . . . 28

1.7 This figure and caption is from Ref. [146]. Observed (solid line) and expected (dashed line) 95% CL upper limits on the $T\bar{T}$ cross-section versus mass for the combination and the standalone analyses in black and coloured lines, respectively. The (a) singlet and (b) doublet scenarios [147] are displayed. The shaded bands correspond to ± 1 and ± 2 standard deviations around the combined expected limit. The rapidly falling thin red line and band show the theory prediction and corresponding uncertainty [148], respectively. . . . 29

1.8 This figure and caption is from Ref. [146]. Observed (solid line) and expected (dashed line) 95% CL upper limits on the $B\bar{B}$ cross-section versus mass for the combination and the standalone analyses in black and colored lines, respectively. The (a) singlet and (b) (T, B) doublet scenarios [147] are displayed. The shaded bands correspond to ± 1 and ± 2 standard deviations around the combined expected limit. The rapidly falling thin red line and band show the theory prediction and corresponding uncertainty [148], respectively. 30
1.9 This figure and caption is from Ref. [146]. Observed lower limits at 95% CL on the mass of the (a) T and (b) B as a function of branching ratio assuming $\mathcal{B}(T \to Ht) + \mathcal{B}(T \to Zt) + \mathcal{B}(T \to Wb) = 1$ and $\mathcal{B}(B \to Ht) + \mathcal{B}(B \to Zt) + \mathcal{B}(B \to Wb) = 1$ The yellow markers indicate the branching ratios for the SU(2) singlet and doublet scenarios for VLQ masses above 800 GeV where the branching ratios become approximately independent of the VLQ mass [147]. 30
1.10 This figure and caption is from Ref. [149]. Expected (a,c) and observed (b,d) 95% CL lower limits from the combination of the pair-production channels on the mass of vector-like quarks for all combinations of BRs for (a,b) $T \to Zt$, $T \to Ht$, $T \to Wb$, and (c,d) $B \to Zb$, $B \to Hb$, $B \to Wt$, adding up to unity. The white lines are contours for fixed values of M_{VLQ}. 31
1.11 This figure and caption is from Ref. [149]. Upper limits at 95% CL on the cross section times BR to Zt of single production (SP) of a T-quark. The expected limits are shown for the individual channels and for the combination of the channels, as are the observed limits for the combination. The expected cross section times BR to Zt for single-T-quark production is also shown for a coupling $\kappa_T = 0.5$, which corresponds to a coupling of $c_W = \sqrt{c_{W,L}^2 + c_{W,R}^2} = 0.45$ from Ref. [150]. The BR assumed here corresponds to the singlet benchmark model, i.e. $\approx 25\%$. 32
1.12 This figure and caption is from Ref. [149]. Expected (a) and observed (b) lower limit from the combination of the single-production channels on the mass of the T quark as a function of the couplings of the T quark to the W boson, $\sqrt{c_{W,L}^2 + c_{W,R}^2}$, and to the Z boson, $\sqrt{c_{Z,L}^2 + c_{Z,R}^2}$ with the assumption of equal BRs for $T \to Zt$ and $T \to Ht$ in the limit of large T-quark masses. The gray area corresponds to a region that is not excluded for any mass value tested because of the limited sensitivity of the analysis for very small T-quark masses. The white lines are contours for fixed values of M_{VLQ}. 32
1.13 This figure and caption is from Ref. [151]. The 95% CL expected and observed upper limits on the cross section of $T\bar{T}$ (upper row) and $B\bar{B}$ (lower row) production after combining all channels for the singlet (left) and doublet (right) branching fraction scenarios. The predicted cross sections are shown by the red curve, with the uncertainty indicated by the width of the line. 33
1.14 This figure and caption is from Ref. [151].The 95% CL expected (left) and observed (right) lower limits on the T quark (upper row) and B quark (lower row) mass, expressed in GeV, after combining all channels for various branching fraction scenarios. 34

1.15 This figure and caption is from Ref. [4]. Observed and expected limits at 95% CL on the product of the single production cross section and branching fraction for the singlet LH T quark produced in association with a b quark (left) and for the doublet RH T quark produced in association with a t quark (right), where the T quark has a narrow width and decays to tZ. The inner green and outer yellow bands represent the 1 and 2 standard deviation uncertainties in the expected limit. The red lines indicate theoretical cross sections, as calculated at next-to-leading order in Ref. [4]. The branching fraction $\mathcal{B}(\mathrm{T}\rightarrow \mathrm{tZ})$ is 0.25 (0.5) for the left (right) plot. 35

1.16 This figure and caption is from Ref. [4]. Observed (upper) and expected (lower) limits at 95% CL on the product of the single production cross section and branching fraction for the singlet LH T quark produced in association with a b quark (left) and for the doublet RH T quark produced in association with a t quark (right), where the T quark has a width from 10% to 30% of its mass and decays to tZ. The solid black lines indicate theoretical cross sections, as calculated at leading order using a modified version of the model constructed by the authors of Refs. [137, 152, 153] and reported in Table 1.4. In each plot, the excluded region lies to the left of the line, except in the lower-left plot where the entire region shown is excluded. 36

2.1 Examples of topologies containing only one VLQ propagator for the $PP \rightarrow W^+bW^-\bar{b}$ and $PP \rightarrow ZtZ\bar{t}$ processes. 39

2.2 Ratio of FW corrections with respect to the NWA relative to the $V-A$ case of a $V+A$ charged decay current. 41

2.3 Number of events at partonic level for $Q\bar{Q}$ pair production and for different LHC energies and luminosities. The corresponding cross-sections have been computed using HATHOR[167] with MSTW2008nnlo68 PDFs[168]. . 43

2.4 Contours with constant Γ/M ratio as function of T mass and mixing angle for T belonging to different representations and with different mixing hypotheses. The excluded (shaded) regions from [169] have been superimposed. 44

2.5 Relative difference between the full signal cross-section and the cross-section of QCD pair production for T mixing with the SM top quark. . . 45

2.6 Partonic level differential cross-sections for the $HtHt$ channel. From left to right and top to bottom: η_t, p_{Tt}, η_H and p_{TH}. All distributions correspond to a T mass of 600 GeV, for which $\sigma_S \sim \sigma_X$ almost independently of the T width. 46

2.7 Partonic level differential cross-sections for the $ZtZt$ channel. From left to right and top to bottom: η_t, p_{Tt}, η_Z and p_{TZ}. All distributions correspond to a T mass of 800 GeV, for which $\sigma_S \sim \sigma_X$ almost independently of the T width. 47

2.8 Relative difference in cross-section between the total $2 \rightarrow 4$ process, including the SM background and the sum of QCD pair production and SM backgrounds. Top row: final states on the diagonal of the matrix in Eq. 2.6 (third generation mixing); bottom row: off-diagonal final states (third generation mixing). 48

2.9 Relative contribution of the interference between the full signal and the SM background. $HtHt$ is the only channel for which this contribution can reach values above 10% in size. 49
2.10 Recast bounds in the $(M_T, \Gamma_T/M_T)$ plane with a set of ATLAS (top row) and CMS (bottom row) searches at 8 TeV for diagonal final states. 50
2.11 Cross-section and efficiency of the best ATLAS SR (bCd_bulk_d of [172]) for the $WbWb$ channel, compared with the bound. 50
2.12 Same as Fig. 2.10 for the ATLAS search at 13 TeV [163] implemented in CheckMATE. The plot for the $WbWb$ channel is not shown because within the explored range the recasting does not set any limit. 51
2.13 Examples of neutral-current topologies for heavy quarks with large width mixing with first generation. 51
2.14 Same as Fig. 2.5 for T mixing with first generation. 52
2.15 Same as Fig. 2.8 for T mixing with first generation. 53
2.16 Same as Fig. 2.9 for T mixing with first generation. 53
2.17 Same as Fig. 2.10 for T mixing with first generation. 54
2.18 Cross-section and efficiency of the best ATLAS SR (SR01_c.2jt of [173]) for the $ZuZu$ channel, compared with the bound. 54

3.1 Examples of topologies containing only one XQ propagator for final states compatible with XQ pair production and decay into scalar or vector DM and SM quarks of first or third generation. 61
3.2 Relative difference between the full signal and the QCD pair production cross sections for a T coupling to a DM particle (coupling to third generation) of mass 10 GeV, 500 GeV and 1000 GeV. Top row: scalar DM; bottom row, vector DM. 64
3.3 Differential distributions of transverse momentum of the top quark and E_T^{miss} along the cancellation line for scalar and vector DM. 65
3.4 CheckMATE results for a T coupling to a DM particle (coupling to third generation) of mass 10 GeV, 500 GeV and 1500 GeV. The black (grey) line show which part of the parameter space is excluded for the scalar (vector) DM scenario. 66
3.5 Top row: full signal cross sections for the scalar DM case. Bottom row: efficiencies of the SR tN_high from the analysis ATLAS-CONF-2016-050 [182] for different scalar DM masses. 66
3.6 Top row: full signal cross sections for the vector DM case. Bottom row: efficiencies of the SR tN_high from the analysis ATLAS-CONF-2016-050 [182] for different vector DM masses. 67
3.7 Differential distributions along the bound for a T with mass $M_T = 1100$ GeV coupling to the top quark and scalar DM with mass $M_{DM} = 10$ GeV. 68
3.8 Exclusion bounds for a T interacting with the SM top quark and DM for different hypotheses on the chirality of the couplings: for a VLQ T pure left-handed and pure right-handed couplings, and for a ChQ T pure scalar (vector) or pseudoscalar (axial-vector) couplings if T interacts with scalar (vector) DM. 69
3.9 Examples of topologies which are peculiar to scenarios with heavy quarks coupling to first generation. 69

3.10 Relative difference between the full signal and the QCD pair production cross sections for a T coupling to a DM particle (coupling to first generation) of mass 10 GeV, 500 GeV and 1000 GeV. Due to the large differences between cross sections, the ratio is plotted as $\log[1+(\sigma_S-\sigma_X)/\sigma_X]$ instead of $(\sigma_S-\sigma_X)/\sigma_X$. Notice that in that case the contours at 0.1, 0.2, 0.3, 0.5 and 1 respectively correspond to a value of $(\sigma_S-\sigma_X)/\sigma_X$ equal to 26%, 58%, 100%, 216% and 900%. Top row: scalar DM; bottom row, vector DM. 70
3.11 CheckMATE results for a T coupling to a DM particle (coupling to first generation) of mass 10 GeV, 500 GeV and 1000 GeV. The black (grey) line shows which part of the parameter space is excluded in the scalar (vector) DM scenario. . . . 71
3.12 Top row: full signal cross sections for the scalar DM case. Bottom row: efficiencies of the SR 2jm from the ATLAS search [180] for different scalar DM masses. . . . 72
3.13 Top row: full signal cross sections for the vector DM case. Bottom row: efficiencies of the SR 2jm from the ATLAS search [180] for different scalar DM masses. . . . 73
3.14 Exclusion bounds for a T interacting with the SM up quark and DM for different hypotheses on the chirality of the couplings: for a VLQ T pure left-handed and pure right-handed couplings, and for a ChQ T pure scalar (vector) or pseudoscalar (axial-vector) couplings if T interacts with scalar (vector) DM. . . . 73
3.15 Bounds in the $(M_T, M_{\rm DM})$ plane for T quark coupling DM particle and first (left panel), second (center panel) and third (right panel) generations of SM quarks for different values of Γ_T/M_T. . . . 74

4.1 Complete list of the generic topologies for final states compatible with single VLQ production in the 5FS. Topologies on the left column can be described in both the NWA and LW regimes while topologies on the right column are neglected in the NWA approximation. Here, V represents the W and Z bosons of the SM. . . . 81
4.2 Example on the left of a subset of interfering topologies in the process $bb \to bW^+\bar{t}$ mediated by a T VLQ and different SM bosons. The diagrams on the right show analogous contributions from the SM background, which interferes with the signal. . . . 82
4.3 Distributions of the transverse momentum of the leading b-tagged jet for two processes. Left panel: $pp \to tWj$ (in the 5FS) or $pp \to tWjb$ (in the 4FS); right panel: $pp \to bZj$ (in the 5FS) or $pp \to bZjb$ (in the 4FS), with subsequent on-shell decays of the SM states in both cases. The comparison is made for a B mass of 1200 GeV and for different values of the width-over-mass ratio (Γ_Q/M_Q) of the VLQ. . . . 85
4.4 95% CL largest allowed cross-sections (in pb) for the Wbj final state as a function of M_T and of Γ_T/M_T for a VLQ T coupling to the third SM quark generation and decaying 100% to bW. . . . 87
4.5 Cross section (in pb) for the Wbj final state as a function of M_T and of Γ_T/M_T and 95% exclusion line (in black) for a VLQ T decaying 100% to bW (left panel) or singlet-like (right panel). . . . 88

4.6 95% CL excluded cross-sections (in pb) and exclusion bound (black line) as a function of M_Q and Γ_Q/M_Q for a VLQ T (top row) and B (bottom row) coupling to the first (top and bottom-left panels) or third (bottom-right panel) SM quark generation. 89
4.7 The 13 TeV $\hat{\sigma}$ values (left) and the signal cross-section (right), both given in pb, as a function of M_Q and Γ_Q/M_Q for a VLQ T coupling to the third generation shown together with the exclusions line obtained using the $\hat{\sigma}$ data (in dashed blue) and with the original exclusion line (in black, same as Fig. 4.5), assuming negligible interference contributions from any source. 90
4.8 $\hat{\sigma}^{\text{int}}_{SB_{\text{irr}}}$ values at 13 TeV (in pb) for the process $pp \to bWj$ mediated by a T interacting with third generation SM quarks exclusively through charged current, for the interference between signal and SM background with dominant LH (RH) coupling chirality of the T in the left (right) panel. . . 91
4.9 $\hat{\sigma}_{S,\text{eff}}$ and $\hat{\sigma}^{\text{int}}_{SB_{\text{irr}},\text{eff}}$ values at 13 TeV (in pb) for the process $pp \to bWj$ mediated by a T interacting with third generation SM quarks exclusively through charged current, for the pure signal (left panel) and for the interference between signal and SM background with dominant LH coupling chirality of the T (right panel). The signal region corresponding to the efficiencies is the single electron from the CMS search [190]. 92
4.10 Upper panel: values of σ_{eff} with (solid line) and without (dashed line) interference contribution. Lower panel: relative contribution of the interference term to it (lower panel) at 13 TeV as function of the c_W coupling. The process is $pp \to bWj$ mediated by a T with $M_T = 600$ GeV and $\Gamma_T/M_T = 10\%$ interacting with third generation SM quarks exclusively through charged current. The maximum value of c_W in the plot corresponds to a partial width equivalent to 10% of the mass. Limits at two different LHC luminosities are also shown (see text for details). 93

List of Tables

1.1 Fermion content of the SM [27]. 6

1.2 Allowed representations for VLQs, with quantum numbers under $SU(2)_L$ and $U(1)_Y$ and Yukawa mixing terms in the Lagrangian. Depending on the chosen representation, the Higgs boson may be H or H^c, therefore it has been noted as $H^{(c)}$ when necessary. The gauge invariant mass term common to all representations is a peculiar feature of VLQs. 19

1.3 Neutral current parameters f_L and f_R. 20

1.4 Theoretical reduced cross sections $\bar{\sigma}_{FW}$ for single production of a T quark with a b or a t quark, where the T quark decays to tZ and its width is 10, 20, and 30% of its mass, for the benchmark masses considered in the analysis. The corresponding leading order cross sections σ are shown in parentheses. 36

4.1 Benchmark points and corresponding coupling relations. 84

4.2 Comparison of the experimental and recasted efficiencies for the different signal regions for a $pp \to T(\to Wb)jb$ signal in the 4FS with $m_T = 1000$ GeV in the NWA. 86

Declaration of Authorship

I, Dermot O'Brien, declare that the thesis entitled *Large Hadron Collider Phenomenology of Vector-like Quarks beyond the Narrow Width Approximation* and the work presented in the thesis are both my own, and have been generated by me as the result of my own original research. I confirm that:

- this work was done wholly or mainly while in candidature for a research degree at this University;
- where any part of this thesis has previously been submitted for a degree or any other qualification at this University or any other institution, this has been clearly stated;
- where I have consulted the published work of others, this is always clearly attributed;
- where I have quoted from the work of others, the source is always given. With the exception of such quotations, this thesis is entirely my own work;
- I have acknowledged all main sources of help;
- where the thesis is based on work done by myself jointly with others, I have made clear exactly what was done by others and what I have contributed myself;
- parts of this work have been published as: [1], [2], [3] and I have contributed to the production of numerical results for [4].

Signed:.....

Date:.....

Acknowledgements

These last 3 years working on my PhD has been incredibly education not only in particle physics phenomenology, but also in advanced programming, presenting seminars and learning about carrying out academic research. I also gained invaluable industrial hands-on experience both for building electronic systems to perform tasks such as the ignition, flight firing system of a low orbit cube satellite launcher and learning about Natural Language Processing (NLP) for Named Entity Recognition (NER) using Deep Learning (DL) techniques. These incredible opportunities would never have presented themselves to me outside the framework of this PhD, also providing access to and benefiting from international networks such SEPnet and DISCnet. I was taken aback by the enthusiasm and their helpfulness I found from the people I came into contact with who are working within these networks.

I would like to first thank in particular Stefano Moretti who gave me the chance to do my PhD at Southampton University. Without this first step, I would not have had the chance to work with and get to know not only Stefano but also other colleagues at the university. I would also like to thank Stefano and in addition Luca Panizzi very much for always being there for me when I needed guidance, and supporting me not only in my daily research challenges, but also in all I wanted to do during my PhD. They helped me as well to deal with making choices of and applications for internships, secondments, conferences and industrial placements all of which gave me separate skills as part of my PhD work. I was incredibly lucky to have the experience to work in collaboration with such special people and especially that fact that I got along with them so well and really enjoyed their company as people.

Thank you to my family who has given my incredible emotional and financial support throughout my studies and who have always encouraged me to work on topics that I find fascinating.

Finally I have left the person I am most appreciative of during my PhD research, namely Hugo Prager. I am incredibly lucky to have collaborated with such a wonderful person who was not only great to work with, when it comes to his professional attitude and interest in discussing all aspects of our collaborative research but also all aspects of physics. He has become one and will remain one of my closest friends. I will deeply miss living and working with such an incredible and unique person.

Nomenclature

LHC	Large Hadron Collider
SM	Standard Model
BSM	Beyond the Standard Model
SUSY	Supersymmetry
DM	Dark Matter
ChQ	Chiral Quarks
VL	Vector-Like
VLQ	Vector-Like Quark
XQ	eXtra Quark inculdes ChQs and VLQs
CKM	Cabibbo-Kobayashi-Maskawa
vev	Vacuum Expectation Value
$\mathcal{B}$	Branching Ratio
NWA	Narrow-Width Approximation
FW	Finite Width
LW	Large Width
SR	Signal Region
FCNCs	Flavour Changing Neutral Currents
$U(1)_Y$	The electromagnetic gauge group
$SU(2)_L$	The weak gauge group
$SU(3)_c$	The QCD gauge group
h.c.	The hermitian conjugated

Chapter 1

Introduction

The Standard Model (SM) [5, 6] is a theoretical description of all the observed fundamental forces of Nature, apart from gravity, and has been since its completion towards the end of the 60s very successful in its agreement with experiments [7, 8]. The main experimental discoveries contained within the SM are listed as follows:

- 1974, J/ψ meson, consisting of a charm and anti-charm quark [9].
- 1976, D^0 meson, consisting of a charm and anti-up quark [10].
- 1976, Tau lepton [11].
- 1977, Bottom quark [12].
- 1978, Weak interaction measured, mediated by Z boson [13].
- 1979, Gluon [14].
- 1983, Observation of Z and $W^{\pm}$ bosons [15, 16]
- 1995, Top quark [17].
- 2012, Higgs boson [18].

The incredible success that Particle Physics has had over the last 50 years can be seen from the above discoveries, each requiring unprecedented experimental precision including some impressively accurate predictions of processes which involve QED interactions [19].

The discovery at the Large Hadron Collider (LHC) of the Higgs boson in 2012 was considered to be the last piece in the jigsaw of the SM. It was generally expected that with the LHC reaching higher energy and luminosity new physics would emerge beyond that predicted by the SM leading to the so called Beyond the Standard Model (BSM) theory. This expectation has to date not been fulfilled with results showing for example

that the Higgs boson is behaving very much as a SM-like Higgs [20] and providing no hints for a BSM theory. This may change when the properties of the Higgs boson are measured very precisely, or if the new physics presents itself from other measurements at the LHC or other experiments. With all the success of the SM, one must note that it is certainly not the final theory as it does not contain gravity within its framework but only contains a description for the weak, strong and electromagnetic forces of nature.

This thesis is organised with first introducing the LHC, as my analyses are aimed at interpreting data produced at such an accelerator. Subsequently, the SM is briefly summarised, listing some of the many theoretical and experimental issues that the SM has to date, followed by touching upon some methods and concepts used when considering possible BSM scenarios. The second half of the introduction focuses entirely on setting up the models and frameworks required for the papers this thesis is based on, namely the addition of a new type of heavy quark to the SM called a Vector-Like Quark (VLQ). The papers presented involve the production of VLQs either via visible interactions only [1, 3] or considering interactions to Dark Matter (DM) [2]. Numerical results I have produced for VLQ single production have been included in [4]. This thesis is finalised with the conclusions.

1.1 The Large Hadron Collider

The LHC is a proton-proton circular collider consisting of two accelerated beams controlled by very powerful magnets spanning a tunnel of 27 kilometres. It can be considered to be the most complex experimental machine ever created, not only due to its size, being the largest single machine ever built, but also due to the shear complexity of the detectors and the volumes of raw data being so large most of it has to be discarded.

It took over 10 years for the LHC to become operational, starting operations and testing from September 2008 until the end of 2009. Run I of the LHC was from 2010 to 2013, starting at a centre of mass energy of 7 TeV and then at 8 TeV in April of 2012. The most notable discovery was the Higgs boson, among bound states and rare decays. The LHC then went into upgrade from 2013 to 2015 to enable collisions up to an energy of 14 TeV. Run II of the LHC then commenced in April 2015, with an energy of 13 TeV. The collected integrated luminosity reached by one of its biggest detector called the Compact Muon Solenoid (CMS) each year is shown in Fig. 1.1.

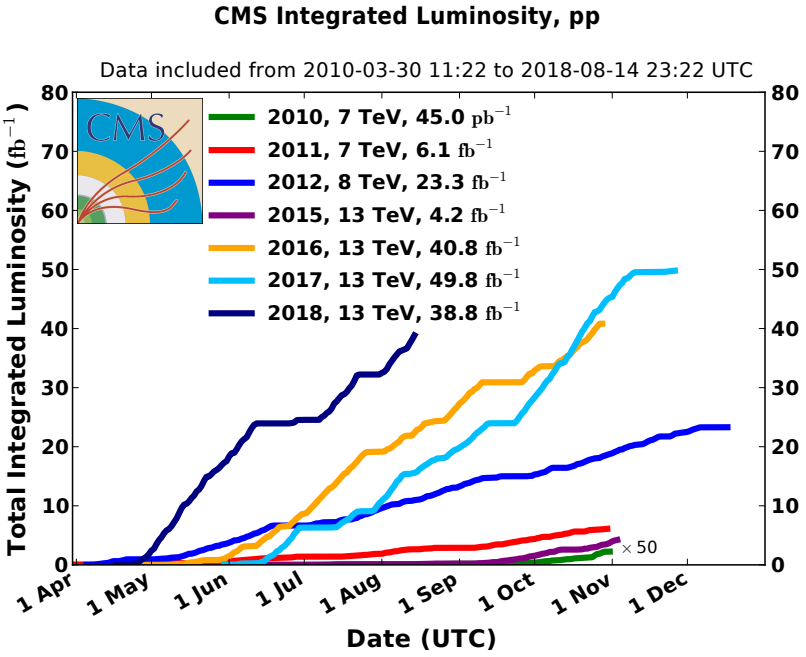

Figure 1.1: Amount of collected integrated luminosity (fb^{-1}) recorded at CMS for the years that the LHC was running and collecting data, at proton-proton beam energies 7, 8 and 13 TeV [21]. The values for ATLAS are similar to that shown from CMS.

The LHC is comprised of seven different detectors, each following a different methodology for their experiments. These experimental collaborations with detectors at the LHC are listed as follows:

- CMS
- A Toroidal LHC Apparatus, ATLAS
- LHCbeauty, LHCb
- A Large Ion Collider Experiment, ALICE
- TOTal Elastic and diffractive cross section Measurements, TOTEM
- Monopole and Exotics Detector At the LHC, MoEDAL
- LHCforward, LHCf

where the last three listed are experiments for very specific and optimised analyses and are of much smaller scale than the 4 main experiments listed first.

The summary plot for the exotic searches performed by CMS shown in Fig. 1.2 was presented at the conference ICHEP in 2016 and shows the exclusion range for 8 TeV and 13 TeV data. CMS and the LHC have found no significant signs of new BSM physics,

with bounds being set on the BSM scenarios searched for each year, although many of these bounds can differ significantly when different assumptions on the specific model are altered.

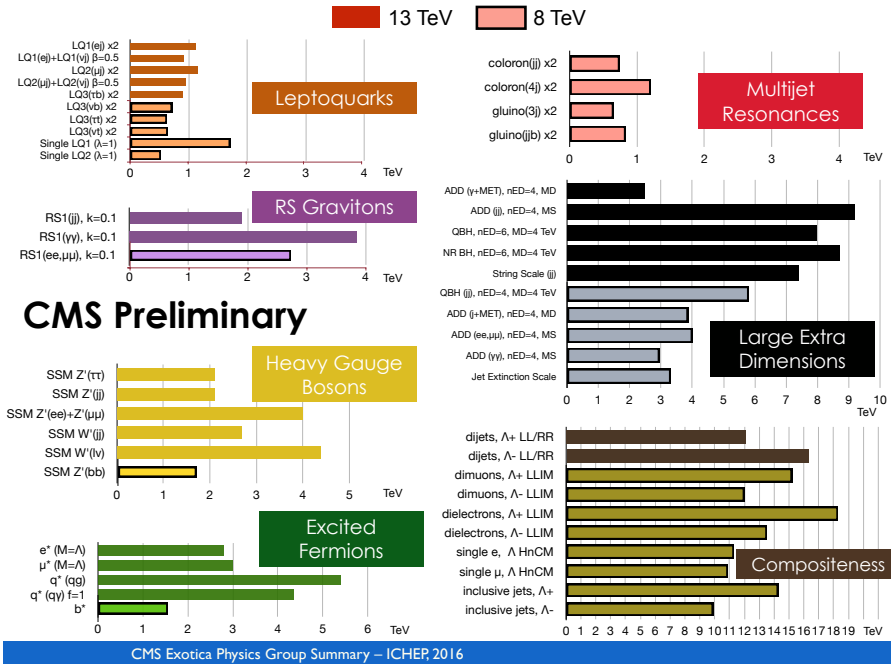

Figure 1.2: Exotica summary plots for resonances, extra dimensions, etc. from CMS, presented at ICHEP 2016 [22].

Future upgrades to the LHC enabling high luminosity, the HL-LHC, planned for 2026 would vastly improve the integrated luminosity. This would benefit many BSM theories, receiving increased sensitivity to rare decays and improving statistically sensitive measurements.

1.2 The Standard Model

To summarise the SM in a consistent but brief manner, two sets of notes have been closely followed [23, 24]. For a more complete review and discussion some of the best books on the matter can be found here [25, 26].

1.2.1 Gauge symmetry

The SM framework exists within a non-abelian gauge group symmetry.

$$\mathcal{G}_{SM} = SU(3)_C \otimes SU(2)_L \otimes U(1)_Y. \tag{1.1}$$

The $SU(3)_C$ term is responsible for Quantum Chromodynamical (QCD) interactions, in the form of the strong interaction between quarks and gluons which are the constituents of protons, neutrons and other hadrons for example mesons. The remaining two factors $SU(2)_L \otimes U(1)_Y$ account for the electroweak (EW) theory that generates nuclear decays, this symmetry is spontaneously broken down to $U(1)_{EM}$ by the Higgs mechanism, where the $U(1)_{EM}$ symmetry is responsible for electromagnetic (EM) interactions. Together these symmetries form the SM gauge group $\mathcal{G}_{SM}$. The model includes gauge bosons and the Higgs boson which mediates all of the possible interactions.

1.2.2 Fermion matter content

There are three generations of matter fields for the fermion content of the SM which consists of particles with spin $\frac{1}{2}$, these distinct families are indistinguishable from each other except for their masses after symmetry breaking. The families are shown in Table 1.1 where the leptons in each family transform trivially under QCD while the quarks transform non-trivially under QCD. The experimentally observed mass and charge values are also given.

Fermions		Mass [GeV]	Charge [e^-]
Quarks:	u	0.002	$\frac{2}{3}$
three	d	0.005	$-\frac{1}{3}$
generation	c	1.28	$\frac{2}{3}$
pairs	s	0.10	$-\frac{1}{3}$
	t	173.21	$\frac{2}{3}$
	b	4.18	$-\frac{1}{3}$
Leptons:	e^-	0.000511	-1
three	ν_e	massless in SM	0
generation	μ	0.11	-1
pairs	ν_μ	massless in SM	0
	τ	1.78	-1
	ν_τ	massless in SM	0

Table 1.1: Fermion content of the SM [27].

1.2.3 Spontaneous symmetry breaking

The final key component of the SM is the Higgs mechanism, through which $SU(2)_L \otimes U(1)_Y$ is broken down to the electromagnetic gauge group $U(1)_{EM}$. This is performed in the SM by introducing a complex scalar field ϕ, which transforms as a doublet of $SU(2)_L$. The potential of this complex scalar doublet is given by

$$V = -\mu^2|\phi|^2 + \lambda|\phi|^4. \tag{1.2}$$

The potential V possesses a minimum at a non-zero value of $\phi^\dagger\phi$ if μ^2 and λ are positive. At the minimum of the potential the vacuum expectation value (vev) is

$$< \phi^\dagger\phi >= \frac{\mu^2}{2\lambda} := \frac{v^2}{2}. \tag{1.3}$$

The scalar field ϕ can then be rotated into the unitary gauge by using the $\mathcal{G}_{SM}$ gauge symmetry and taking the corresponding vev to be real. In this form it can be seen that the vev is responsible for generating the masses of all of the gauge bosons of $SU(2)_L \otimes U(1)_Y$ except one unbroken generator which remains massless (photon), and also generating mass for the fermions through their interaction with the Higgs field. The value of v in the unitary gauge

$$v =< \phi_0 > \sim 180 \text{ GeV}, \tag{1.4}$$

is fixed by experiment and is used to define the electroweak scale (EWS), which is the point where the SM gauge symmetry breaks. The massless gauge boson for the remaining

symmetry group couples to the unbroken linear combination

$$Q_{EM} = T_3 + Y, \tag{1.5}$$

where Q_{EM} is the electric charge, T_3 is the diagonal generator of $SU(2)_L$ and Y the generator of $U(1)_Y$. The surviving symmetry group accounts for the electromagnetic interactions, under which the fields transform with charges given by Q_{EM}. The surviving gauge group below the EWS is

$$SU(3)_c \otimes U(1)_{EM}. \tag{1.6}$$

Three out of four real components of $\phi^\dagger\phi$ are absorbed by the now-massive gauge fields named $W^\pm$ and Z^0 as longitudinal polarisations, while a surviving real scalar h, describes excitations around the new vacuum

$$< \phi_0 >= \frac{1}{\sqrt{2}} \begin{pmatrix} 0 \\ v \end{pmatrix} \tag{1.7}$$

$$\phi_0 = \frac{1}{\sqrt{2}}(v + h), \tag{1.8}$$

which is called the Higgs boson, detected at a mass of $m_h \simeq 125$ GeV. Tree-level Dirac fermion masses are obtained through the Higgs mechanism and the Lagrangian that contains the coupling terms between the Higgs doublet and the fermion matter states [24] is as follows

$$\mathcal{L}^{Yuk}_{quark} = -\sqrt{2}[\lambda^{ij}_d \bar{Q}^i_L \phi d^j_R + \lambda^{ij}_u \epsilon^{\alpha\beta} \bar{Q}^{\alpha,i}_L \phi^{\dagger\beta} u^J_R + h.c.], \tag{1.9}$$

where L and R are indices denoting chirality. Since an invariant of $\mathcal{G}_{SM}$ of the form fermion-fermion does not exist for charged particles, the Lagrangian does not include any mass term for these fields. Such terms are forbidden by the fact that $SU(2)_L$ only transforms left-handed fields. This is only true however, as long as the symmetry is not spontaneously broken.

1.2.4 Coupling of fermion matter states to Higgs doublet

This section makes use of [24] for notation and methodology.

The weak interaction groups the 6 SM quarks into pairs of $SU(2)_L$ doublets, each with an assigned hypercharge of $Y = \frac{1}{6}$ such that after symmetry breaking the corrected empirically observed electric charges are obtained.

$$Q_L = \begin{pmatrix} u^j_L \\ d^j_L \end{pmatrix} = \left(\begin{pmatrix} u_L \\ d_L \end{pmatrix}, \begin{pmatrix} c_L \\ s_L \end{pmatrix}, \begin{pmatrix} t_L \\ b_L \end{pmatrix} \right) \tag{1.10}$$

and the right-handed component of the $SU(2)_L$ singlets are

$$u_R^j = (u_r, c_R, t_R), \qquad d_R^j = (d_R, s_R, b_R). \tag{1.11}$$

The quarks are coupled to the $SU(2) \otimes U(1)$ electroweak gauge bosons via the following Lagrangian term

$$\mathcal{L}_{quark}^{EW} = \bar{Q}_L^j i(\gamma^\mu D_\mu) Q_L^j + \bar{u}_R^j i(\gamma^\mu D_\mu) u_R^j + \bar{d}_R^j i(\gamma^\mu D_\mu) d_R^j. \tag{1.12}$$

Before the symmetry breaking the quark-Higgs couplings take the following general form

$$\mathcal{L}_{quark}^{Yuk} = -\sqrt{2}[\lambda_d^{ij}(\bar{u}_L^i, \bar{d}_L^i)\phi d_R^j + \lambda_u^{ij}\epsilon^{\alpha\beta}\bar{Q}_L^{\alpha,i}\phi^{\dagger\beta}u_R^j + h.c.]. \tag{1.13}$$

It can be noted that $\mathcal{L}_{quark}^{EW}$ violates C and P invariance and $\mathcal{L}_{quark}^{Yuk}$ only respects CP invariance if the matrix elements of $\lambda_{u,d}^{ij}$ are real. The SM's chiral fermionic matter field content does not form real representations of $\mathcal{G}_{SM}$, which means that the tree-level Dirac masses are forbidden due to gauge invariance. To inspect the mass terms in $\mathcal{L}_{quark}^{Yuk}$, the symmetry must be broken by the Higgs mechanism and several transformations are required, the procedure is listed below.

- Expand around the Higgs vev.
- Diagonalise the Yukawa matrices.
- Transform the quark fields $u_L^i, d_L^i \to V_L^u u_L^i, V_L^d d_L^i$ and $u_R^i, d_R^i \to V_R^u u_R^i, V_R^d d_R^i$.
- Transform the Dirac adjoint fields with corresponding Hermitian adjoint matrices.
- Rotate into the unitary gauge where $\phi_0^T = \frac{1}{\sqrt{2}}(0, v + h(x))$.

After symmetry breaking the Lagrangian of Eq (1.13) takes the following form

$$\mathcal{L}_{quark}^{Yuk} = -\left[(\bar{u}_L, \bar{d}_L)M^d d_R + \bar{d}_R \bar{M}^d \begin{pmatrix} u_L \\ d_L \end{pmatrix} + (-\bar{d}_L, \bar{u}_L)M^u u_R + \bar{u}_R \bar{M}^u \begin{pmatrix} -d_L \\ u_L \end{pmatrix}\right], \tag{1.14}$$

where the diagonalisation procedure performed on the Yukawa matrices $\lambda_{u,d}$ such that diagonal matrices $M^{u,d}$ have been formed by rotating into the unitary gauge after transforming the quark fields. The quark mass matrices then have the quark masses as elements, as can be seen in the following equations

$$M^u = \begin{pmatrix} m_u & 0 & 0 \\ 0 & m_c & 0 \\ 0 & 0 & m_t \end{pmatrix} = \frac{v}{\sqrt{2}} V_L^u \lambda_u V_R^{u\dagger}, \quad M^d = \begin{pmatrix} m_d & 0 & 0 \\ 0 & m_s & 0 \\ 0 & 0 & m_b \end{pmatrix} = \frac{v}{\sqrt{2}} V_L^d \lambda_d V_R^{d\dagger}, \tag{1.15}$$

where V is a 3×3 unitary matrix. The unitary gauge transformation used to get Eq (1.14) into its form was

$$\lambda_d^{ij}\bar{Q}_L^i\phi d_R^j \rightarrow \bar{Q}_L\phi V_L^{d\dagger}V_L^d M^d V_R^{d\dagger}V_R^d d_R = \bar{Q}_L\phi M^d d_R. \tag{1.16}$$

This transformation of the quark fields in Eq (1.16) has not left the doublet term $\bar{Q}_L i(\gamma^\mu D_\mu)Q_L$ in the Lagrangian Eq. (1.12) unaffected. The singlet terms $\bar{u}_R i(\gamma^\mu D_\mu)u_R + \bar{d}i(\gamma^\mu D_\mu)d_R$ are invariant under the above transformation. This doublet term is what is responsible for the interaction between the quark terms and $W^\pm$. The charge currents $J^\pm$ appearing in the Lagrangian as $\frac{-g}{2\sqrt{2}}J^{\mu\pm}W_\mu^\pm$ are transformed in the following way

$$\frac{1}{2}J^{\mu,+} = \bar{u}_L^i\gamma^\mu d_L^i \rightarrow \bar{u}_L^i\gamma^\mu(V_L^{\dagger u}V_L^d)^{ij}d_L^j, \tag{1.17}$$

with

$$V_L^{\dagger u}V_L^d = V_{CKM} = \begin{pmatrix} V_{ud} & V_{us} & V_{ub} \\ V_{cd} & V_{cs} & V_{cb} \\ V_{td} & V_{ts} & V_{tb} \end{pmatrix}. \tag{1.18}$$

The elements of this matrix have been determined empirically, as the SM cannot derive these values analytically.

1.3 Phenomena the SM cannot account for

In this section some of the many theoretical issues and observed phenomena that are not included in or explained by the SM are discussed.

Dark matter: Conventionally, DM can be classified based on their velocities being ultra relativistic and light or non-relativistic and heavy, referred to as hot and cold dark matter respectively. The temperature anisotropies of the CMB [28, 29], as well as structure formation can be explained through the presence of cold dark matter [30]. This is a consequence of CMB possessing velocities much less than the speed of light, causing it to congregate around the galactic constituents inside a cluster. Contrary to this, hot DM possesses relativistic speeds comparable to those scales matching super cluster lengths. Given the evidence provided by regarding the filamentary small scale structures in the universe, as implied by the nearly homogeneous microwave background, hot dark matter is incapable of explaining small scale structure, and a combination of cold and hot dark matter is necessary to reproduce these experimental observations.

There is an extraordinary amount of observational evidence indicating that there exists this massive, neutral, weakly interacting, non-relativistic, non-baryonic matter. A few of the main discoveries are listed here:

- Rotation curve of spiral galaxies [31] : Although the discrepancy between the velocity of stars within our galaxy had been reported by numerous physicists previously (by Jan Hendrik Oort in 1932 [32], among others), it was not until 1970 that Vera Rubin [33] showed that Newtonian gravity was not sufficient to describe her highly accurate measurements (for the technology at the time seen in Fig. 1.3), a possible explanation given was that more than half of the mass of the galaxy was formed by some dark galactic halo that had yet to be observed.

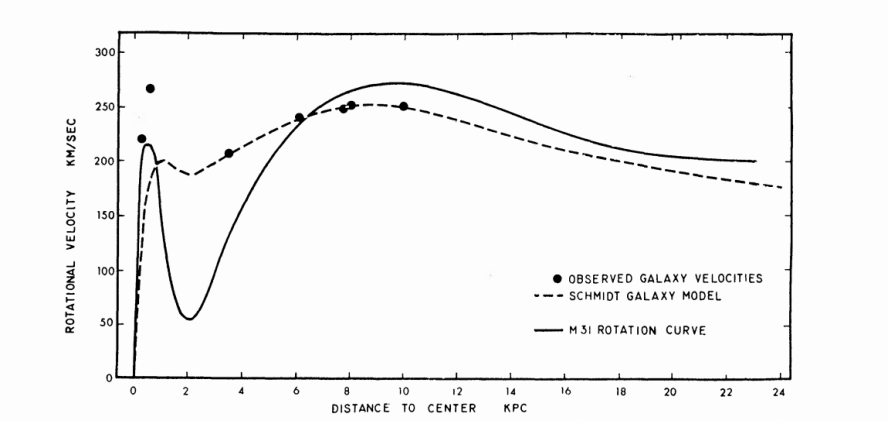

Figure 1.3: Comparison of rotation curves for M31 and the Galaxy as a function from the centre. Solid line: rotation curve for M31, dashed line: rotation curve from Schmidt model of the galaxy, Filled circles, observed rational velocities [33].

- Velocity dispersion observations of elliptical galaxies: Fritz Zwicky postulated the existence of what he referred to as DM from observations of motions of galaxies within the Coma Cluster [34, 35]. By applying the virial theorem, he noted that the velocity of the outer galaxies was far too great for the visible mass that could be accounted for. However his estimations where magnitudes of orders off todays observed values (as the observed value of the Hubble constant in 1929, by Edwin Hubble using the Hooker telescope [36], used for the calculation was 500 compared to the value observed today of 73.52+-1.62 by Hubble Space Telescope [37]).

- Gravitational Lensing, where massive galactical objects can act like lenses to magnify distant objects by bending light [38, 39] was postulated by Einstein [40] as a result of General Relativity, has been well observed (both strong and weak gravitational lensing).

- Bullet Cluster and other large scale collisions [41, 42]:

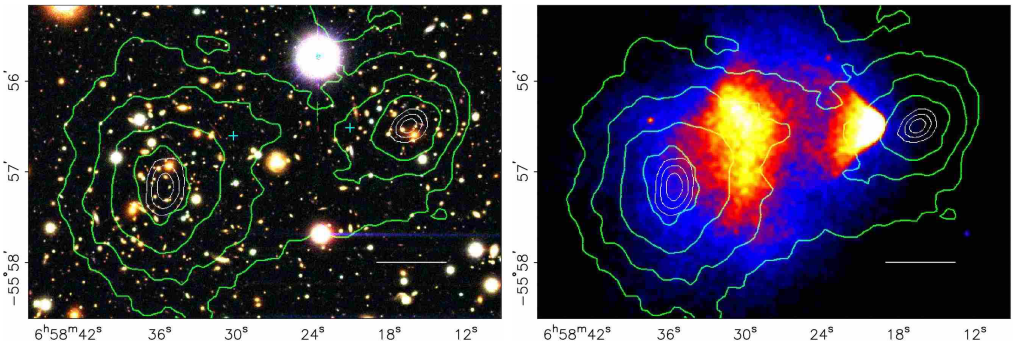

(a) (b)

Figure 1.4: This figure and caption is from Ref. [41]. Shown above in the top panel is a colour image from the Magellan images of the merging cluster 1E0657−558, with the white bar indicating 200 kpc at the distance of the cluster. In the bottom panel is a 500 ks Chandra image of the cluster. Shown in green contours in both panels are the weak lensing κ reconstruction with the outer contour level at $\kappa = 0.16$ and increasing in steps of 0.07. The white contours show the errors on the positions of the κ peaks and correspond to 68.3%, 95.5%, and 99.7% confidence levels. The blue +s show the location of the centers used to measure the masses of the plasma clouds.

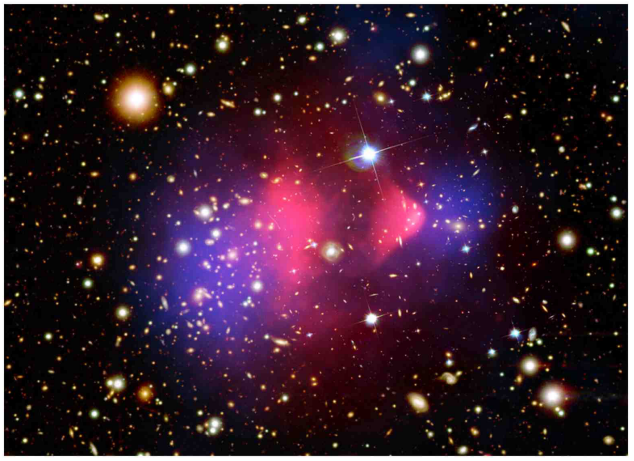

Figure 1.5: This figure and caption is from Ref. [42], this analysis was provided the image courtesy of Chandra X-ray Observatory [43]. False colour image of Bullet Cluster 1E0657-558. The surface density $\sum$-map reconstructed from X-ray imaging observations is shown in red and the convergence κ-map as reconstructed from strong and weak gravitational lensing observations is shown in blue.

In Figs. 1.4, 1.5 two colliding galaxies have been depicted, there are three items to take note of.

1. The stars of the galaxies seen clearly by the point sources of visible light observed, are very slightly slowed by gravity but otherwise passing through unaffected.
2. The regions which appear reddish-yellow (reddish-pink) are hot gas in each of the colliding galaxies which is interacting electromagnetically causing the baryonic matter to slow down relative to the stars of each respective galaxy
3. The DM regions are detected by the gravitational lensing effects that occur near the star content of each galaxy (DM halo). These regions of DM follow properties theorised, that DM is only weakly self-interacting and so is not slowed as with the baryonic gas content of the galaxies.

The issue today is not a lack of evidence that this new type of matter exists, but actually detecting this hypothesised particle directly [44, 45] from cosmology, or indirectly from collider experiments [46].

Massive neutrinos One of the most obvious short comings of the SM is that it has no mathematical framework to describe neutrino oscillations, or similarly a property that follows from empirically observed neutrino oscillations is the fact that neutrinos are not massless (minimum two out of three neutrino states are massive [47], ignoring the less favoured possibility that there is also a sterile neutrino [48]). Neutrino oscillation has been well documented from many experiments (such as Icecube [49] or KamLAND [50] among many others) which have examined neutrinos from different sources (beam experiments [47], cosmic ray collisions [51] with the atmosphere, nuclear reactor and neutrinos produced by our sun [47], or from even recently from a Blazar [52]). A more complete review of these experiments can be found in Ref [53]. All of which have confirmed the fact that neutrinos do indeed oscillate between states and that neutrinos are therefore massive in nature.

The matter anti-matter asymmetry The universe which can be observed has a radius of roughly 13.8 billion light years and is formed mostly of matter (not anti-matter), yet during the first infinitesimal moments of the universes existence, it is thought that there should have been roughly an even distribution of matter and anti-matter. So where has all the anti-matter gone? Unfortunately even though the SM contains some CP violating terms, the value is not sufficient to account for the matter-antimatter asymmetry required [54, 55]. In 1967 Andrei Sakharov used certain assumptions for his description of the evolution of a universe, it was later noted that he used the minimum three conditions required for baryogengesis to occur in nature. These three vital assumptions are called the Sakharov conditions:

- At least one Baryon number violating process.

- C and CP violating terms
- Particle interactions outside of thermal equilibrium

That is with the assumption that under consideration is a universe that started off with $B = 0$ during the Big Bang and is currently in a state that has a very large value. For more information on the wide literature on the subject please refer to [56, 57, 58]

The strong CP problem The full SM Lagrangian permits a CP-violating term:

$$\frac{\theta}{32\pi^2} F_{\mu\nu}\bar{F}^{\mu\nu}. \tag{1.19}$$

From this QCD Lagrangian term one could expect to have θ of order 1, yet it has been shown empirically to have an upper bound of 10^{-10} from measurements of the electric dipole moment of the neutron [59], which would have had large contributions if $\theta \sim 1$. The suppression which is required for θ to be small by experimental constraints is called the Strong CP problem [60, 61] (due to the term arising from the QCD gauge part of the Lagrangian). The SM cannot provide any reasons for this term to be small enough as to basically have negligible CP-violating effects.

Gravity: It is clear that the SM was never considered as a theory that completely describes nature as it does not include gravity. The best description of gravity we have for the moment is General Relativity (GR) but it is not compatible with the SM. These two theories can be considered as effective theories of a yet unknown theory where all the forces are unified [62, 63, 64, 65] at a higher energy scale. The attempts so far to quantise gravity have faced many difficulties [66], including the theories being non-renormalisable.

Dark energy: There is observational evidence since the 1990s that the universe is not only expanding [67] but that this expansion is occurring at an accelerated rate [68, 69, 70, 71, 72, 73]. Where such observations include the following.

1. Cosmic Microwave Background (CMB) [29, 74, 75, 66, 76]
2. Early Universe Structure Formation [77, 78, 79]

One of the more popular explanations for this is a new form of energy that exists homogeneously throughout all of space and only interacts via gravity [80, 81, 82, 83, 84].

The hierarchy problem: It was shown empirically that the Higgs mass is approximately 125 GeV [85, 86]. The issue with the Higgs is that it is the first scalar discovered in Nature and scalar masses are sensitive to quantum corrections [87]. The corrections to the Higgs mass are related to the cut-off squared (i.e. its mass is quadratically divergent). There are two possibilities that can be considered:

1. One is that if the Higgs mass potential squared is chosen such that it cancels these massive contributions that the scalar mass is sensitive to when taking the cut-off to be around the Planck scale. This amount of fine-tuning is disliked due to the fact that it is very unnatural.

2. A generally more favoured solution is that there is new physics at higher scales that has been impossible to probe due to a lack of sufficient energy present at colliders. New theories at this higher energy scale often perform these corrections via not yet discovered symmetries. These theories may still contain divergences (therefore there is still the need for new theories at even higher scales to completely remove the need for fine-tuning). Other theories like composite Higgs models side-step the hierarchy problem (like with the pion mass problem in QCD being solved upon the discovery that the pion is a composite particle [88], the Higgs could also be a composite [89, 90]).

Patterns that appear in the SM Some of the deeper questions which we hope a fundamental theory of physics would contain answers to and which physicists have been considering since the creation of the SM are:

- the existence of three generations for quarks and leptons, three colours and the electromagnetic charge being quantised by a third.
- the reason for the experimentally observed mass hierarchy of the three fermion generations, values of which are listed in Table 1.1.
- the reason for living in three space plus one time dimensions.
- why the SM gauge group $\mathcal{G}$ requires this exact gauge symmetry.
- how come there are so many parameters in the SM which are mostly only measured by experiment and have no theoretical predictions? One would hope that these quantities should be derivable in a more fundamental theory.

It is with this that we now move on to consider how to carry forward BSM in a consistent way that can explain some of the above issues of the SM. Some of the proposed solutions that could be tested at the LHC will be briefly mentioned before outlining the framework required for the research that has been performed in this thesis on VLQ phenomenology.

1.4 New quarks as a probe of physics beyond the SM

It can often be useful in phenomenology to first find and consider a common feature of different BSM theories, an example of such a feature could be the existence of a new heavy fermion. This approach is called the bottom-up approach, where instead of focusing on specific models in studies one can consider a common element in the predictions of the different classes of models, i.e. the addition of new quarks. The focus of the research performed in this thesis is on a bottom-up approach with the addition of a new quark which is among the easiest new particles to produce in a hadron collider. The other possible method is to follow a model-dependent top-down approach, that is studying a specific model from the framework of a BSM theory and the resulting phenomenological implications.

Fourth Generation Chiral Fermions The possibility of having one or more generations of chiral fermions has been heavily constrained by experimental searches which exclude chiral fermions above a mass of 600 GeV [91], due to the fermionic mass terms arising through their couplings to the Higgs field. Indeed the Higgs production via gluon fusion is increased 9 fold when including a fourth generation chiral fermion that interacts with the SM [92], when 40% is the largest value currently allowed [93]. The current bounds include a lower mass limit set for a fourth generation chiral quark (ChQ) above 1.3 TeV [94, 95] (where it was assumed that a ChQ decays into a $W^{\pm}$ boson and a third generation SM quark). There are also issues with the current electroweak data [96]. This can be fixed by allowing some new particles contained in a loop to cancel out the electroweak and Higgs production loop contributions [97] to current data. This can be achieved by including in the ChQ model an extended scalar sector of the SM [92], or one could also couple the new ChQ to the invisible sector such that its is not impacted by the bounds coming from Higgs production [3].

Vector-like Quarks VLQs are a different kind of quark that we will describe in detail in the next section and they are by nature not affected by the Higgs bounds cited previously. The current mass exclusion limits for VLQs do not rule out many favourable models, where the bound on the VLQs depends on many factors ranging from charge, mixing properties, the number of VLQ states and also depends on which decay channel is considered, the current experimental mass bound will be different or non-existent in more complex scenarios as shown in this study [98]. This is why these particles are interesting to study, in addition to the fact that many BSM theories have incorporated VLQs into their models.

There are many BSM theories which require the presence of VL-fermions, some of which are listed below. While some of these theories that incorporate new quarks are listed

here, it is important to stress that in our performed research, a model-independent and bottom-up approach is followed.

Little Higgs In these models, the gauge symmetries are extended such that there is a naturally occurring light Higgs field, where the quadratic divergences which contribute to the Higgs mass potential are cancelled by VL fermionic partners with the same statistics at the TeV scale [99, 100, 101, 102, 103, 104, 105, 106].

Composite Higgs In this type of model, the Higgs is described by a bound state of the top quark with a VL singlet [107, 108, 109, 110, 111, 112, 113, 114, 115, 116, 117, 118, 119, 120]. These composite Higgs models are one of the only ways to truly get around the hierarchy problem. This is similar to the pion mass in QCD which no longer has the hierarchical issues it previously had when it was thought to be a fundamental scalar of nature, when in fact it is a bound state of up and down quarks [121].

Extra Dimension The effective Higgs potential is finite without the need for fine-tuning in these model thanks to the addition of a gauge field interacting with the Higgs field via extra dimensions [122, 123, 124, 125]. Some of the possible extra dimension scenarios also require the addition VL-fermions to the model.

Supersymmetry (SUSY) In minimal supersymmetric extensions of the SM, the corrections to the quadratic divergences of the Higgs mass potential are lowered to logarithmic divergences by introducing SUSY partners, which cancel some of these divergences. In non-minimal extensions of the SM the logarithmic divergence can be further reduced by introducing VL matter. [126, 127, 128, 129, 130, 106, 131].

1.5 Model framework of VLQs

For a particle in spinor representation ϕ, the left and right handed components are given by $\phi = \phi_R + \phi_L = \mathcal{P}_R\phi + \mathcal{P}_L\phi$. Where the projection operators are defined as

$$\mathcal{P}_R = \frac{1+\gamma^5}{2}, \quad \mathcal{P}_L = \frac{1-\gamma^5}{2}. \tag{1.20}$$

A fermion is defined as Vector-like (VL) under a specific gauge group $\mathcal{G}$ if its left and right-handed projections belong to the same representation of such a group. The SM gauge group has been used in our model and has already been defined as

$$\mathcal{G}_{SM} = SU(3)_C \otimes SU(2)_L \otimes U(1)_Y. \tag{1.21}$$

To understand where the name "vector-like quark" originates from, it is useful to examine the charge current part of the SM Lagrangian

$$\mathcal{L} = \frac{g}{\sqrt{2}}(\mathcal{J}^{\mu+}W_{\mu}^{+} + \mathcal{J}^{\mu-}W_{\mu}^{-}), \tag{1.22}$$

it has been observed empirically that SM fermions are in agreement with a Vector−Axial (V-A) structure of the weak interaction if they only have left-handed charge currents

$$\mathcal{J}_{\mu+} = \mathcal{J}_{L}^{\mu+} = \bar{t}_{L}\gamma^{\mu}b_{L} = \bar{t}\gamma_{\mu}\frac{(1-\gamma^{5})}{2}b. \tag{1.23}$$

Now considering the situation where the left- and right-handed projections transform identically under the SM $SU(2)_L$ gauge groups,

$$\mathcal{J}^{\mu+} = \mathcal{J}_{L}^{\mu+} + \mathcal{J}_{R}^{\mu+} = \bar{T}\gamma^{\mu}\frac{(1-\gamma^{5})}{2}B + \bar{T}\gamma^{\mu}\frac{(1+\gamma^{5})}{2}B = \bar{T}\gamma^{\mu}B. \tag{1.24}$$

The resulting charge current in Eq (1.24) has only a vector component (V).

1.5.1 Symmetries, interactions and representations

The minimal scenarios with the presence of VLQs besides SM particles are those in which the new states interact with SM quarks and the Higgs boson through Yukawa couplings as in Eq (1.25):

$$\mathcal{L}_{Y} = -y_{ij}\bar{\mathcal{Q}}_{i}Hq_{j} + h.c.\,, \tag{1.25}$$

where Q_i is a VLQ added to the model and interacting with the SM quarks q_j and the Higgs H through the Yukawa coupling y_{ij}. The following sections are considering the representation of these particles in $SU(2)_L$.

1.5.1.1 Interaction terms

To add a new quark to the SM in a model independent way, it is not important which theory predicts the new state, but what is key is to understand the observable consequence of this SM extension. It is then useful to consider different representations of the SM gauge group for SM quarks and the VLQ:

$$(SU(3)_C, SU(2)_L, U(1)_Y) \rightarrow \begin{cases} \mathcal{Q}_L \simeq (3, S_L, Y_L) = (\boldsymbol{S_L}, Y_L) \\ \mathcal{Q}_R \simeq (3, S_R, Y_R) = (\boldsymbol{S_R}, Y_R) \end{cases} \tag{1.26}$$

For the SM quarks which are chiral there is the following isospin S and hypercharge Y structure:

$$\begin{cases} \text{left doublet: } S_L = 2,\ Y_L = \frac{1}{6}, \\ \text{right singlet: } S_R = 1,\ Y_R^u = \frac{2}{3},\ Y_R^d = -\frac{1}{3}, \end{cases} \tag{1.27}$$

while for VLQs there is the following structure:

$$S_L = S_R = S \text{ and } Y_L = Y_R = Y. \tag{1.28}$$

The interaction of a new VLQ with a SM chiral quark q and a neutral scalar Higgs boson $SU(2)_L$ doublet, H. The interaction term is therefore $\bar{\mathcal{Q}}Hq$ which allows only a limited subset of representations. Note that since we have a scalar boson, the coupling links quarks of opposite chirality.

$$\begin{aligned}
&\bar{\mathcal{Q}}_R \otimes H \otimes q_L \rightarrow \quad (\mathbf{2}, \pm\tfrac{1}{2}) \otimes (\mathbf{2}, \tfrac{1}{6}) = (\mathbf{1}, \tfrac{1}{6} \pm \tfrac{1}{2}) \oplus (\mathbf{3}, \tfrac{1}{6} \pm \tfrac{1}{2}) \quad \rightarrow (\boldsymbol{S_R}, Y_R) = (\mathbf{1}, \frac{1}{6} \pm \frac{1}{2}) \text{ or } (\mathbf{3}, \frac{1}{6} \pm \frac{1}{2}) \\
&\bar{\mathcal{Q}}_L \otimes H \otimes u_R \rightarrow \qquad (\mathbf{2}, \pm\tfrac{1}{2}) \otimes (\mathbf{1}, \tfrac{2}{3}) = (\mathbf{2}, \tfrac{2}{3} \pm \tfrac{1}{2}) \qquad = (\boldsymbol{S_L}, Y_L) \\
&\bar{\mathcal{Q}}_L \otimes H \otimes d_R \rightarrow \qquad (\mathbf{2}, \pm\tfrac{1}{2}) \otimes (\mathbf{1}, -\tfrac{1}{3}) = (\mathbf{2}, -\tfrac{1}{3} \pm \tfrac{1}{2}) \qquad = (\boldsymbol{S_L}, Y_L)
\end{aligned}$$

Therefore, the only allowed representations are:

$$\left\{ \begin{array}{l} \mathcal{Q}_L \simeq (\boldsymbol{S_L}, Y_L) \\ \mathcal{Q}_R \simeq (\mathbf{1}, \frac{1}{6} \pm \frac{1}{2}) \end{array} \right. \quad \left\{ \begin{array}{l} \mathcal{Q}_L \simeq (\boldsymbol{S_L}, Y_L) \\ \mathcal{Q}_R \simeq (\mathbf{3}, \frac{1}{6} \pm \frac{1}{2}) \end{array} \right. \quad \left\{ \begin{array}{l} \mathcal{Q}_L \simeq (\mathbf{2}, \frac{1}{6} \pm \frac{1}{2} \pm \frac{1}{2}) \\ \mathcal{Q}_R \simeq (\boldsymbol{S_R}, Y_R) \end{array} \right. \tag{1.29}$$

For a VLQ which has $S_L = S_R$ and $Y_L = Y_R$ this simplifies the previous relation to the following:

$$\left\{ \begin{array}{l} \mathcal{Q}_L \simeq (\mathbf{1}, \frac{1}{6} \pm \frac{1}{2}) \\ \mathcal{Q}_R \simeq (\mathbf{1}, \frac{1}{6} \pm \frac{1}{2}) \end{array} \right. \quad \left\{ \begin{array}{l} \mathcal{Q}_L \simeq (\mathbf{3}, \frac{1}{6} \pm \frac{1}{2}) \\ \mathcal{Q}_R \simeq (\mathbf{3}, \frac{1}{6} \pm \frac{1}{2}) \end{array} \right. \quad \left\{ \begin{array}{l} \mathcal{Q}_L \simeq (\mathbf{2}, \frac{1}{6} \pm \frac{1}{2} \pm \frac{1}{2}) \\ \mathcal{Q}_R \simeq (\mathbf{2}, \frac{1}{6} \pm \frac{1}{2} \pm \frac{1}{2}) \end{array} \right. \tag{1.30}$$

This means that the particle content of a

- **Singlet** under $SU(2)_L$ with hypercharge $\frac{1}{6} + \frac{1}{2} = \frac{2}{3}$ is (T) and $\frac{1}{6} - \frac{1}{2} = -\frac{1}{3}$ for (B).
- **Doublet** under $SU(2)_L$ with hypercharge $\frac{1}{6} + \frac{1}{2} + \frac{1}{2} = \frac{7}{6}$ is (X, T) and $\frac{1}{6} + \frac{1}{2} - \frac{1}{2} = \frac{1}{6}$ for (T, B) and $\frac{1}{6} - \frac{1}{2} - \frac{1}{2} = -\frac{1}{6}$ for (B, Y).
- **Triplet** under $SU(2)_L$ with hypercharge $\frac{1}{6} + \frac{1}{2} = \frac{2}{3}$ is (X, T, B) and $\frac{1}{6} - \frac{1}{2} = -\frac{1}{3}$ is for (T, B, Y).

Where X, T, B and Y are the possible VLQs with a charge of $+\frac{5}{3}$, $+\frac{2}{3}$, $-\frac{1}{3}$ or $-\frac{4}{3}$ respectively.

1.5.1.2 Mass terms

The mass terms for the new quarks can be written in a gauge-invariant way without requiring the Higgs mechanism, only in the VL scenario because under $SU(2)$

$$M\bar{Q}Q = M\bar{Q}_L Q_R \simeq S_L \otimes S_R = S \otimes S = 1 \oplus ... \tag{1.31}$$

is always allowed.

1.5.1.3 Summary of allowed representations

Classifying VLQs in multiplets of $SU(2)_L$, it is possible to write gauge-invariant interaction terms only for singlets, doublets and triplet representations. The possible multiplets of VLQs are shown in Table 1.2.

	SM quarks q			Singlets T_R, B_R		Doublets Q_L			Triplets Q_R	
	$\begin{pmatrix} u \\ d \end{pmatrix}$	$\begin{pmatrix} c \\ s \end{pmatrix}$	$\begin{pmatrix} t \\ b \end{pmatrix}$	T	B	$\begin{pmatrix} X \\ T \end{pmatrix}$	$\begin{pmatrix} T \\ B \end{pmatrix}$	$\begin{pmatrix} B \\ Y \end{pmatrix}$	$\begin{pmatrix} X \\ T \\ B \end{pmatrix}$	$\begin{pmatrix} T \\ B \\ Y \end{pmatrix}$
$SU(2)_L$	$q_L = 2$ $q_R = 1$			1		2			3	
$U(1)_Y$	$q_L = 1/6$ $u_R = 2/3$ $d_R = -1/3$			$2/3$	$-1/3$	$7/6$	$1/6$	$-5/6$	$2/3$	$-1/3$
$\mathcal{L}_Y$	$-y_u^i \bar{q}_L^i H^c u_R^i$ $-y_d^i \bar{q}_L^i V_{CKM}^{i,j} H d_R^j$			$-\lambda_u^i \bar{q}_L^i H^c T_R$ $-\lambda_d^i \bar{q}_L^i H B_R$		$-\lambda_u^i \bar{Q}_L H^{(c)} u_R^i$ $-\lambda_d^i \bar{Q}_L H^{(c)} d_R^i$			$-\lambda_i \bar{q}_L^i \sigma^a H^{(c)} Q_R^a$	
$\mathcal{L}_m$	not allowed			$-M_{VLQ}\, \bar{Q}\, Q$		$-M_{VLQ}\, \bar{Q}\, Q$			$-M_{VLQ}\, \bar{Q}\, Q$	

Table 1.2: Allowed representations for VLQs, with quantum numbers under $SU(2)_L$ and $U(1)_Y$ and Yukawa mixing terms in the Lagrangian. Depending on the chosen representation, the Higgs boson may be H or H^c, therefore it has been noted as $H^{(c)}$ when necessary. The gauge invariant mass term common to all representations is a peculiar feature of VLQs.

1.5.1.4 Mixing of allowed representations and modified couplings

As shown in Table 1.2 the mixing occurs in the left-handed sector for the singlet and triplet representations and in the right-handed sector for the doublet representation. The mass eigenstates will be labelled as:

$$\{X_{5/3}, t', b', Y_{-4/3}\}. \tag{1.32}$$

The mass matrices for the SM-partners t' and b' can be diagonalized by unitary 4×4 matrices $V_L^{t,b}$ and $V_R^{t,b}$:

$$\begin{pmatrix} m_u & & & \\ & m_c & & \\ & & m_t & \\ & & & m_{t'} \end{pmatrix} = (V_L^t)^\dagger \cdot \mathcal{M}_t \cdot (V_R^t), \tag{1.33}$$

$$\begin{pmatrix} m_d & & & \\ & m_s & & \\ & & m_b & \\ & & & m_{b'} \end{pmatrix} = (V_L^b)^\dagger \cdot \mathcal{M}_b \cdot (V_R^b), \tag{1.34}$$

where the actual expressions of $\mathcal{M}_t$ and $\mathcal{M}_b$ depend on the chosen representations and on the assumptions on the mixing parameters. The couplings with gauge bosons also depends on the chosen representations, but a common feature of every VLQ scenario is that tree-level FCNCs are developed through the mixing with SM quarks. The general form of Zqq couplings with the presence of VLQs is:

$$\begin{aligned} g_{ZL}^{IJ} &= \tfrac{g}{c_W}\left(T_3 - Qs_W^2\right)\delta^{IJ} + f_L \tfrac{g}{c_W}(V_L^{t,b})^{*,q'I}(V_L^{t,b})^{q'J}, \\ g_{ZR}^{IJ} &= \tfrac{g}{c_W}\left(-Qs_W^2\right)\delta^{IJ} \quad + f_R \tfrac{g}{c_W}(V_R^{t,b})^{*,q'I}(V_R^{t,b})^{q'J}, \end{aligned} \tag{1.35}$$

where I, J run on all quarks, including VLQs, $T_3 = \pm 1/2$ is the weak isospin of top or bottom in the SM, and $f_{L,R} = \{0, \pm 1/2, \pm 1\}$ are parameters which depend on the VLQ representation and satisfy the relation $T_3^{q'} = T_3 + f_L = f_R$; they are listed in Tab. 1.3 for each representation.

		Singlets		Doublets			Triplets	
$U(1)_Y$		$2/3$	$-1/3$	$7/6$	$1/6$	$-5/6$	$2/3$	$-1/3$
t'	f_L	$-1/2$		-1	0		$-1/2$	$+1/2$
	f_R	0		$-1/2$	$+1/2$		0	$+1$
b'	f_L		$+1/2$		0	$+1$	$-1/2$	$+1/2$
	f_R		0		$-1/2$	$1/2$	-1	0

Table 1.3: Neutral current parameters f_L and f_R.

From (1.35) two consequences can be inferred the first being that Flavour Changing Neutral Currents (FCNCs) are present between the new state and SM quarks, but can also be induced between SM quarks themselves, if mixing with light families is allowed. Secondly even flavour conserving neutral currents ($I = J$) are modified by the presence of VLQs.

Constraints on FCNCs, if the VLQS mix with lighter generations which leads to large deviations arising for couplings that have the following structure, Wq_1q_2 or Zq_1q_2, affects a large number of observables and can therefore provide strong bounds on the coupling between the VLQs and SM particles where the deviations in question depend on the mixing parameters [132]. These contributions to the affected SM observables will arise at tree-level from FCNCs when normally they only occur at loop-level. The two main observables that see large differences at tree-level due to FCNCs are as follows.

- **Rare FCNC top decays** The CMS collaboration has performed a study on said decays showing that there is a limit for $\mathcal{B}(t \to Zq) < 0.24\%$ when in the SM regime, the limit for $\mathcal{B}(t \to Zq) < \mathcal{O}(10^{-14})\%$. Bounds on combinations of non-diagonal mixing matrix elements can be formed from this limit in both the left- and right-handed sector.

- **Meson mixing and decays** With the inclusion of VLQs, FCNCs can be an important factor in the mixing and decay of mesons, which allows for some processes that would normally only occur at loop-level to also occur at tree-level. There have been a large number of measurements involving the branching ratios and mixing parameters which provide heavy constraints on the VLQ mixing parameters. Mixing and decays of mesons have been thoroughly studied in the literature, an analytical description of these contributions occurring with the presence of VLQs can be found in [133, 134, 135, 136].

Charged currents are modified too. The general form of Wq_1q_2 couplings with the presence of VLQs is:

$$g_{WL}^{IJ} = \frac{g}{\sqrt{2}}(V_{CKM}^{L})^{IJ} = \frac{g}{\sqrt{2}}(V_{L}^{t})^{\dagger} \cdot \hat{\delta}_{L} \cdot \tilde{V}_{CKM}^{L} \cdot V_{L}^{b}, \tag{1.36}$$

$$g_{WR}^{IJ} = \frac{g}{\sqrt{2}}(V_{CKM}^{R})^{IJ} = \frac{g}{\sqrt{2}}(V_{R}^{t})^{\dagger} \cdot \hat{\delta}_{R} \cdot \tilde{V}_{CKM}^{R} \cdot V_{R}^{b}, \tag{1.37}$$

where $I, J = 1, 2, 3(, 4)$ and the matrices $V^{t,b}$ may or may not be present depending on the scenario considered. The matrices $\hat{\delta}_{L,R}$ are defined as:

$$\hat{\delta}_{L} = \left(\begin{array}{ccc|c} 1 & & & \\ & 1 & & \\ & & 1 & \\ \hline & & & 1 \end{array}\right), \qquad \hat{\delta}_{R} = \left(\begin{array}{ccc|c} 0 & & & \\ & 0 & & \\ & & 0 & \\ \hline & & & 1 \end{array}\right), \tag{1.38}$$

where the lines mean that the size of the matrices depend on the chosen scenario; in particular, g_{WR} exists only if both an up- and down-type VLQ are present simultaneously. The matrices $\tilde{V}_{CKM}^{L,R}$ represent the misalignment between SM quarks in the left- and right-handed sector; $\tilde{V}_{CKM}^{L}$ corresponds to the measured CKM matrix in the absence of VLQs. Two CKM matrices can thus be defined in the presence of VLQs, for the left- and right-handed sectors. If VLQs exist, the measured CKM matrix corresponds to the 3×3 block $(V_{CKM}^{L})^{ij}$, with $i, j = 1, 3$. A further consequence of the introduction of VLQs is that the measured 3×3 CKM block is not unitary, and it is possible to check that deviations from unitarity are proportional to the mixing between SM quarks and VL states.

Charged currents may also be present between the exotic states $\{X_{5/3}, Y_{-4/3}\}$ and up- or down-type quark respectively. The couplings are:

$$\begin{aligned} g_W^{XI} &= \frac{g}{\sqrt{2}}\left((V_L^t)^{4I} + (V_R^t)^{4I}\right), \\ g_W^{YI} &= \frac{g}{\sqrt{2}}\left((V_L^b)^{4I} + (V_R^b)^{4I}\right). \end{aligned} \tag{1.39}$$

1.5.1.5 Coupling to the Higgs boson

Finally, the couplings to the Higgs bosons can be written as:

$$\begin{aligned} C_u^{IJ} &= \frac{1}{v}\begin{pmatrix} m_u & & & \\ & m_c & & \\ & & m_t & \\ & & & m_t' \end{pmatrix} - \frac{M}{v}(V_L^t)^{*,4I}(V_R^t)^{4J} \\ C_d^{IJ} &= \frac{1}{v}\begin{pmatrix} m_d & & & \\ & m_s & & \\ & & m_b & \\ & & & m_b' \end{pmatrix} - \frac{M}{v}(V_L^b)^{*,4I}(V_R^b)^{4J}. \end{aligned} \tag{1.40}$$

From these expressions it can be inferred that the presence of a VLQ can modify the mechanism of production and decay of the Higgs boson with respect to SM predictions.

1.5.2 The Lagrangian term for VLQs

In the studies performed in this thesis, the addition of only one VL-top T was considered, where the general couplings between the electroweak gauge bosons and a single T can be parametrised using the same method as Ref. [137], as is done with the following Lagrangian.

$$\begin{aligned} \mathcal{L}_{T_{single}} &= \kappa_W V_{L/R}^{4i}\frac{g}{\sqrt{2}}[\bar{T}_{L/R}W_\mu^+\gamma^\mu d_{L/R}^i] + \kappa_Z V_{L/R}^{4i}\frac{g}{2c_W}[\bar{T}_{L/R}Z_\mu\gamma^\mu u_{L/R}^i] \\ &- \kappa_H V_{L/R}^{4i}\frac{M}{v}[\bar{T}_{R/L}H u_{L/R}^i] + h.c.\,, \end{aligned} \tag{1.41}$$

where M is the mass of the VLQ, $V_{L/R}^{4i}$ represents the mixing matrices between the VLQ and the three SM generations labelled by i, and the parameters κ_V $(V = W, Z, H)$ encodes the couplings to the three bosons. The coupling with the photon and gluon are standard and are dictated by gauge invariance[1]. The following normalisation is used $\kappa_W = \kappa_Z = \kappa_H = 1$, and in the following studies it was chosen that the VL-top would decay 100% to either Z, H or $W^\pm$, in the asymptotic limit when the mass of the VL-top goes to infinity, depending on the channel in question. The values of κ_ν depends

[1] Couplings to the Z, and to the W and other VL quarks, are also in general present and they depend on the representation of $SU(2)_L$ T belongs to.Ref. [137]

upon the $SU(2)_L$ representation of T chosen and is determined by mixing with other VL-representations.

An assumption which was used in the simulations of the papers presented in this thesis is based on a discussion of suppressed terms performed by Ref [137], and is summarised by the following reasoning. In the more general case where not only a single T is in consideration, T can have a large coupling to both the left- and right-handed SM quarks q. In the scenario considered in the research presented in this thesis, the addition of only a single VLQ to the SM (commonly studied experimentally), it can be shown that only one mixing angle is large as the other is suppressed by a factor of m_q/M_{VLQ} [138]. Due to this fact the above Lagrangian can be simplified by neglecting the suppressed mixing angle by only containing one of the chiral couplings. This assumption is well justified for all the SM quarks apart from the top quark, although a discussion of the terms suppressed by the top mass has been performed in Appendix B of Ref. [137] which provides correction terms and in the case where it is a sizeable correction in a region of phenomenological interest (for $T \to Ht$) it was included in the general effective Lagrangian Eq. (1.55) without the need to add a new parameter. The partial width terms in the above Lagrangian are given in each channels by the following:

$$\Gamma(T \to Wb, Zt, Ht) = \kappa^2_{W,Z,H}|V^{4i}_{L/R}|^2 \frac{M^3 g^2}{64\Pi m^2_W} \times \Gamma_{W,Z,H}(M_T, m_{W,Z,H}, m_{b,t,t}), \quad (1.42)$$

with the kinematic relations given by:

$$\Gamma_{W,Z} = \frac{1}{2}\lambda^{\frac{1}{2}}\left(1, \frac{m^2_q}{M^2_T}, \frac{m^2_{W,Z}}{M^2_T}\right)\left[\left(1 - \frac{m^2_q}{M^2_T}\right)^2 + \frac{m^2_{W,Z}}{M^2_T} - 2\frac{m^4_{W,Z}}{M^4_T} + \frac{m^2_q m^2_{W,Z}}{M^4_T}\right]$$

and

$$\Gamma_H = \frac{1}{2}\lambda^{\frac{1}{2}}\left(1, \frac{m^2_q}{M^2_T}, \frac{m^2_H}{M^2_T}\right)\left[1 + \frac{m^2_q}{M^2_T} - \frac{m^2_H}{M^2_T}\right]. \quad (1.43)$$

The partial width has been expressed in a way that utilises a universal coupling factor such that the only difference between the channels depends on the masses, which for the light quarks is weak and values for the other generations of quarks can be assumed. This is possible for all but the top quark which can have mass relevant effects, these effects have been discussed in detail by Ref [137]. The branching ratios when neglecting all quark masses can be defined in the following form

$$\mathcal{B}(T \to Vq_i) = \frac{\kappa^2_V |V^{4i}_{L/R}|^2 \Gamma^0_V}{\left(\sum^3_{j=1} |V^{4j}_{L/R}|^2\right)\left(\sum_{V'=W,Z,H} \kappa^2_{V'} \Gamma^0_{V'}\right)} \quad (1.44)$$

The kinematic functions Γ^0_V for zero quark mass $m_q = 0$ are given by:

$$\Gamma^0_W = \left(1 - 3\frac{m^4_W}{M^4} + 2\frac{m^6_W}{M^6}\right) \sim 1 + \mathcal{O}(M^{-4}), \quad (1.45)$$

$$\Gamma_Z^0 = \frac{1}{2}\left(1 - 3\frac{m_Z^4}{M^4} + 2\frac{m_Z^6}{M^6}\right) \sim \frac{1}{2} + \mathcal{O}(M^{-4})\,, \tag{1.46}$$

$$\Gamma_H^0 = \frac{1}{2}\left(1 - \frac{m_H^2}{M^2}\right)^2 \sim \frac{1}{2} - \frac{m_H^2}{M^2} + \mathcal{O}(M^{-4})\,. \tag{1.47}$$

It is useful to write these branching ratios in terms of four independent parameters that contain all the relevant information:

$$\zeta_i = \frac{|V_{L/R}^{4i}|^2}{\sum_{j=1}^3 |V_{L/R}^{4j}|^2}\,, \quad \sum_{i=1}^3 \zeta_i = 1\,, \xi_V = \frac{\kappa_V^2 \Gamma_V^0}{\sum_{V'=W,Z,H} \kappa_{V'}^2 \Gamma_{V'}^0}\,, \quad \sum_{V=W,Z,H} \xi_V = 1\,; \tag{1.48}$$

so that

$$\mathcal{B}(T \to V q_i) = \zeta_i \xi_V\,. \tag{1.49}$$

When considering experimental scenarios where the decays into the first or second generation quarks cannot be distinguished, one can express all the results in terms of decay rates into light generations via $\zeta_{jet} = \zeta_1 + \zeta_2 = 1 - \zeta_3$:

$$\mathcal{B}(T \to Zj) = \zeta_{jet}\xi_Z\,, \quad \mathcal{B}(T \to Zt) = (1 - \zeta_{jet})\xi_Z\,, \tag{1.50}$$

$$\mathcal{B}(T \to Hj) = \zeta_{jet}(1 - \xi_Z - \xi_W)\,, \quad \mathcal{B}(T \to Ht) = (1 - \zeta_{jet})(1 - \xi_Z - \xi_W)\,, \tag{1.51}$$

$$\mathcal{B}(T \to W^+ j) = \zeta_{jet}\xi_W\,, \quad \mathcal{B}(T \to W^+ b) = (1 - \zeta_{jet})\xi_W\,. \tag{1.52}$$

In the pair production scenario that is dominated by model-independent QCD processes which depend only on the mass of the VLQ, the phenomenology of the T for this reason can be described by the following four independent parameters: M_{VLQ}, ξ_W, ξ_Z and ζ_{jet}.

The Lagrangian in Eq.(1.55) can then be expressed with the 5 relevant parameters as follows:

$$\begin{aligned}\mathcal{L} \;=\; & \kappa_T \left\{ \sqrt{\frac{\zeta_i \xi_W}{\Gamma_W^0}} \frac{g}{\sqrt{2}} \left[\bar{T}_{L/R} W_\mu^+ \gamma^\mu d_{L/R}^i\right] + \sqrt{\frac{\zeta_i \xi_Z}{\Gamma_Z^0}} \frac{g}{2c_W} \left[\bar{T}_{L/R} Z_\mu \gamma^\mu u_{L/R}^i\right] \right. \\ & \left. - \sqrt{\frac{\zeta_i (1 - \xi_Z - \xi_W)}{\Gamma_H^0}} \frac{M}{v} \left[\bar{T}_{R/L} H\; u_{L/R}^i\right] \right\} + h.c. \end{aligned} \tag{1.53}$$

where $\zeta_3 = 1 - \zeta_1 - \zeta_2$ and the additional parameter κ_T is the overall coupling strength measure and is not important for the branching ratios or for pair production (QCD dominated processes). It is on the other hand useful to determine the strength of single production and can be written in the following form:

$$\kappa_T = \sqrt{\sum_{i=1}^3 |V_{L/R}^{4i}|^2} \sqrt{\sum_V \kappa_V^2 \Gamma_V^0}\,. \tag{1.54}$$

The complete effective Lagrangian that contains interactions for the 4 possible VLQs for leading left-handed mixing, where one can inter-change the left- and right-handed

chirality's ($L \to R$) for the leading right-handed coupling is as follows.

$$\begin{aligned}\mathcal{L}_L = \kappa_T \Bigg\{ & \sqrt{\frac{\zeta_i \xi_W^T}{\Gamma_W^0}} \frac{g}{\sqrt{2}} \left[\bar{T}_L W_\mu^+ \gamma^\mu d_L^i\right] + \sqrt{\frac{\zeta_i \xi_Z^T}{\Gamma_Z^0}} \frac{g}{2c_W} \left[\bar{T}_L Z_\mu \gamma^\mu u_L^i\right] \\ & - \sqrt{\frac{\zeta_i \xi_H^T}{\Gamma_H^0}} \frac{M_T}{v} \left[\bar{T}_R H u_L^i\right] - \sqrt{\frac{\zeta_3 \xi_H^T}{\Gamma_H^0}} \frac{m_t}{v} \left[\bar{T}_L H t_R\right] \Bigg\} \\ + \kappa_B \Bigg\{ & \sqrt{\frac{\zeta_i \xi_W^B}{\Gamma_W^0}} \frac{g}{\sqrt{2}} \left[\bar{B}_L W_\mu^- \gamma^\mu u_L^i\right] + \sqrt{\frac{\zeta_i \xi_Z^B}{\Gamma_Z^0}} \frac{g}{2c_W} \left[\bar{B}_L Z_\mu \gamma^\mu d_L^i\right] - \sqrt{\frac{\zeta_i \xi_H^B}{\Gamma_H^0}} \frac{M_B}{v} \left[\bar{B}_R H d_L^i\right] \Bigg\} \\ + \kappa_X & \left\{ \sqrt{\frac{\zeta_i}{\Gamma_W^0}} \frac{g}{\sqrt{2}} \left[\bar{X}_L W_\mu^+ \gamma^\mu u_L^i\right] \right\} + \kappa_Y \left\{ \sqrt{\frac{\zeta_i}{\Gamma_W^0}} \frac{g}{\sqrt{2}} \left[\bar{Y}_L W_\mu^- \gamma^\mu d_L^i\right] \right\} + h.c. \end{aligned} \tag{1.55}$$

For the allowed decay rates of the above Lagrangian please refer to Ref. [137] or to the Appendix. The effective Lagrangian Eq (1.55) has been implemented in FeynRules [139], this implementation is described in detail in the Appendix C of [137]. The complete FeynRules files, together with the CalcHEP and MadGraph outputs, are available on the FeynRules website for the general model [140] and for specific cases such as that of a T singlet among other scenarios. There is also a HEP model database project found on this website [141].

1.6 The Narrow Width Approximation (NWA)

If one considers the width Γ of the VLQs to be small with respect to its mass, the Breit-Wigner distribution in the propagator can be replaced by a Dirac delta in the $\Gamma/M \to 0$ limit, this is what we call the NWA. This allows complex processes to be factorised into production and decay such that the cross-section can be expressed in a form that significantly simplifies simulations, especially when the production cross-section only depends on the mass of the VLQ.

For example if one considers the total matrix element squared of a process involving a scalar particle, it contains its propagator squared which is a Breit-Wigner distribution

$$\frac{1}{(q^2 - M^2)^2 + M^2\Gamma^2}. \tag{1.56}$$

Knowing the following limit

$$\lim_{\epsilon \to 0} \frac{\epsilon}{\epsilon^2 + x^2} = \pi \delta(x), \tag{1.57}$$

where the width is $\Gamma \ll M$ and the following simplification can be made

$$\frac{1}{\Gamma M^3} \frac{\Gamma/M}{(q^2/M^2 - 1)^2 + (\Gamma/M)^2} \to \pi \frac{\delta(q^2/M^2 - 1)}{\Gamma M^3} = \pi \frac{\delta(q^2 - M^2)}{\Gamma M}. \tag{1.58}$$

It can be seen by using the above assumption that the scalar intermediate particle in question has been made on-shell by the δ-function and at leading order the production

will be factorised from decay. So for a process involving pair production of VLQs Q and $\bar{Q}$, the NWA permits the following simplification of calculation of the cross-section in the NWA regime, σ_X

$$\sigma_X \equiv \sigma_{2\to2}\mathcal{B}(Q)\mathcal{B}(\bar{Q}), \tag{1.59}$$

where $\sigma_{2\to2}$ is the two to two scattering process producing the VLQs and the branching ratio $\mathcal{B}$ is the ratio of the partial decay width of the VLQ into the final state particles over the total decay width of the VLQ. For single production of a VLQ, this NWA cross-section becomes

$$\sigma_X \equiv \sigma_{2\to2}\mathcal{B}(Q). \tag{1.60}$$

One of the key topics researched was to understand the relevance of the VLQ width in processes of pair and single production at the LHC. If the width is large, it is not possible to factorise production and decay processes, and the kinematics can be sizeably different. In turn this affects the efficiencies of experimental analyses for a given final state, and therefore it is not necessarily possible to simply rescale the experimental bounds computed in the NWA to obtain the bounds for finite widths.

1.7 Pair and single production of VLQs

The addition of only one VL-top was considered in the research carried out. Adding several VLQs could have added additional complications such as interference effects between the different VLQ which was already studied in Ref. [142]. The two production methods of VLQs examined in the studies performed are as follows.

- **Pair production**: it is dominated by QCD production topologies easily allowing us to do a model independent approach as the only dependence is on the mass of the new VLQ.
- **Single production**: in this case the model dependence is larger since the production also depend on the coupling strength of the VLQ to the SM quarks. Also the VLQ can be produced
  - in association with tops;
  - in association with jets (where jet denotes any light quark, including the b quark);
  - in association with a boson, including $W^{\pm}$, Z and the Higgs H;

  This model-independent approach was suggested and examined in detail by Ref. [137], their analysis provides good motivation for many possible VLQ studies.

1.7.1 Pair production

The pair production processes are the following ones

$$q\bar{q}, gg \rightarrow \bar{Q}Q \rightarrow V^{H,W^{\pm},Z}V^{H,W^{\mp},Z}q\bar{q} \tag{1.61}$$

where $V^{H,W^{\pm},Z}$ is a $H, W^{\pm}$ or Z boson. The main contribution to the pair production of VLQs is the QCD production via gluons, with subleading contributions from topologies involving electroweak gauge bosons. This is due to the fact that the production probability is proportional to the coupling constants of the strong and electroweak interactions. The fact that the strong coupling constant is much greater than the electromagnetic or weak coupling means that the production is dominated by the strong interaction. This means that the neutral current diagrams where the productions is via a Z or γ that have the same final states as QCD production are negligible. The reason pair production topologies involving a t-channel propagating Higgs boson will not be considered is due to the fact that they are heavily suppressed by the Yukawa coupling between the light generation SM quarks being small and with the Higgs mass inclusion in the propagator.

The QCD leading topologies contributing to the cross-section only depend on the mass of the VLQ and therefore is model-independent as previously mentioned. These leading topologies become less important as higher VLQ mass ranges are studied, this is due to a suppression arising from the PDFs.

1.7.2 Single production

Processes of VLQ production in association with SM states crucially depend on the couplings between the VLQs and the SM quarks, but for fixed couplings the cross-section for single production scales with the VLQ mass more slowly than the cross-section for pair production. Eventually, for a large enough VLQ mass, the single production processes become the dominant channels. Therefore, as bounds on VLQ masses increases, it is worth exploring the phenomenology of single production processes alongside pair-production.

The cross section from single production is model dependent as all the topologies involving only one VLQ always contain an electroweak coupling, so the cross section is related to not only the mass of the VLQ but also to the size of the coupling between the VLQ and the resulting SM decay particles.

One caveat is that single production scales differently due to the cross-section not suffering from the same PDF suppression as pair production. The PDF suppression effects are compensated by a weaker flavour bound on the couplings which allows the single production to be the dominant production method when considering larger mass regions of VLQs.

An important subtlety arises when one is deciding what topologies are of interest for their single production study, which is the choice of the initial state flavour scheme of the proton in the collision. This will be discussed in more detail in a later chapter, but to summarise it was assumed in the 2 to 3 single production study that the bottom was a constituent part of the proton in the so-called 5 Flavour-Scheme (5FS), another possible choice was the 4FS where the bottom cannot appear in the initial state, though they can appear from gluon splitting. The key phenomenological reasoning that this choice can be made is that any difference between the two schemes would vanish if it was possible to describe the processes at all orders in QCD perturbation theory[2]. The topologies for single production in the 5FS are represented in Fig. 4.1. (Notice that some of these only exist in the Large Width (LW) regime, not in the NWA).

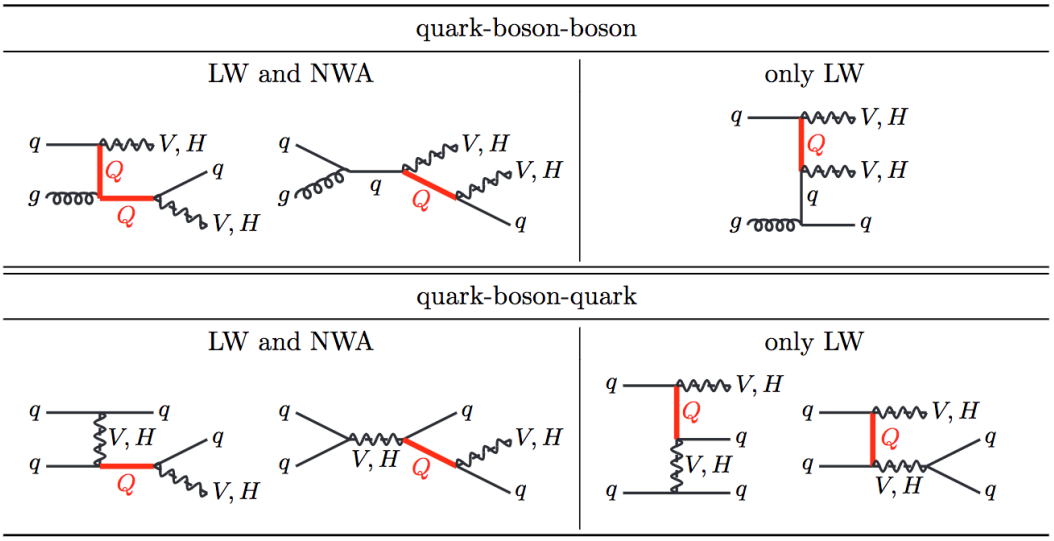

Figure 1.6: Complete list of the generic topologies for final states compatible with single VLQ production in the 5FS. Topologies on the left column can be described in both the NWA and LW regimes while topologies on the right column are neglected in the NWA approximation. Here, V represents the W and Z bosons of the SM.

[2]For specific details we refer to the wide literature on this subject (see for example [143, 144, 145] for single top production).

1.8 Current state of experimental VLQ searches at the LHC

1.8.1 Pair and single production searches for VLQs at ATLAS

1.8.1.1 Combined decays of $T \to Wb, Zt, Ht$ or $B \to Wt, Zb, Hb$ VLQ analysis

ATLAS has performed a combined analysis for pair production of a VL-top and -bottom quark at $\sqrt{s}$ =13 TeV with 31.1 fb^{-1} of data [146] in the following decay channels

$$T \to Zt, Wb, Ht. \quad \text{and} \quad B \to Zb, Wt, Hb. \tag{1.62}$$

The data observed matched the expected SM background predicted in each individual search, the upper limits with combined 95% confidence-level are set for a range of VLQ scenarios, which are then combined to increase the mass range accessible then what the searches alone could achieve. This study has set a mass bound of 1.31 TeV for the VL-top singlet (left plot of Fig. 1.7) and for the VL-bottom the excluded region is up to 1.22 TeV (left plot of Fig. 1.8). When considering a weak isospin (T, B) doublet the analysis has also provided exclusion limits up to 1.37 TeV (right plots of Fig. 1.7 and Fig. 1.8).

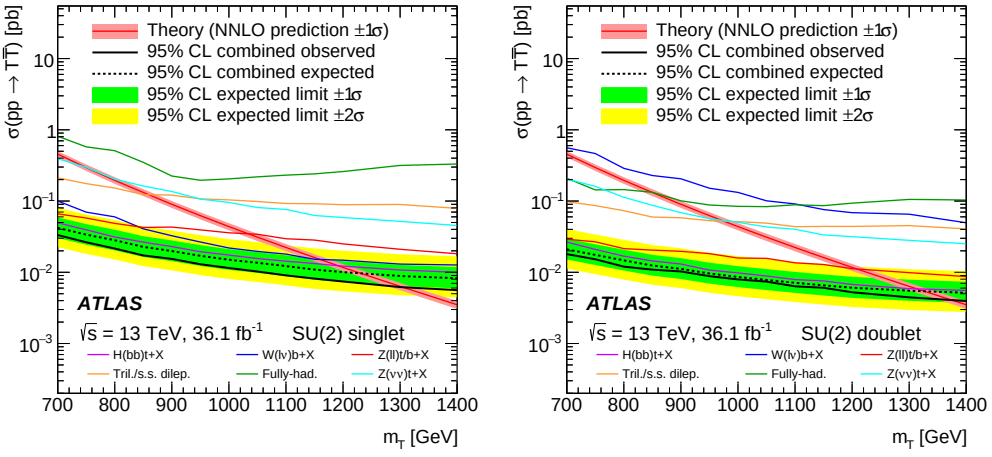

(a) (b)

Figure 1.7: This figure and caption is from Ref. [146]. Observed (solid line) and expected (dashed line) 95% CL upper limits on the $T\bar{T}$ cross-section versus mass for the combination and the standalone analyses in black and coloured lines, respectively. The (a) singlet and (b) doublet scenarios [147] are displayed. The shaded bands correspond to ±1 and ±2 standard deviations around the combined expected limit. The rapidly falling thin red line and band show the theory prediction and corresponding uncertainty [148], respectively.

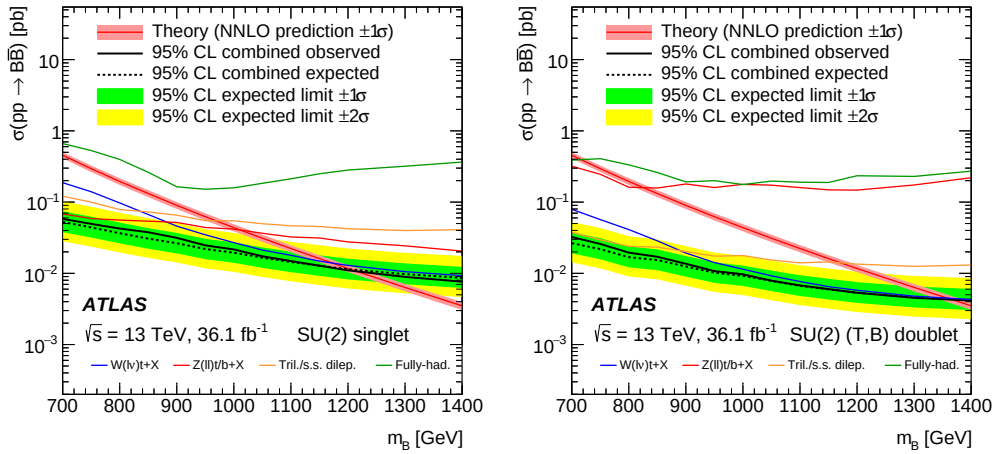

(a) (b)

Figure 1.8: This figure and caption is from Ref. [146]. Observed (solid line) and expected (dashed line) 95% CL upper limits on the $B\bar{B}$ cross-section versus mass for the combination and the standalone analyses in black and colored lines, respectively. The (a) singlet and (b) (T, B) doublet scenarios [147] are displayed. The shaded bands correspond to ± 1 and ± 2 standard deviations around the combined expected limit. The rapidly falling thin red line and band show the theory prediction and corresponding uncertainty [148], respectively.

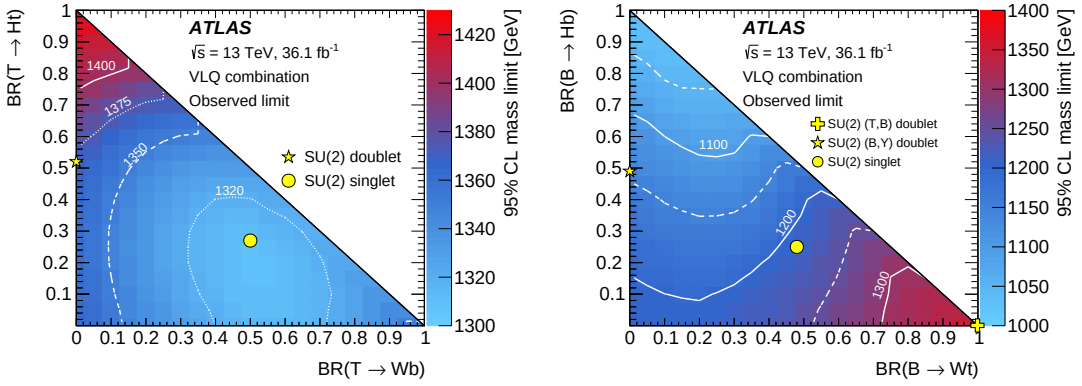

(a) (b)

Figure 1.9: This figure and caption is from Ref. [146]. Observed lower limits at 95% CL on the mass of the (a) T and (b) B as a function of branching ratio assuming $\mathcal{B}(T \to Ht) + \mathcal{B}(T \to Zt) + \mathcal{B}(T \to Wb) = 1$ and $\mathcal{B}(B \to Ht) + \mathcal{B}(B \to Zt) + \mathcal{B}(B \to Wb) = 1$ The yellow markers indicate the branching ratios for the SU(2) singlet and doublet scenarios for VLQ masses above 800 GeV where the branching ratios become approximately independent of the VLQ mass [147].

This combination of seven different analyses of pair production searches of VLQs performed by the ATLAS collaboration, excluding the VL-T, B quarks below a mass of 1.31 TeV and 1.03 TeV respectively (left and right plots of Fig. 1.9).

1.8.1.2 Search for VLQ involving a decay $T, B \to Zq$ analysis

Another analysis recently performed by the ATLAS collaboration was on a search using five channels optimised for targeting the decay of a VLQ into a Z boson along with a SM top (bottom) for the VL-top (-bottom) $T \to Zt$ ($B \to Zb$) case. A combination of the $\sqrt{s} = 13$ TeV, with 36.1 fb^{-1} worth of LHC data recorded in 2015 and 2016 was used by this analysis [149]. A high transverse momentum Z boson in the final state is reconstructed from b-tagged jets and a pair of same-flavour opposite-sign leptons. This analysis performed was not only for pair production but also single production.

Three channels were combined and used to provide an exclusion region up to 1030 GeV (1010 GeV) for a T (B) singlet and 1210 GeV (1140 GeV) exclusion limits in the T (B) doublet model case shown in Fig. 1.10.

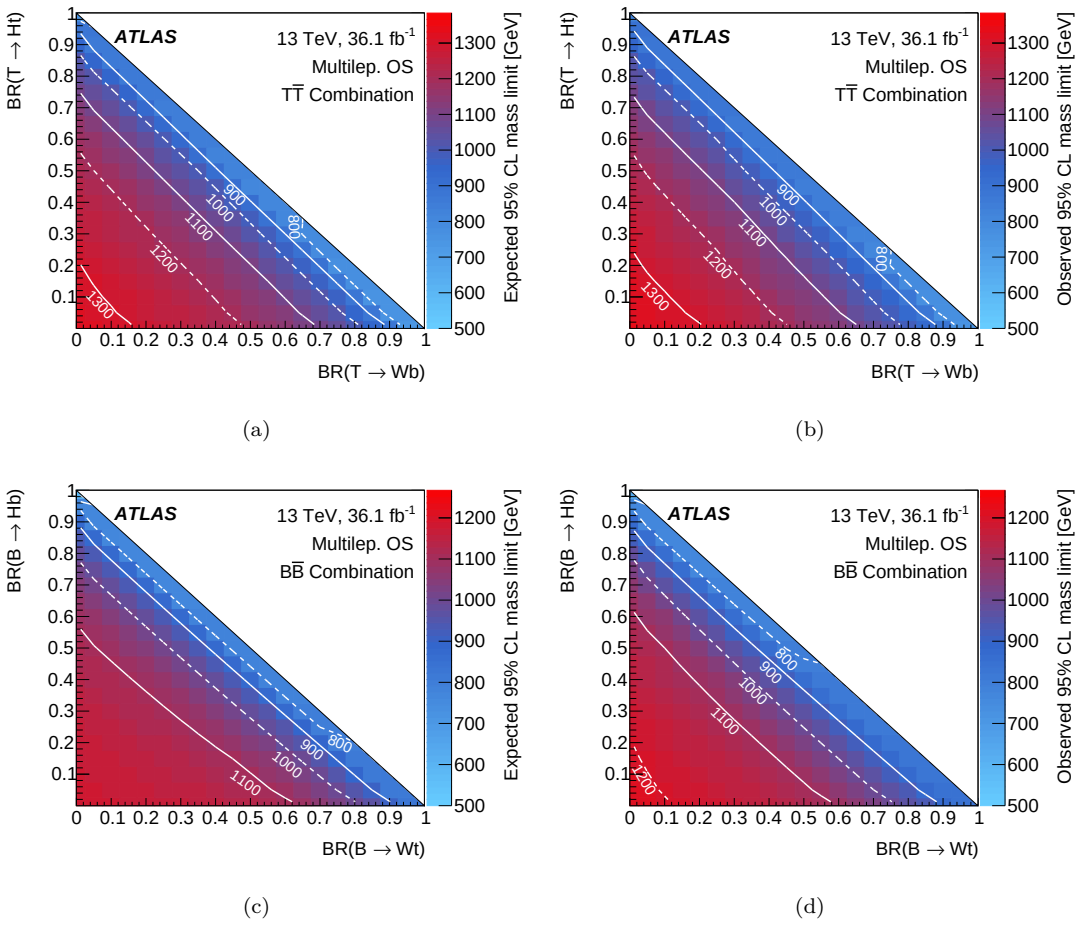

Figure 1.10: This figure and caption is from Ref. [149]. Expected (a,c) and observed (b,d) 95% CL lower limits from the combination of the pair-production channels on the mass of vector-like quarks for all combinations of BRs for (a,b) $T \to Zt$, $T \to Ht$, $T \to Wb$, and (c,d) $B \to Zb$, $B \to Hb$, $B \to Wt$, adding up to unity. The white lines are contours for fixed values of M_{VLQ}.

The limits on the production cross section times branching fraction into Zt $\mathcal{B}(T \to Zt)$ are in the range of 0.16 to 0.18 pb at $M_T = 700$ GeV and decreases to 0.03-0.05 pb at $M_T = 2000$ GeV, relative to the value of the coupling that ranges from $\kappa_T = 0.1$ to 1.6 seen in Fig. 1.12.

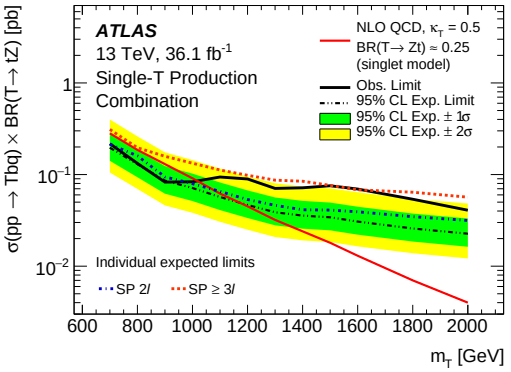

Figure 1.11: This figure and caption is from Ref. [149]. Upper limits at 95% CL on the cross section times BR to Zt of single production (SP) of a T-quark. The expected limits are shown for the individual channels and for the combination of the channels, as are the observed limits for the combination. The expected cross section times BR to Zt for single-T-quark production is also shown for a coupling $\kappa_T = 0.5$, which corresponds to a coupling of $c_W = \sqrt{c_{W,L}^2 + c_{W,R}^2} = 0.45$ from Ref. [150]. The BR assumed here corresponds to the singlet benchmark model, i.e. $\approx 25\%$.

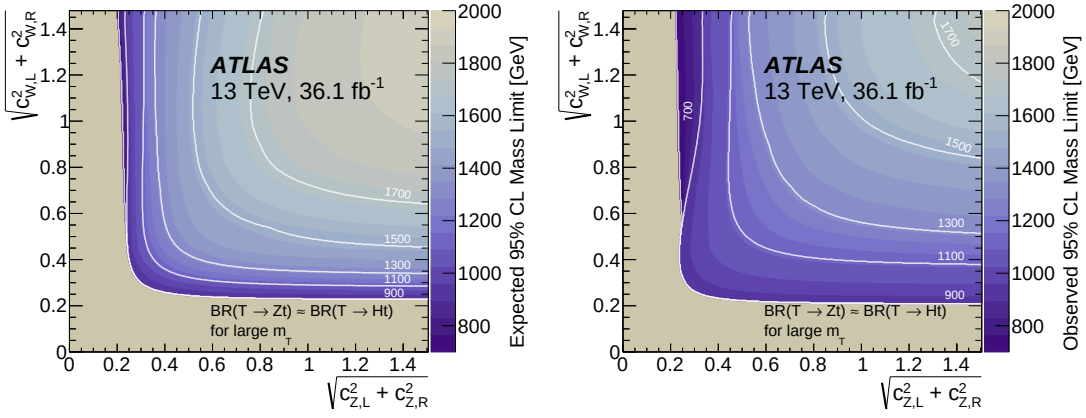

(a) (b)

Figure 1.12: This figure and caption is from Ref. [149]. Expected (a) and observed (b) lower limit from the combination of the single-production channels on the mass of the T quark as a function of the couplings of the T quark to the W boson, $\sqrt{c_{W,L}^2 + c_{W,R}^2}$, and to the Z boson, $\sqrt{c_{Z,L}^2 + c_{Z,R}^2}$ with the assumption of equal BRs for $T \to Zt$ and $T \to Ht$ in the limit of large T-quark masses. The gray area corresponds to a region that is not excluded for any mass value tested because of the limited sensitivity of the analysis for very small T-quark masses. The white lines are contours for fixed values of M_{VLQ}.

1.8.2 Pair and single production searches for VLQs at CMS

1.8.2.1 Combined decays of $T \to Wb, Zt, Ht$ or $B \to Wt, Zb, Hb$ VLQ analysis

The CMS collaboration has presented a data sample of 35.9 fb^{-1} integrated luminosity at $\sqrt{s} = 13$ TeV [151]. The channels examined by this search are those involving a lepton, a pair of same sign leptons and three or more leptons in the final state. These channels are then combined such that at 95% CL T (B) quarks are excluded up to a mass of 1200 GeV (1170 GeV) for the case of a T (B) singlet and 1280 GeV (940 GeV) in the case of a T (B) doublet, as can been seen in Figure 1.13.

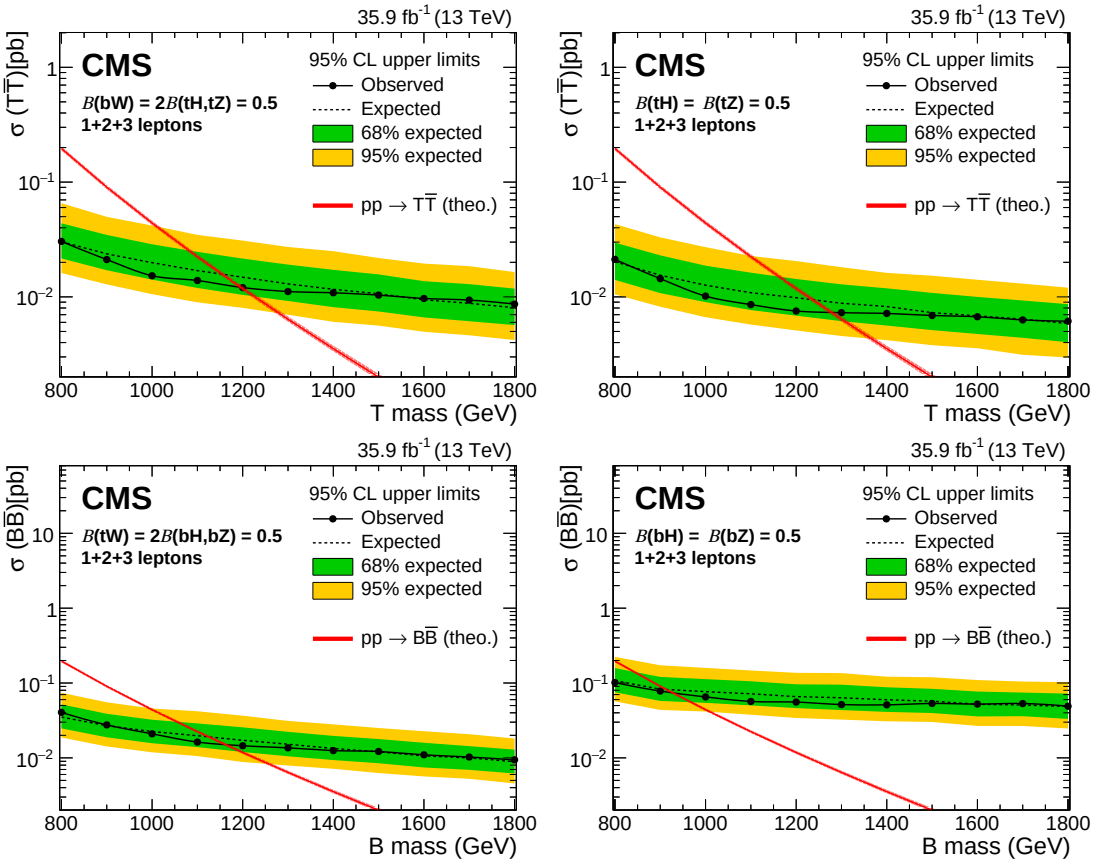

Figure 1.13: This figure and caption is from Ref. [151]. The 95% CL expected and observed upper limits on the cross section of $T\bar{T}$ (upper row) and $B\bar{B}$ (lower row) production after combining all channels for the singlet (left) and doublet (right) branching fraction scenarios. The predicted cross sections are shown by the red curve, with the uncertainty indicated by the width of the line.

This analysis also produced expected and observed limits from scans involving the possible branching fraction scenarios which excludes T (B) quark masses up to a range of 1140-1300 GeV (910-1240 GeV). These results can be seen in Figure 1.14.

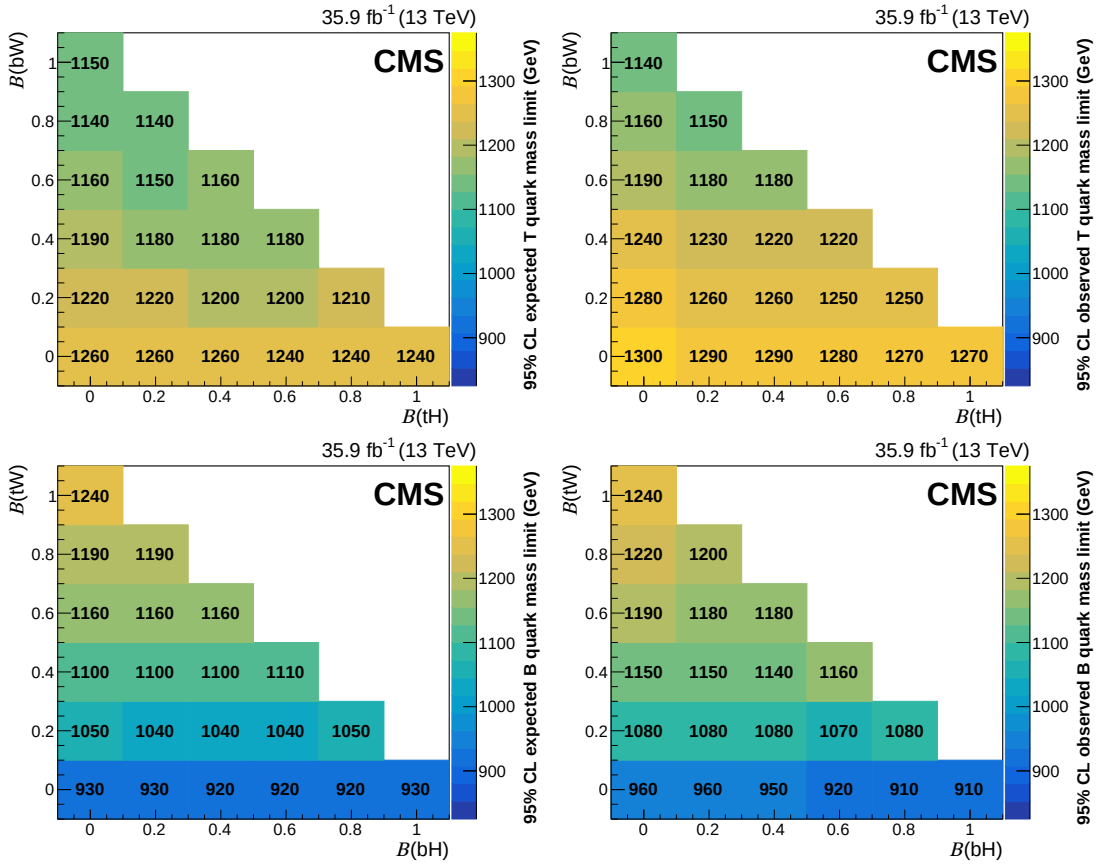

Figure 1.14: This figure and caption is from Ref. [151].The 95% CL expected (left) and observed (right) lower limits on the T quark (upper row) and B quark (lower row) mass, expressed in GeV, after combining all channels for various branching fraction scenarios.

1.8.2.2 Search for VLQ involving a decay of $T \to Zt$ analysis

This single production search for VLQs [4] is especially relevant to this thesis as I contributed to this analysis in the form of helping to develop the formalism of the reduced cross section ($\bar{\sigma}_{FW}$) and by computing the cross sections which appear in Table 1.4.

The analysis performed by [4] presented results for a search involving decay of a VL-top decaying into a Z and t quark. It provided upper limits at 95% CL on the product of the cross section and branching fraction ranging from 0.26 pb to 0.04 pb (from 0.14 pb to 0.04 pb) for the production of a left-handed T associated with a b quark $T(b)$ (right-handed T associated with a t quark), for a mass range of 0.7 TeV to 1.7 TeV as can be viewed in Fig. 1.15. This exclusion limit was set under that NWA assumption, using a simplified approach described by Ref. [150].

The observed and expected upper limits at 95% CL is presented in Fig. 1.16, where the mass exclusion limit for the production of a left-handed T singlet associated with a b quark $T(b)$ was set around 1.34 TeV to 1.42 TeV and for the production of the

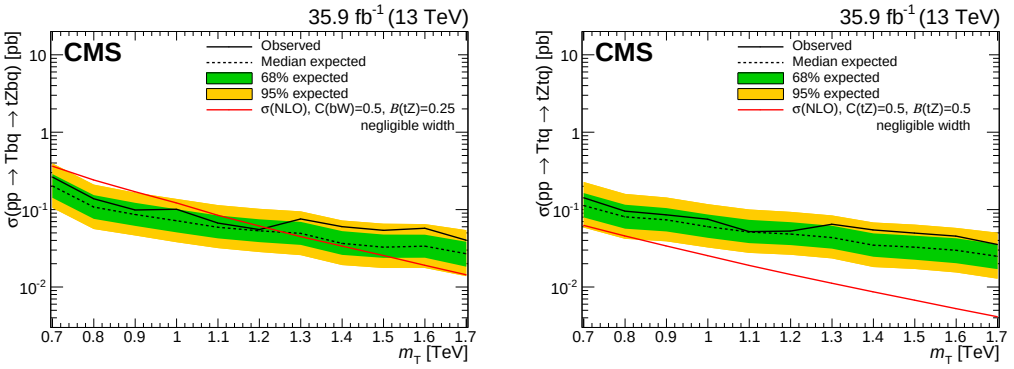

Figure 1.15: This figure and caption is from Ref. [4]. Observed and expected limits at 95% CL on the product of the single production cross section and branching fraction for the singlet LH T quark produced in association with a b quark (left) and for the doublet RH T quark produced in association with a t quark (right), where the T quark has a narrow width and decays to tZ. The inner green and outer yellow bands represent the 1 and 2 standard deviation uncertainties in the expected limit. The red lines indicate theoretical cross sections, as calculated at next-to-leading order in Ref. [4]. The branching fraction $\mathcal{B}(\mathrm{T}\rightarrow \mathrm{tZ})$ is 0.25 (0.5) for the left (right) plot.

right-handed T doublet associated with a t quark was set at around 0.82 TeV to 0.94 TeV. The analysis of the experimental results are compared to results in the case that large width effects are considered (referred to as finite width (FW) in this study), the range of which was from 10% to 30% of the VL-top mass. This comparison to LO theoretical cross sections was done using a modified version of a VLQ model made by the contributors of Refs. [137, 152, 153]. The theoretical reduced cross sections $\bar{\sigma}_{FW}$ for single production of a VL-T in association with a b or a t quark decaying into Zt are presented in Table 1.4, where the solid black line in Fig. 1.16 represents the theoretical cross sections. The contributions I made to this study are in the form of helping develop the formalism of the reduced cross section and by computing the cross sections which appear in Table 1.4.

The total production cross section for a T quark with a FW, σ_{FW}, is related to the reduced cross section $\bar{\sigma}_{FW}$ (the physical cross section after factorising the production cross section and the decay couplings) by the following equation.

$$\sigma_{FW}(C_1, C_2, M_T, \Gamma(C_1, C_2, C_i, M_T, m_j)) = C_1^2 C_2^2 \bar{\sigma}_{FW}(M_T, \Gamma(C_1, C_2, C_i, M_T, m_j)), \tag{1.63}$$

where $\Gamma(C_1, C_2, C_i, M_T, m_j)$ is the width of the VL-top quark, the VL-top is coupled to the SM quarks and bosons via C_1 and C_2 respectively. All possible couplings that allow the VL-top to decay into final state particles are incorporated into C_i and m_j is the mass term for the decay products of the VL-top, with M_T representing the mass of the VL-top.

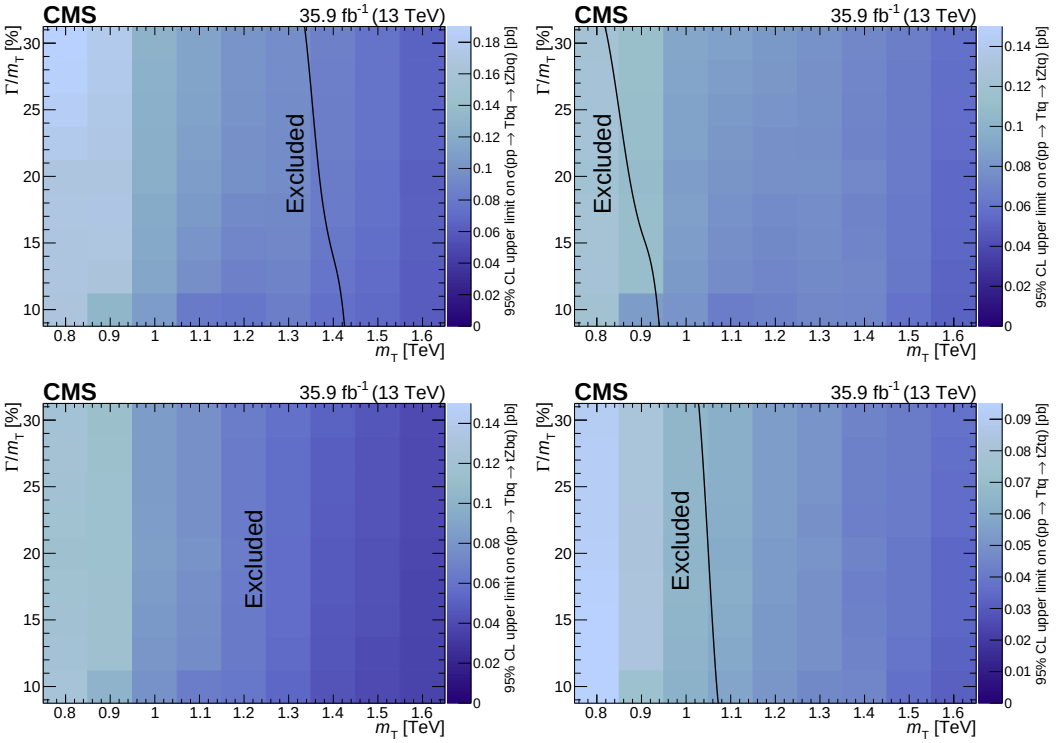

Figure 1.16: This figure and caption is from Ref. [4]. Observed (upper) and expected (lower) limits at 95% CL on the product of the single production cross section and branching fraction for the singlet LH T quark produced in association with a b quark (left) and for the doublet RH T quark produced in association with a t quark (right), where the T quark has a width from 10% to 30% of its mass and decays to tZ. The solid black lines indicate theoretical cross sections, as calculated at leading order using a modified version of the model constructed by the authors of Refs. [137, 152, 153] and reported in Table 1.4. In each plot, the excluded region lies to the left of the line, except in the lower-left plot where the entire region shown is excluded.

Table 1.4: Theoretical reduced cross sections $\bar{\sigma}_{FW}$ for single production of a T quark with a b or a t quark, where the T quark decays to tZ and its width is 10, 20, and 30% of its mass, for the benchmark masses considered in the analysis. The corresponding leading order cross sections σ are shown in parentheses.

Mass [TeV]	$\bar{\sigma}_{FW}(\sigma)$ for $pp \to Tbq \to tZbq$ [pb]			$\bar{\sigma}_{FW}(\sigma)$ for $pp \to Ttq \to tZtq$ [pb]		
	10%	20%	30%	10%	20%	30%
0.8	226 (0.675)	108 (0.650)	70 (0.631)	19 (0.144)	9.3 (0.144)	6.0 (0.135)
1.0	183 (0.314)	87 (0.299)	55 (0.284)	17 (0.075)	7.9 (0.072)	5.0 (0.069)
1.2	145 (0.158)	68 (0.149)	43 (0.141)	14 (0.042)	6.4 (0.039)	4.1 (0.037)
1.4	112 (0.084)	52 (0.079)	33 (0.074)	11 (0.024)	5.0 (0.022)	3.2 (0.021)
1.6	85 (0.047)	39 (0.043)	29 (0.041)	8.2 (0.014)	3.8 (0.013)	2.4 (0.012)

Chapter 2

Production of extra quarks at the Large Hadron Collider beyond the Narrow Width Approximation

2.1 Introduction

It has been mentioned previously that experimentalists wanting to be as model independent as possible, have performed experimental searches for VLQs that exploit an economical approach, assuming that only one new VLQ is present beyond the SM, considering QCD processes alone and parametrising the production and decay dynamics using the NWA. This chapter focuses on examining the use of the NWA and whether there are important large width effects that can describe important contributions that would otherwise be neglected.

It is well known that, in the case of the top quark, effects induced onto the inclusive cross-section by its finite width are of $\mathcal{O}(\Gamma_t/m_t)^2$, hence generally negligible, as $m_t \approx 173$ GeV and $\Gamma_t \approx 1.5$ GeV. A study of finite width effects in final states corresponding to top pair production has been performed in Ref.[154]. One would naively expect that similar effects in the case of VLQs would be of the same size, i.e., of $\mathcal{O}(\Gamma_{\rm VLQ}/M_{\rm VLQ})^2$. However, it should be noted that, as $M_{\rm VLQ}$ is unknown, also $\Gamma_{\rm VLQ}$ is, so that the aforementioned corrections may not be negligible, if $\Gamma_{\rm VLQ}/M_{\rm VLQ}$ is not very small. In fact, also differences between the case of the top quark and a VLQ due to the different structure of their couplings in the charged decay currents would play a role[1]. In this

[1]Notice that VLQs may also decay through flavour changing neutral currents, involving both the Higgs and Z bosons.

connection, one should recall that, in taking the NWA, as generally done in most Monte Carlo (MC) programs used in phenomenological and experimental analyses, one neglects off-diagonal spin effects which stem from the quark (top or vector-like) being massive and whose size is intimately related to the vector/axial (or left/right) composition of the fermionic state entering the charged decay currents and, of course, to the value of the ratio $\Gamma_{\rm VLQ}/M_{\rm VLQ}$. Furthermore, these very same two aspects also enter the interfering terms between the heavy quark (top or vector-like) signal (whichever way this is defined in terms of Feynman diagrams) and the background (which would then be represented by all the other graphs leading to the same final state). Needless to say, one should then not assume that what is valid for the treatment of off-shellness effects of the top quark (and consequent interferences) remains so for VLQs as well.

Very recently experimental searches for VLQs have started to explore the large width regime, considering single production of top and bottom VLQ partners [155, 156]. However, to our knowledge, no experimental limit has been set for topologies compatible with the pair production channels. It is the purpose of this paper to assess the regions of validity of the NWA for final states compatible with pair production and decay of a VLQ with charge 2/3 but where, due to its finite width, the VLQ is produced, via both QCD and EW interactions, in pairs or even singly. Interference effects of various nature will also be considered. We will do so under the assumption that all the decay products of the heavy quark are visible SM states. The plan of this chapter is as follows. In the next two sections we describe our conventions and the computational tools we adopted while in the following two we present our numerical results, first for the case of finite width corrections then for interference effects. Finally, we conclude in the last section.

2.2 Setup

2.2.1 Definitions

To understand the effects of large widths on the signal, we will consider different processes, all leading to the same four-particle final state:

- *QCD pair production and decay of on-shell VLQs*

  This process is usually considered in experimental searches of VLQs. In the NWA it is possible to separate and factorise production and decay of the heavy quarks, thus allowing for a model-independent analysis of the results. The cross-section for this process is given by (hereafter, in our formulae, Q denotes a VLQ):

$$\sigma_X \equiv \sigma_{2\to 2}\ {\rm BR}(Q)\ {\rm BR}(\bar{Q}) \tag{2.1}$$

  where, obviously, $\sigma_{2\to 2}$ only takes into account pure QCD topologies.

- *Full signal*

  In this process all the topologies which contain *at least one* VLQ propagator are taken into account. The only assumption is that the QCD and EW order of the processes are the same as in the processes above, for consistency. The full signal includes the pair production process without the on-shell condition described above. The cross-section of this process will be labelled as σ_S. Some example topologies for this process which are not included in the previous ones are in Fig. 2.1. The full signal contains topologies which are generally subleading in the NWA, but that become more and more relevant as the width of the VLQ increases.

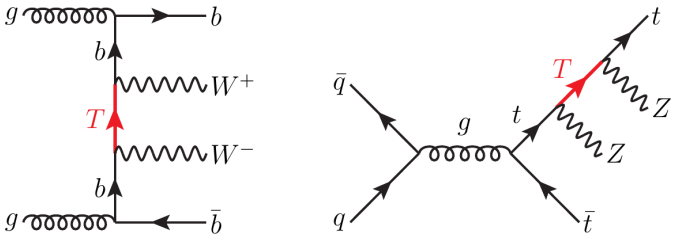

Figure 2.1: Examples of topologies containing only one VLQ propagator for the $PP \to W^+bW^-\bar{b}$ and $PP \to Zt\bar{Z}\bar{t}$ processes.

- *SM irreducible background*

  This process trivially corresponds to all the $2 \to 4$ topologies which do not involve any VLQ propagators. The cross-section will be labelled as σ_B.

- *Total process*

  This process includes the full signal, the SM background and the interference terms. The cross-section will be labelled as σ_T and is related to the previous cross-sections by the following relation:

$$\sigma_T = \sigma_S + \sigma_B + \sigma_{\text{interference}} \tag{2.2}$$

In order to determine the effect of large widths on the cross-section, we will consider a number of variables:

- $\frac{\sigma_S - \sigma_X}{\sigma_X}$: this ratio takes into account both the off-shell and the subleading contributions given by topologies which contain at least one VLQ propagator. It measures in practice how much the full signal differs from the approximate pair-production-plus-decay signal in the NWA.

- $\frac{\sigma_T - (\sigma_X + \sigma_B)}{\sigma_X + \sigma_B}$: this ratio measures the correction factor to apply to obtain the full cross-section starting with the pair-production in the NWA and the SM background considered independently.

- $\frac{\sigma_T-(\sigma_S+\sigma_B)}{\sigma_S+\sigma_B}$: this ratio measures the size of the interference effects between signal and SM background.

2.2.2 Tools and validation

Our numerical results at partonic level have been obtained using MadGraph 5 [157, 158] with the public VLQ model [159] implemented in FeynRules [160]. We have produced events in the five-flavour scheme (5FS), using the cteq6l1 [161] PDF set. Hadronisation and parton showering have been obtained through the Pythia 8 code [162]. To obtain the width-dependent bounds on the VLQ mass we have considered a combination of searches at 8 TeV and an ATLAS search [163] at 13 TeV. All the searches we considered are present in the database of the code CheckMATE 2 [164], which exploits the Delphes 3 framework [165]. We stress here that the purpose of our recasting is not to obtain bounds for large width VLQs but to study the performance of sets of cuts currently adopted in searches for pair production of VLQs or optimised for different final states. Determining an optimised set of selection and kinematics cuts to enhance the sensitivity to the kinematics of a T with large width (and therefore determine a reliable bound in the mass-width plane) will be the scope of a future dedicated study.

Furthermore, to fully validate our analysis of the NWA results versus the off-shell ones, we developed a separate code where the Dirac function is obtained as the appropriate limit of the Breit-Wigner distribution, we have also prepared a dedicated $2 \to 6$ program (hence also including the fermionic decays of the bosons stemming from the two T decays, which are SM-like), wherein we have adopted a suitable mapping of the integrand function, via the standard change of variable

$$p^2 - M^2 = M\Gamma \tan\theta, \tag{2.3}$$

where p^2 is the (squared) moment flowing through a resonance with mass M and width Γ. This factorises the Jacobian

$$dp^2 = \frac{1}{M\Gamma}[(p^2 - M^2)^2 + M^2\Gamma^2]d\theta, \tag{2.4}$$

which thus incorporates the resonant behaviour in the sampling of the phase space itself, thereby rendering the multi-dimensional numerical integration (done via importance sampling) very efficient. Finally, upon multiplying the integrand function by $\Gamma/\Gamma_{\rm tot}$, where $\Gamma_{\rm tot}$ is the decaying particle's intrinsic total width, and taking the limit $\Gamma \to 0$, we obtain self-consistently the above transition from the off-shell to the NWA results. The results obtained this way closely match those obtained through MadGraph 5 for the aforementioned $2 \to 2$ (on-shell, times BR) and $2 \to 4$ (off-shell) processes.

As the SM top quark, t, and the heavy quark with same Electro-Magnetic (EM) charge, T, have a common decay channel, i.e., bW^+, as a preliminary exercise meant to address the impact of a potentially very different chiral structures in the transitions $t \to bW^+$ and $T \to bW^+$, we have defined the following quantity

$$R(X) = \frac{\sigma(pp \to X \to bW^+\bar{b}W^- \to 6 \text{ fermions})_{\text{FW}}}{\sigma(pp \to X \to bW^+\bar{b}W^- \to 6 \text{ fermions})_{\text{NWA}}}, \tag{2.5}$$

which measures inclusively the effect of a Finite Width (FW) for the cases $X = t$ (a heavy quark with pure $V - A$ couplings, i.e., top-like) and $X =$ Right (heavy quark with pure $V + A$ couplings). Clearly, these are extreme coupling choices, as an interaction eigenstate of a VLQ would have an admixture of $V - A$ and $V + A$ couplings. However, it should be recalled that VLQ couplings have always a dominant chirality: this has been demonstrated in Refs.[166, 137]. In Fig. 2.2 we plot the ratio $R(\text{Right})/R(t)$ mapped as a function of the heavy quark mass M_{VLQ} and relative width $x = \Gamma_{\text{VLQ}}/M_{\text{VLQ}}$ over the ranges [1000 GeV, 2500 GeV] (i.e., up to the typical mass reach of the LHC for pair production) and [0, 0.5] (i.e., up to the width limit beyond which the VLQ can no longer be considered a resonance), respectively. One can see that differences are phenomenologically irrelevant.

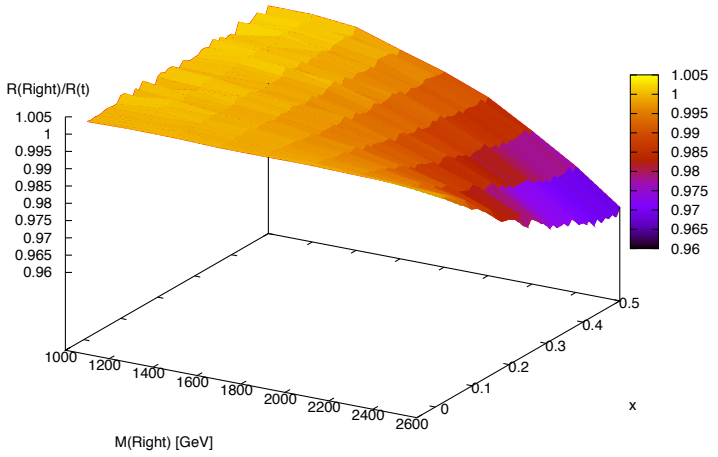

Figure 2.2: Ratio of FW corrections with respect to the NWA relative to the $V - A$ case of a $V + A$ charged decay current.

2.3 Benchmarks and constraints

In the present analysis we will consider the processes of production of a heavy top-like quark T. In principle, from a model-independent point of view, the T quark is allowed to interact with all SM quark generations, but to evaluate the effects of large widths in

different scenarios, only specific interactions will be switched on in the different examples we will consider.

Since the purpose of this analysis is to evaluate the effects of large widths on channels commonly explored by experimental analysis, we will consider only final states allowed by T pair production and decay. The full set of channels in which a pair-produced T quark can decay is given by the following matrix:

$$T\bar{T} \rightarrow \left(\begin{array}{ccc|ccc|ccc} WdW\bar{d} & WdZ\bar{u} & WdH\bar{u} & WdW\bar{s} & WdZ\bar{c} & WdH\bar{c} & WdW\bar{b} & WdZ\bar{t} & WdH\bar{t} \\ ZuW\bar{d} & ZuZ\bar{u} & ZuH\bar{u} & ZuW\bar{s} & ZuZ\bar{c} & WdH\bar{c} & ZuW\bar{b} & ZuZ\bar{t} & ZuH\bar{t} \\ HuW\bar{d} & HuZ\bar{u} & HuH\bar{u} & HuW\bar{s} & HuZ\bar{c} & WdH\bar{c} & HuW\bar{b} & HuZ\bar{t} & HuH\bar{t} \\ \hline WsW\bar{d} & WsZ\bar{u} & WsH\bar{u} & WsW\bar{s} & WsZ\bar{c} & WdH\bar{c} & WsW\bar{b} & WsZ\bar{t} & WsH\bar{t} \\ ZcW\bar{d} & ZcZ\bar{u} & ZcH\bar{u} & ZcW\bar{s} & ZcZ\bar{c} & WdH\bar{c} & ZcW\bar{b} & ZcZ\bar{t} & ZcH\bar{t} \\ HcW\bar{d} & HcZ\bar{u} & HcH\bar{u} & HcW\bar{s} & HcZ\bar{c} & WdH\bar{c} & HcW\bar{b} & HcZ\bar{t} & HcH\bar{t} \\ \hline WbW\bar{d} & WbZ\bar{u} & WbH\bar{u} & WbW\bar{s} & WbZ\bar{c} & WdH\bar{c} & WbW\bar{b} & WbZ\bar{t} & WbH\bar{t} \\ ZtW\bar{d} & ZtZ\bar{u} & ZtH\bar{u} & ZtW\bar{s} & ZtZ\bar{c} & WdH\bar{c} & ZtW\bar{b} & ZtZ\bar{t} & ZtH\bar{t} \\ HtW\bar{d} & HtZ\bar{u} & HtH\bar{u} & HtW\bar{s} & HtZ\bar{c} & WdH\bar{c} & HtW\bar{b} & HtZ\bar{t} & HtH\bar{t} \end{array}\right) \quad (2.6)$$

We will focus on two blocks of this matrix, the top-left (corresponding to a T interacting with the first SM generation) and the bottom-right (T interacting with the third SM generation). As we are interested in the width dependence of ratios of cross-sections and of mass bounds, we expect that the scenario of mixing with the second generation will not give sizeably different results with respect to the mixing with first generation, so we will not consider it in this analysis. Performing the analysis by selecting specific final states doesn't mean that we are assuming that the T quark only interacts with first or third generation. Effects of large width are different depending on the kinematics of the process and by selecting representative scenarios it is possible to reconstruct intermediate configurations (VLQs interacting partly with heavy and partly with light SM generations).

This analysis is of phenomenological interest only for mass values for which the number of final events is (ideally) larger than 1. In Fig. 2.3 we show the number of events for different LHC luminosities for the X channel, which is common to all scenarios. The number of events in Fig. 2.3 has been computed considering a NNLO cross-section, however the results in the next sections will correspond to LO cross-sections, as we are assuming that for processes of pair production the kinematics won't change appreciably and all the differences can be factorised through a K-factor. From Fig. 2.3 it is possible to see that the ideal practical validity of our results is limited to mass values of around 1500 GeV for LHC@8TeV, 2500 GeV (2700 GeV) for LHC@13TeV with 100/fb (300/fb) integrated luminosity. Of course we are not considering here effects due to experimental acceptances and efficiencies.

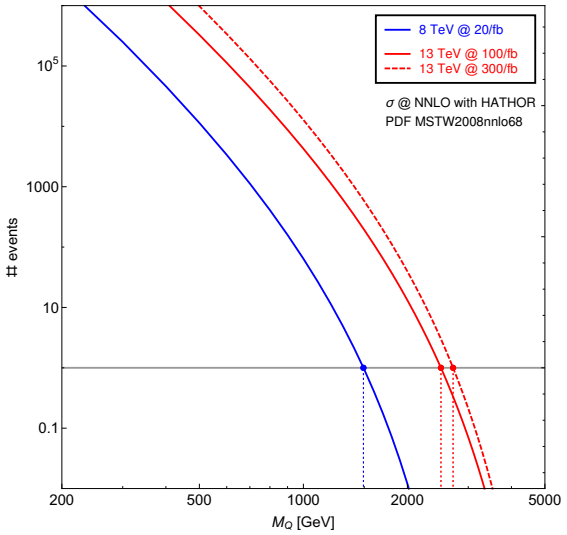

Figure 2.3: Number of events at partonic level for $Q\bar{Q}$ pair production and for different LHC energies and luminosities. The corresponding cross-sections have been computed using HATHOR[167] with MSTW2008nnlo68 PDFs[168].

2.3.1 How large can the width be?

In a simplified model where the SM is only augmented by the presence of a VLQ representation containing a T quark the couplings of the VLQ are constrained by different observables [132]. In contrast, a T VLQ with a large width in such a scenario can only be obtained if its couplings are large. It is therefore important to determine how large the width can be in simplified scenarios if constraints on the T couplings are saturated to the current bounds. Such bounds depend on the specific representation the T state belongs to.

We will consider here as representative scenarios a T singlet and a T as part of a doublet (both $(X,\ T)$ and $(T,\ B)$). In both cases the Branching Ratios (BRs) depend on both mass and width, but for the singlet the couplings are dominantly left-handed, while for the doublet the couplings are dominantly right-handed.

In Fig. 2.4 we show the contours with constant Γ/M ratio for different values of the T mass and mixing angle with the SM top quark, to which we have superimposed the excluded regions from EWPTs and $Zb\bar{b}$ constraints, borrowed from Ref.[169]. These constraints arising from the study performed by [169] was done with a global fit of the parameters of simple VLQ models in minimal representations of $SU(2)L$ to precision data and Higgs rates. The results of this analysis was presented in an EFT framework and show the large degree to which the VLQ model parameters are constrained, largely due to tree-level effects on the $Zb\bar{b}$ coupling in the T singlet case.

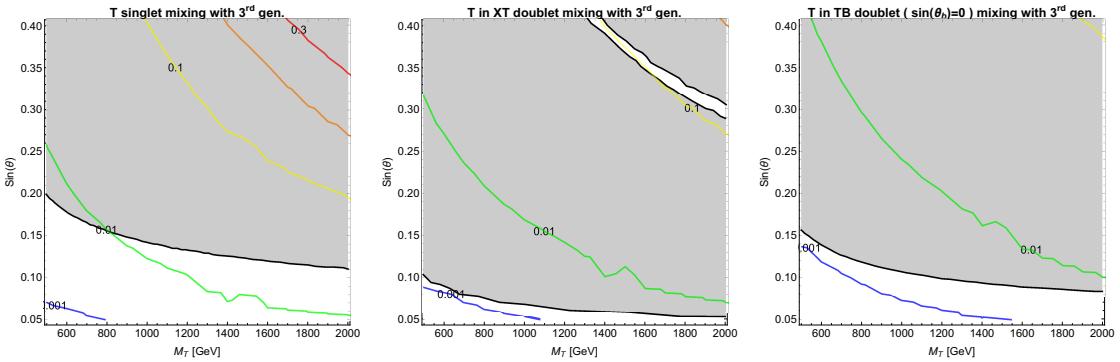

Figure 2.4: Contours with constant Γ/M ratio as function of T mass and mixing angle for T belonging to different representations and with different mixing hypotheses. The excluded (shaded) regions from [169] have been superimposed.

The situation mentioned in the previous paragraph which has strong constraints are for simplified models where the SM is extended with one VLQ representation containing a T with large mixing. In this case the T width cannot become larger than few % of the mass (at best). The scenarios are even more constrained for T quarks mixing with light generations, for which the bounds are tighter [135, 132].

However these constraints are relaxed or all together disappear if there exists the presence of further (yet undiscovered) new states lighter than the T VLQ, which results in a larger number of decay channels into further BSM particles, and/or because of mixing with other VLQs, which will largely effect the constraints previously mentioned from flavour or precision observables because of cancellations of effects. Further details when considering more complex models can be found in [170, 171, 98]

For the purposes of this analysis as a model-independent approach it is then important that the *total width* of the T will be treated as a free parameter, limited to be less than the extreme value of 50% of the mass of the VLQ. In practice, we will consider values up to 40% of the T mass for our numerical evaluations.

2.4 Extra T quark mixing with third generation SM quarks

2.4.1 Large width effects on the signal at parton level

The effect of a large width in the cross-section due to off-shell contributions and to topologies which are absent in the NWA limit is shown in Fig. 2.5. At parton level we will only show results at 13 TeV. We verified that the results at 8 TeV are qualitatively similar.

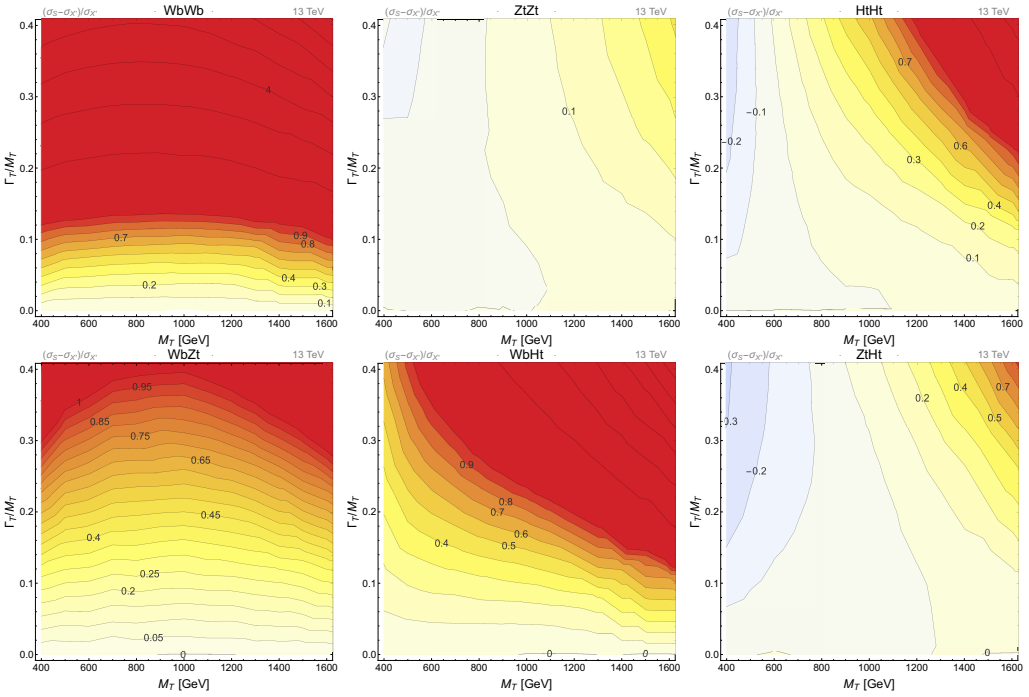

Figure 2.5: Relative difference between the full signal cross-section and the cross-section of QCD pair production for T mixing with the SM top quark.

As a first sanity check of our calculations we observe that, as expected, in the NWA limit the off-shell contributions are negligible. The contributions of off-shellness and new topologies become more and more relevant as the width of the T increases and the cross-section may eventually become several factors larger than in the NWA for some final states. The large increase of the cross-section even for small T masses for channels with the bottom in the final state is explained by the presence of diagrams where the b-jets are radiated directly from the initial state or generated by gluon splittings: such topologies are enhanced by collinear divergences. We will not explore this aspect further, as the isolation and kinematics cuts applied at analysis level usually remove such enhanced contributions, independently of the T mass and width as we will show in Sec. 2.4.3.

For some channels it is possible to notice a cancellation of effects which makes the QCD pair production cross-section similar to the cross-section including off-shell contributions even for large values of the width. The cancellations appear at different values of the T mass, depending on the channel and for processes involving the bottom quark in the final state they are partially masked by the large increase of the cross-section due to the collinear divergences caused by topologies where the bottom quarks arise from gluon splitting, as the one shown in Fig. 3.1. Such cancellations are due to the different scaling of phase space between the large and narrow width regimes. Indeed, if the T VLQ has a large width, the transferred momentum of the process can have values in a larger range than in the NWA case, where it is constrained by the resonant production of the T pair: this means in turn that the PDFs are sampled at different scales and therefore the cross-section receives a non-trivial mass- and width-dependent contribution which

results in the observed behaviour. Of course, this does not necessarily mean that the NWA approximation can be used along the cancellation regions. Sample kinematical distributions of the decay products of the T in different width regimes are shown in Fig. 2.6 for the $HtHt$ channel and $M_T = 600$ GeV and in Fig. 2.7 for the $ZtZt$ channel and $M_T = 800$ GeV. In both cases, while the η distribution does not change significantly as the width increases, the p_T distributions exhibits a visible shift towards the softer region.

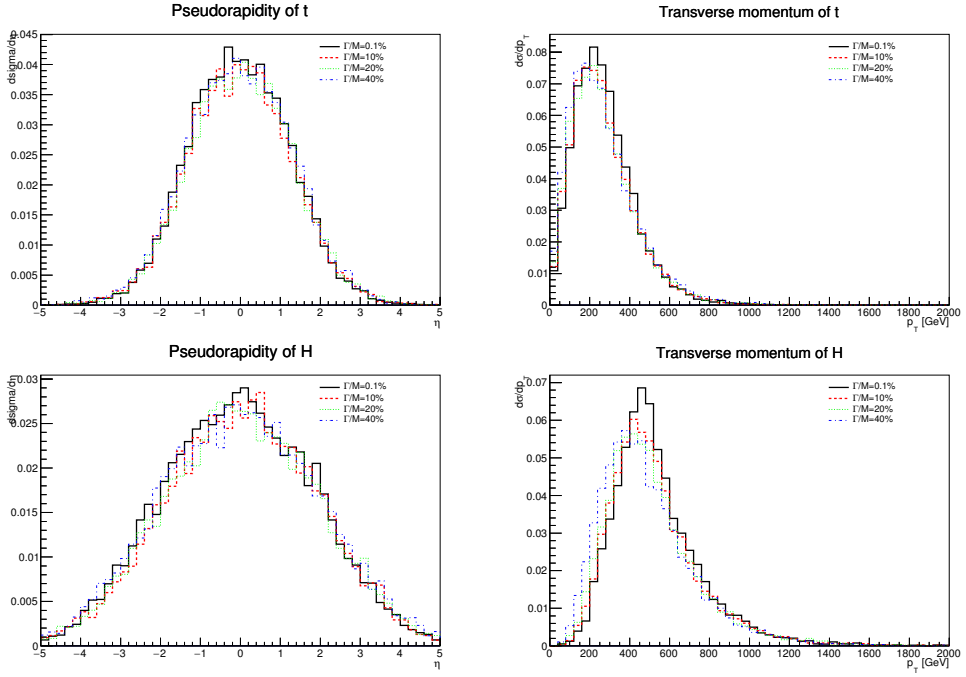

Figure 2.6: Partonic level differential cross-sections for the $HtHt$ channel. From left to right and top to bottom: η_t, p_{Tt}, η_H and p_{TH}. All distributions correspond to a T mass of 600 GeV, for which $\sigma_S \sim \sigma_X$ almost independently of the T width.

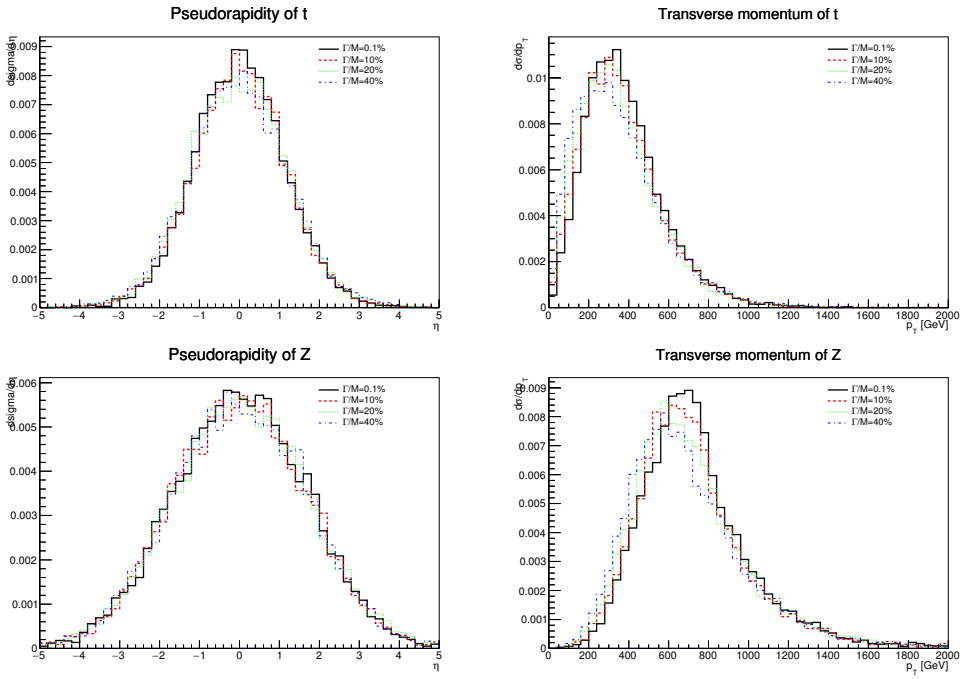

Figure 2.7: Partonic level differential cross-sections for the $ZtZt$ channel. From left to right and top to bottom: η_t, p_{Tt}, η_Z and p_{TZ}. All distributions correspond to a T mass of 800 GeV, for which $\sigma_S \sim \sigma_X$ almost independently of the T width.

2.4.2 Interference with SM background

When considering processes of pair production of heavy quarks in the NWA, interferences with the SM background are zero by construction, but if the width of the heavy quark is large, it is crucial to explore the relevance of interference terms in the determination of the total number of events. Moreover, understanding this contribution for regions which are not usually explored in experimental analyses may be useful in the determination of sets of kinematical cuts for the optimisation of future searches, if any hint of a VLQ with large width appears in the data.

The correction factor between the total cross-section and the sum of NWA pair production and SM background cross-section is plotted in Fig. 2.8. Such correction factors depend on the relative weight of the SM background contribution in the determination of the total cross-section: they are almost negligible in the whole parameter space where the background is the dominant contribution to the total signal, while they are become larger where the new physics signal has a more relevant role. This can easily be understood by considering what affects the various terms of the ratio. Herein, σ_B is a constant term (for fixed final state), σ_X only depends on the T mass and σ_T is the only term which depends on the both the T mass and width. For the $WbWb$ case, however, σ_T is almost entirely dominated by the SM background contribution (mostly by the top pair production process) and therefore the contribution of the T is just a small correction,

which does not produce relevant effects in the whole range of masses and widths we have explored. For the $ZtZt$ and $HtHt$ scenarios, on the contrary, the SM background is comparable or negligible with respect to the signal contribution, and therefore the dependence on the T mass and width is much more evident.

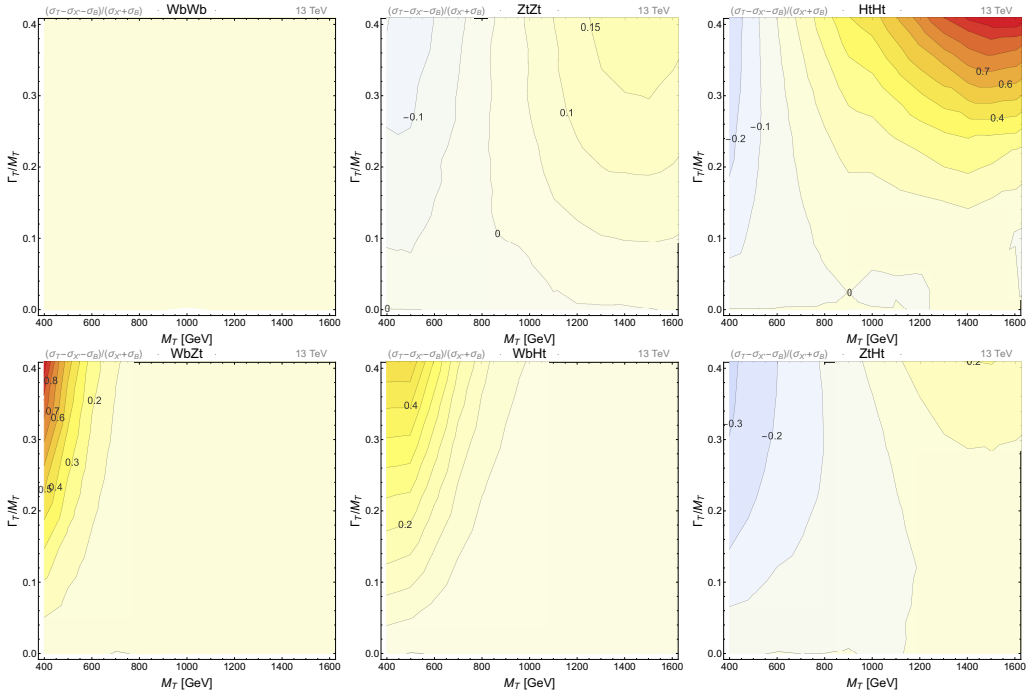

Figure 2.8: Relative difference in cross-section between the total $2 \to 4$ process, including the SM background and the sum of QCD pair production and SM backgrounds. Top row: final states on the diagonal of the matrix in Eq. 2.6 (third generation mixing); bottom row: off-diagonal final states (third generation mixing).

The full contribution of interference terms, considering the full signal instead of the signal in the NWA, is always numerically negligible. In Fig. 2.9 we have shown the only channel for which the contribution can become larger than 10% in absolute value. The inclusion of single-resonance effects, therefore, changes the picture in a substantial way, showing that interference effects between the full signal and the SM background are always negligible, except for the $HtHt$ channel in the large width and large M_T region. This has to be expected because the kinematical properties of signal and background are usually different. However, this can only be seen by taking into account the full signal contribution. This means that, if searches for VLQs with large width are designed, considering the full signal instead of rescaling the NWA results would almost in any case automatically kill any contribution from interference with the SM background, especially for scenarios where the SM background is large.

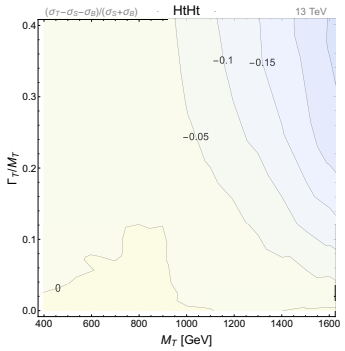

Figure 2.9: Relative contribution of the interference between the full signal and the SM background. $HtHt$ is the only channel for which this contribution can reach values above 10% in size.

2.4.3 Results at detector level

In this section we will study the performance of 8 TeV and 13 TeV searches from both ATLAS and CMS in determining the excluded region in the $\{M_T, \Gamma_T/M_T\}$ plane. We will consider only final states in the diagonal of the matrix of Eq. 2.6 because non-diagonal final states would not represent, by themselves, physically valid scenarios. Such final states arise only if the VLQ has non-zero BRs in different channels, and a consistent treatment would require the combination of diagonal and off-diagonal final states together. As stated above, the purpose of this study is not to set limits, but to study the performance of experimental searches in regions yet unexplored for these scenarios. Indeed, the set of searches we consider are not necessarily optimised for the discovery of VLQs at the LHC, therefore our recast bounds are not likely to be competitive with current bounds for pair production of VLQs in the NWA, and, in this respect, we will not compare our results with other bounds from direct searches for pair production of VLQs.

We show in Fig. 2.10 the exclusion lines for combinations of 8 TeV searches from both ATLAS and CMS for the three diagonal final states compatible with pair production and decay of T VLQs. Our results show that none of the signal regions in the considered searches is sensitive to the large width scenarios: the exclusion bound are, for all final states, analogous to the NWA limit.

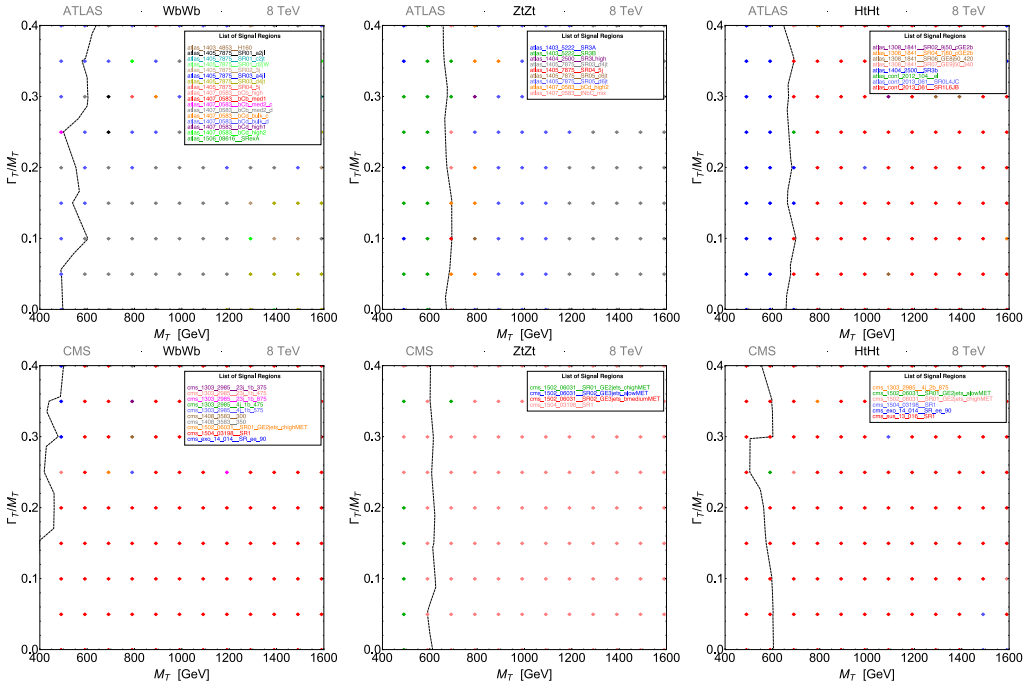

Figure 2.10: Recast bounds in the $(M_T, \Gamma_T/M_T)$ plane with a set of ATLAS (top row) and CMS (bottom row) searches at 8 TeV for diagonal final states.

This can be understood by considering the cross-section of the full signal, σ_S, and the dependence on the T width of the efficiencies of the Signal Regions (SRs) which is most marked near the bounds. In Fig. 2.11 we superimpose the bound from the combination of ATLAS searches at 8 TeV with the cross-section of the full signal for the $WbWb$ channel (the others are qualitatively similar): the dependence on the width of the cross-section is weak in the region where the searches fix the exclusion limit, and becomes slightly stronger for higher (allowed) masses. Moreover, the variation of the kinematics of the final states is not large enough to increase the sensitivity of the search cuts, as can be seen by looking at the efficiency of the the SR bCd_bulk_d of the ATLAS search [172], which depends rather weakly on the width of the T.

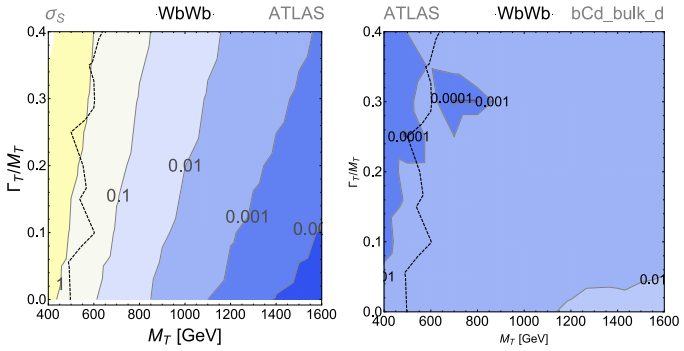

Figure 2.11: Cross-section and efficiency of the best ATLAS SR (bCd_bulk_d of [172]) for the $WbWb$ channel, compared with the bound.

Our results at 13 TeV have been obtained considering a dedicated search for pair production of a T VLQ [163] implemented in CheckMATE. The results exhibit a similar behaviour as the set of 8 TeV ones. Our bounds are rather different from those reported in Ref. [163]. However, we did not rescale the bounds considering different BRs, as we have not factorised the production from decay, and we are mostly interested in the dependence on the width of such bounds. In this respect, the bounds weakly depend on the T width, as can be seen in Fig. 2.12. As for the 8 TeV case, the slight increase in cross-section, and relative deformation of kinematics distribution of the final state objects is compensated by an increase of the efficiencies of the SRs cuts. This information can be exploited for the design of future dedicated searches if the discovery of VLQs with large width are among the goals of the studies.

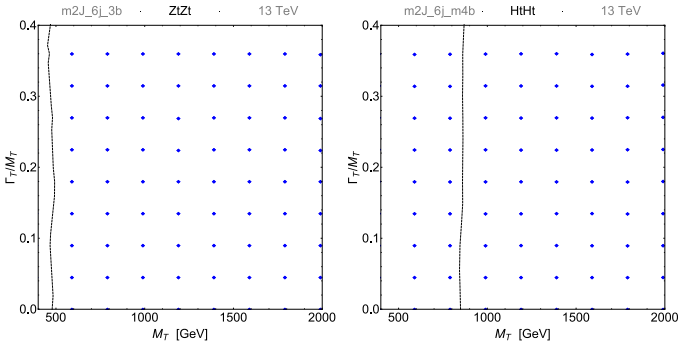

Figure 2.12: Same as Fig. 2.10 for the ATLAS search at 13 TeV [163] implemented in CheckMATE. The plot for the $WbWb$ channel is not shown because within the explored range the recasting does not set any limit.

2.5 Extra T quark mixing with first generation SM quarks

2.5.1 Large width effects on the signal at parton level

If the T interacts with first generation SM quarks, topologies where gluons splitting into light quarks increase the cross-section due to collinear enhancements are present also for neutral currents, as shown in Fig. 2.13. In the case of mixing with third generation, such topologies were not present for neutral currents due to the large top mass.

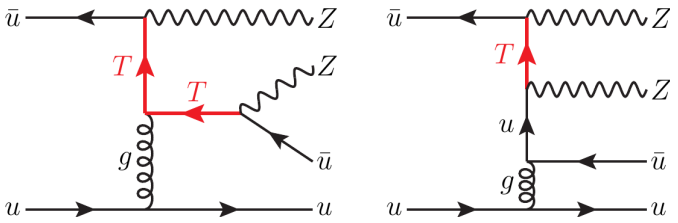

Figure 2.13: Examples of neutral-current topologies for heavy quarks with large width mixing with first generation.

The relative increase of the cross-section with respect to the NWA regime is shown in Fig. 2.14 for an energy of 13 TeV (we have checked that the results at 8 TeV are analogous), where it is possible to notice the large enhancement due to topologies with collinear divergences for all final states.

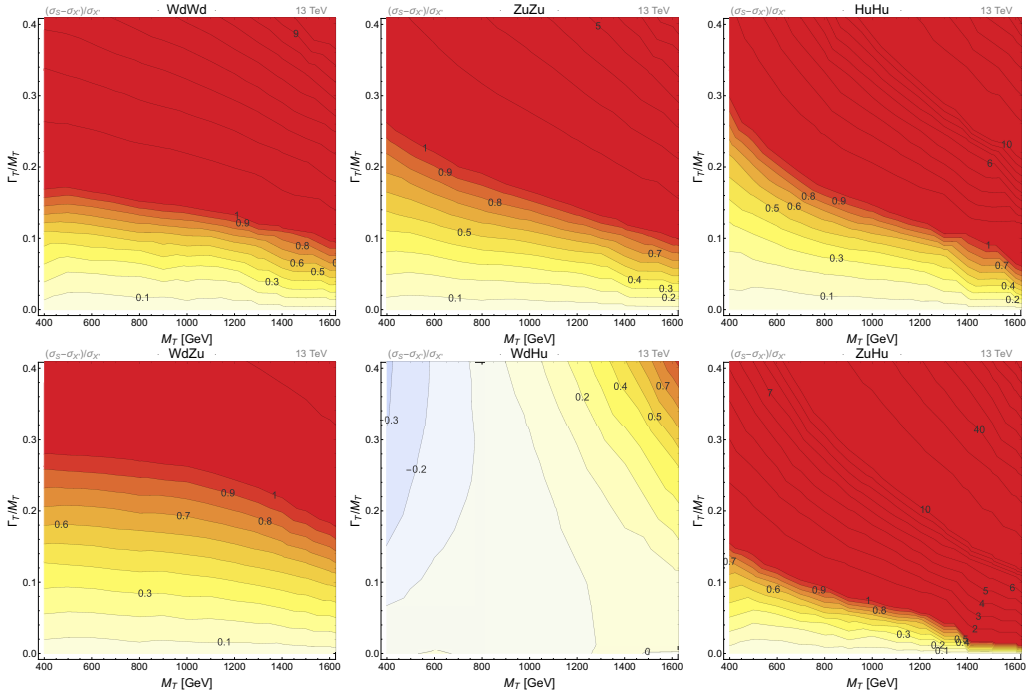

Figure 2.14: Same as Fig. 2.5 for T mixing with first generation.

2.5.2 Interference with SM background

The correction factors to multiply to the sum of NWA cross-section and SM background to obtain the interference term are plotted in Fig. 2.15. For all channels the correction factor becomes quickly large as the T width increases, even if in different fashions depending on the channel. The relative differences between signal and background are small in this case, such that σ_T receives a large contribution from the signal. However, when taking into account the full signal, including the large width effects, the interference effects with the SM background become small or negligible in the whole parameter space. As in the case of mixing with third generation, these results show that searches for the exploration of scenarios where the VLQs mix with light generations and have a large width would be significantly more accurate by considering the full signal instead than reinterpreting the NWA results.

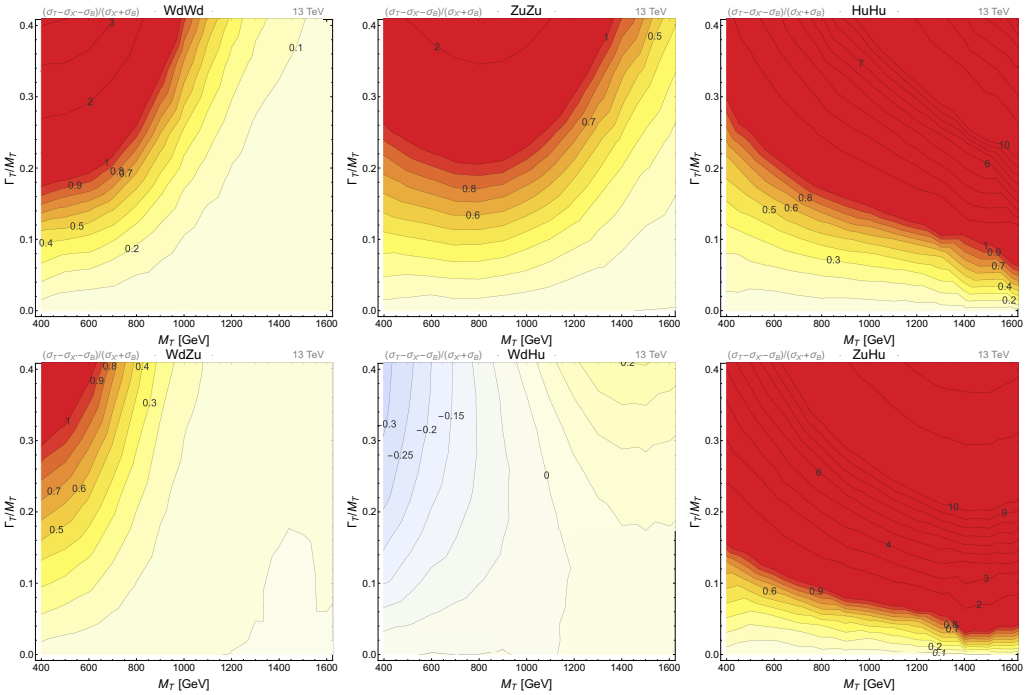

Figure 2.15: Same as Fig. 2.8 for T mixing with first generation.

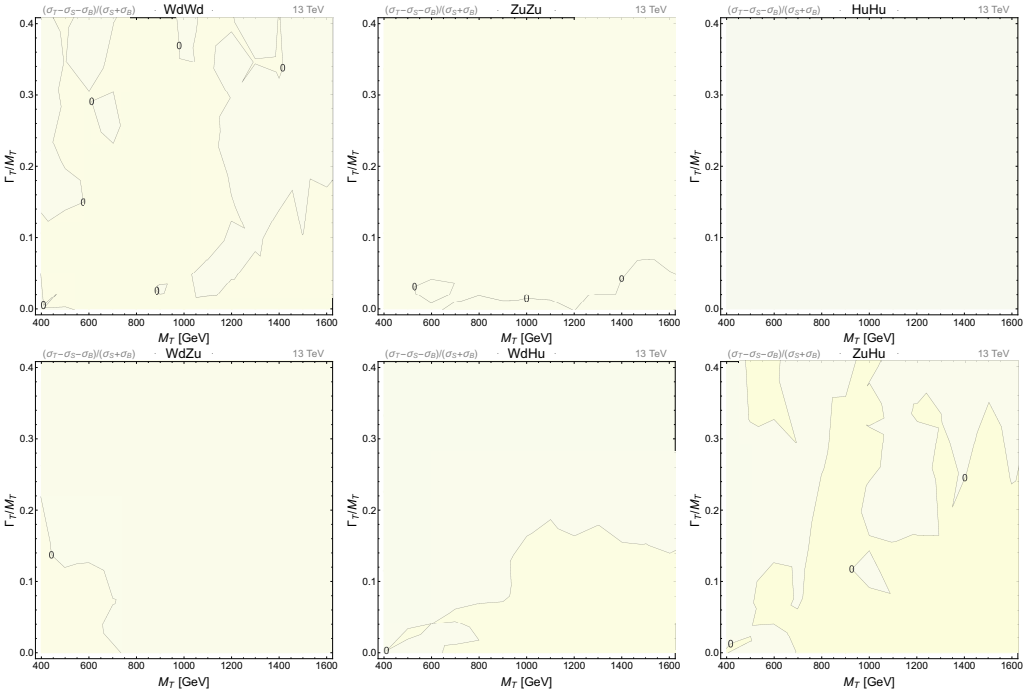

Figure 2.16: Same as Fig. 2.9 for T mixing with first generation.

2.5.3 Results at detector level

Our recast results, obtained considering the same set of ATLAS and CMS searches at 8 TeV as in the case of mixing with third generation, are shown in Fig. 2.17. The

dependence of the bound on the T width is stronger than in the case of mixing with third generation. For all channels the bound on the T mass becomes stronger as the T width increases. This behaviour has again to be put in relation with the dependence of the signal cross-section, σ_S, on the T mass and width, shown in the example of Fig. 2.18 for the bound on the $ZuZu$ channel from ATLAS searches. It is possible to see that the bound roughly tracks the cross-section, which unlike in the case of third generation mixing is much more dependent on the width of the T, and that the width dependence of the efficiency on the other hand is weakly increasing with both width and mass of T along the bound.

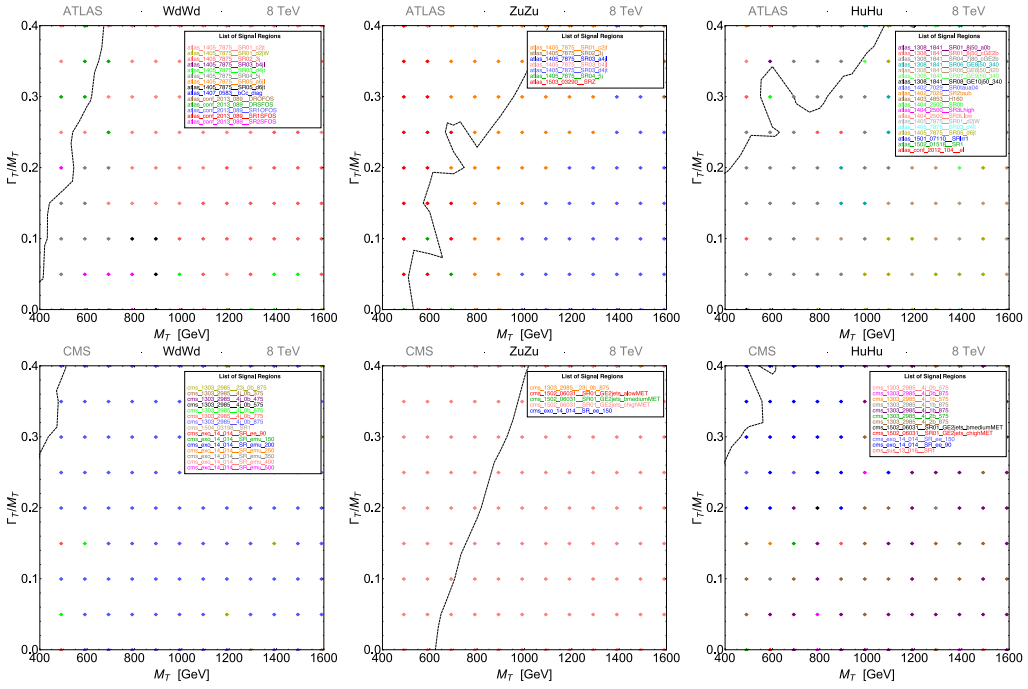

Figure 2.17: Same as Fig. 2.10 for T mixing with first generation.

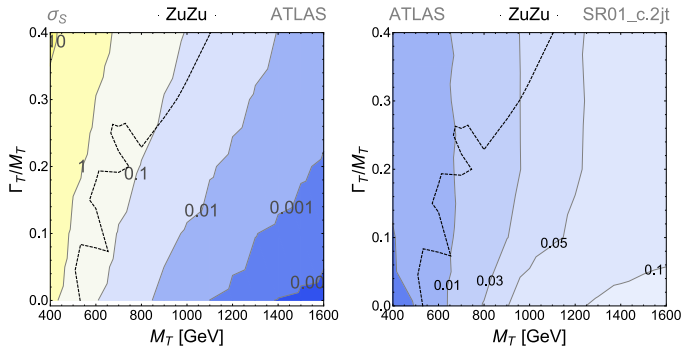

Figure 2.18: Cross-section and efficiency of the best ATLAS SR (SR01_c.2jt of [173]) for the $ZuZu$ channel, compared with the bound.

2.6 Conclusions

We have performed an analysis of off-shell and interference contributions to the process of pair production of heavy quarks at the LHC in the context of minimal scenarios where the SM is extended by adding only a new quark state. As, according to current experimental limits, the latter cannot have the $V-A$ structure of the top quark (unless the Higgs sector is extended, which is not the case in our analysis), we have first assessed how off-shellness impacts on the heavy quark decay signature common to the one of top quark pairs, i.e., $W^-\bar{b}W^+b$, showing that a $V+A$ chiral structure would be similarly affected over the LHC kinematical regime for pair production of heavy quarks which can be profiled through a resonance. In this case then, the implementation of finite width effects for heavy quarks can be subsumed under the well established procedures already put in place for the top quark, by simply rescaling the mass of the fermion. Many more decays are however possible for a generic heavy quark pair. Of all the latter, as representative examples, we have chosen to focus on the production and decay of a heavy vector-like top partner T in the singlet representation and considered two scenarios in which it mixes with either the first or third generation of SM quarks.

The results of our analysis quantify the relevance of the large width regime in the determination of the cross-section and the importance of interference effects between signal and SM background. Clearly, the differences in the cross-section are ultimately reflected in different kinematical distributions, which result in different experimental efficiencies for specific sets of kinematical cuts on the final state. The effect of interference is also found to be generally relevant if the NWA approximation is adopted, while its role is almost negligible if the full signal is considered. Finally, we have evaluated the performance of a set of ATLAS and CMS searches at both 8 and 13 TeV in the determination of the excluded region in the $(M_T, \Gamma_T/M_T)$ plane. We found that the signal regions which are most relevant for the determination of the constraints are weakly sensitive to the T width if the T mixes with the SM top quark, while they can pose higher mass bounds (with respect to the NWA limits) if the T mixes with the up quark.

To summarise, the conclusion of our analysis is that it is not possible to trivially rescale the mass bounds for VLQs decaying to SM states obtained considering processes of pair production and decay in the NWA to determine constraints for VLQ with large widths. Further, given the weak dependence on the T width of a large set of signal regions of 8 TeV analyses from both ATLAS and CMS, and also of signal regions from a dedicated ATLAS analysis [163] at 13 TeV looking at pair production of T VLQs, we think that designing different signal regions in experimental analyses to explore the large width regime by taking into account the full kinematical properties of the signal is advisable for a more comprehensive search of heavy quarks at the LHC. A prerequisite to this is to dismiss at MC generation level both the NWA (which leads to severe mis-estimates) and a naive generalisation to a FW approach using the same topologies as in the NWA

(which is potentially strongly gauge dependent) in favour of a full determination of every contribution (off-shellness and new topologies) to the signal.

Chapter 3

Production of extra quarks decaying to Dark Matter beyond the Narrow Width Approximation at the LHC

3.1 Introduction

In this chapter of the thesis the study performed in paper [2] is presented, where the main focus of this research was to examine large width effects (as was done in the previous chapter) in the scenario of an eXtra Quark (XQ) decaying to DM instead of SM particles. The XQ can be either vector-like (in VLQ scenarios) or chiral (in the ChQ scenarios) as the relevant phenomenology is not largely effected (where ChQs have only been excluded by Higgs data, so can still interact only with DM).

We will focus on a simplified scenario where a top-like XQ (T) interacts with SM quarks and DM candidates and its width is large relatively to its mass (up to 40% of it). We will consider final states compatible with processes of pair production of the T and subsequent decay into a bosonic DM candidate and a SM quark. Then, we will evaluate the effects of large width in the determination of the cross section and in the reinterpretation of bounds from experimental searches. We will distinguish scenarios with a scalar DM from scenarios with a vector DM and we will analyse in detail scenarios where the T state interacts either with the SM up or top quark, such that the final states we will consider are either $2j + E_T^{\text{miss}}$ or $t\bar{t} + E_T^{\text{miss}}$, respectively. For scenarios where T interacts with the charm quark, leading to a final state analogous to the case of the up-quark in terms of reconstructed objects if charm-tagging is not considered, only the main results will be provided. It is important to notice that, unlike in the case of scenarios where the XQs

decay only into SM states [1], interference terms with the SM background are absent if the XQs decay to DM candidates, as the only (irreducible) source of E_T^{miss} in the SM is given by final states containing neutrinos.

The structure of this chapter is as follows: in Section 3.2 we describe the simplified scenarios we consider, providing the relevant Lagrangian terms and relations between couplings, define our naming conventions and identify the final states of interest; in Section 3.3 we describe our setup for the numerical computation and we list the experimental searches we consider in our analysis; in Sections 3.4 and 3.5 we analyse in detail scenarios where the T quarks interacts with third generation and first generation SM quarks, respectively; in Section 3.6 we present the 95% CL exclusion limits in the M_T-M_{DM} plane, including the case of interaction with the charm quark; finally, in Section 3.7 we state our conclusions.

3.2 Model and conventions

3.2.1 Lagrangian terms

We concentrate here, for illustrative purposes, on a minimal extension of the SM with just one XQ state and one DM state[1]. Our notation follows the same conventions of Ref.[176], to which we refer for the most general Lagrangian terms involving different representations of XQs. In the present analysis we limit our investigation to a top-partner XQ and a DM real scalar or real vector singlet: therefore we label the XQ as T if it is a singlet or $\Psi_{1/6} = (T\ B)^T$ if it belongs to a doublet (where 1/6 indicates the weak isospin of the doublet), and the DM states as S^0_{DM} if scalar or $V^{0\mu}_{\text{DM}}$ if vector. The couplings between the XQ, the DM and SM quarks are introduced using the notation λ^q_{ij} if the DM is scalar and g^q_{ij} if the DM is vector, with the labels $i, j \in \{1, 2\}$ indicating the representations of the XQ and DM, respectively (1 for singlet, 2 for doublet), while $q \in \{u, d, c, s, t, b\}$ identifies which SM quark the new states couples to. The relevant Lagrangian terms are therefore:

$$\mathcal{L}_1^S = \left[\lambda_{11}^{u_f}\bar{T}P_R\, u_f + \lambda_{11}^{d_f}\bar{B}P_R\, d_f + \lambda_{21}^{f}\,\overline{\Psi}_{1/6}P_L\begin{pmatrix}u_f\\ d_f\end{pmatrix}\right] S^0_{\text{DM}} + \text{h.c.} \tag{3.1}$$

$$\mathcal{L}_1^V = \left[g_{11}^{u_f}\bar{T}\gamma_\mu P_R\, u_f + g_{11}^{d_f}\bar{B}\gamma_\mu P_R\, d_f + g_{21}^{f}\,\overline{\Psi}_{1/6}\gamma_\mu P_L\begin{pmatrix}u_f\\ d_f\end{pmatrix}\right] V^{0\mu}_{\text{DM}} + \text{h.c.}, \tag{3.2}$$

where f is a flavour index and where we included terms corresponding to a B singlet for completeness.

[1] More realistic constructs including families of XQs have been dealt with from a phenomenological point of view in previous publications of some of us[142, 174, 175].

The XQs can be either vector-like (VLQ) or chiral (ChQ), and the gauge-invariant mass terms depend on the scenario:

$$\mathcal{L}_{\text{VLQ}} = - M_{T_{\text{VLQ}}} \bar{T} T - M_{B_{\text{VLQ}}} \bar{B} B, \tag{3.3}$$

$$\mathcal{L}_{\text{ChQ}} = - y^{B}_{\text{XQ}} \bar{\Psi}_{1/6} H B - y^{T}_{\text{XQ}} \bar{\Psi}_{1/6} H^{c} T + \text{h.c.} \xrightarrow[\text{vev}]{} - M_{T_{\text{ChQ}}} \bar{T} T - M_{B_{\text{ChQ}}} \bar{B} B. \tag{3.4}$$

In the following, for simplicity, we will consider the mass of the XQ as a free parameter, though one should bear in mind that in the chiral case the contribution of the new ChQ to Higgs production and decay processes, even if different from scenarios where a fourth chiral generation mixes with the SM quarks, can be used to impose constraints on the coupling between the XQ and Higgs boson and, consequently, on the maximum mass the ChQ can acquire through the Higgs mechanism. Of course, ChQs can still acquire mass by some different new physics mechanism (e.g., by interacting with a heavier scalar which develops a VEV).

An important consequence of the assumption about the VLQ or ChQ nature of the XQ top-partner is the structure of its couplings. If the XQ is vector-like, either the left-handed or right-handed components of the interactions are allowed, depending if the XQ is a doublet or singlet respectively. If the XQ is chiral, both projections must be present (even if one of the two can be dominant). The difference between a dominant left-handed or right-handed coupling, in the NWA and for couplings with third generation SM quarks, has been explored in Ref.[176], where it was found that the bounds in the XQ-DM mass plane can be slightly different in the two cases, though they have the same qualitative behaviour. In the following analysis we will explore in detail scenarios where the T has a purely left-handed coupling (*i.e.* it belongs to a VLQ doublet), but we will show (for specific benchmarks) how the experimental limits change in the large width regime when considering alternative hypotheses, such as pure right-handed couplings (VLQ singlet) or couplings where the left- and right-handed components are equal in size with same or opposite sign (ChQ scenarios).

A further important aspect we ought to consider is the physical origin of the large width. This can be achieved in two ways: both by increasing the couplings of the XQs to the states they can decay to, and by increasing the number of decay channels. Of course, if the coupling is increased to achieve a large enough width, it can reach values for which the perturbative regime is not valid anymore, and therefore it would not be possible to perform our analysis with the same techniques. Increasing the number of decay channels has the advantage of limiting the size of couplings, and the disadvantage of introducing further new particles, such as new Z_2-odd neutral or charged bosons or further XQs which then chain-decay to the DM candidate and generate further and complementary final states of phenomenological relevance. To avoid running into the problem of describing *how* the XQ gets a large width, and in order to be as model-independent as possible, we will be agnostic about the mechanism at the origin of the XQ width, and we will consider the Γ_{XQ} as an independent free parameter.

3.2.2 Observables and conventions

To understand the effects of large widths on the signal, we will consider two different processes, both leading to the same four-particle final state DM q DM $\bar{q} \equiv q\bar{q} + E_T^{\text{miss}}$, where $q(\bar{q})$ is an ordinary SM (anti)quark.

- *QCD pair production and decay of on-shell XQs* This process is the one usually considered in experimental searches for XQs. In the so-called Narrow Width Approximation (NWA), wherein the Breit-Wigner propagators of the two T states are suitably replaced by Dirac δ distribution functions, it is possible to separate production and decay of the heavy quarks, thus allowing for a model-independent analysis of the results. The cross section for this process is given by (hereafter, in our formulae, Q denotes an XQ):

$$\sigma_X \equiv \sigma_{2\to 2}\ \text{BR}(Q)\ \text{BR}(\bar{Q}) \tag{3.5}$$

  where, for simplicity, $\sigma_{2\to 2}$ only takes into account the dominant (pure) QCD topologies. This factorisation of production and decay only makes sense in NWA so this process is *dynamically* independent of the width, i.e., $\sigma_X \equiv \sigma_X(M_Q)$, though Γ_Q obviously enter in the definition of the BRs of Q and $\bar{Q}$.

- *Full signal*

  In this process all the topologies which lead to the same four-particle final state and contain *at least one* XQ propagator are taken into account. The only assumption we make, to allow a consistent comparison with the NWA results, is that the order of the QCD α_s in the full signal topologies is the same as in the NWA case. The pair production and decay topologies are included, but for the full signal the XQs are not strictly required to be on-shell. Furthermore, diagrams with only one XQ propagator are also included. We stress that the NWA limit is indeed recovered when the XQ width becomes small with respect to its mass: in this limit, factorisation of production and decay can still be done, as the contribution of all the subleading topologies considered in the full signal becomes negligible and the dominant contribution is given only by pair-production topologies where the XQ is on-shell. If the XQ width is large with respect to its mass, the contribution of other topologies becomes relevant and the factorisation is not possible anymore. Hence, this approach, on the one hand, describes accurately scenarios where the widths of the XQs are large and, on the other hand, is fully gauge invariant (like the NWA approach). Furthermore, it takes into account the spin correlations between the Q quark and antiquark decay branches, which are lost in the NWA. The cross section of this process will be labelled as σ_S and depends upon both the mass and width of the XQ: $\sigma_S \equiv \sigma_S(M_Q, \Gamma_Q)$. Some example topologies for this process, which are not included in the previous one, are given in Fig. 3.1.

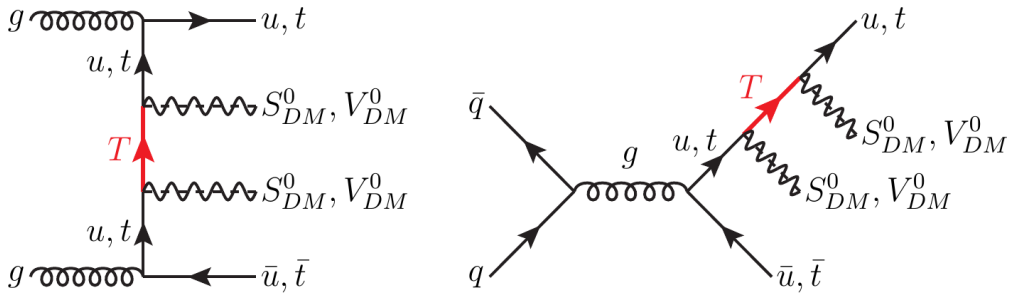

Figure 3.1: Examples of topologies containing only one XQ propagator for final states compatible with XQ pair production and decay into scalar or vector DM and SM quarks of first or third generation.

In order to determine the difference between the two approaches above, we will consider the variable $(\sigma_S - \sigma_X)/\sigma_X$. This ratio takes into account effects of both the off-shellness of T and $\bar{T}$ in their pair production as well as contributions given by topologies which contain at least one XQ propagator (including interference between the two). It measures in practice how much the full signal differs from the approximate pair-production-plus-decay one computed in the NWA.

3.2.3 Channels

In the present analysis we consider the processes of production of a heavy top-like quark T. In principle, from a model-independent point of view, the T quark is allowed to interact with all SM quark generations, but to evaluate the effects of large widths in different scenarios, only specific interactions will be switched on in the different scenarios we will consider.

Since the purpose of this analysis is to evaluate the effects of large widths on channels commonly explored by experimental analysis, we will consider only final states allowed by T pair production and decay. The full set of channels in which a pair-produced T quark can decay is given by the following matrix:

$$
T\bar{T} \rightarrow
\left(\begin{array}{ccc|ccc}
S^0_{DM}u\,S^0_{DM}\bar{u} & S^0_{DM}u\,S^0_{DM}\bar{c} & S^0_{DM}u\,S^0_{DM}\bar{t} & S^0_{DM}u\,V^0_{DM}\bar{u} & S^0_{DM}u\,V^0_{DM}\bar{c} & S^0_{DM}u\,V^0_{DM}\bar{t} \\
S^0_{DM}c\,S^0_{DM}\bar{u} & S^0_{DM}c\,S^0_{DM}\bar{c} & S^0_{DM}c\,S^0_{DM}\bar{t} & S^0_{DM}c\,V^0_{DM}\bar{u} & S^0_{DM}c\,V^0_{DM}\bar{c} & S^0_{DM}c\,V^0_{DM}\bar{t} \\
S^0_{DM}t\,S^0_{DM}\bar{u} & S^0_{DM}t\,S^0_{DM}\bar{c} & S^0_{DM}t\,S^0_{DM}\bar{t} & S^0_{DM}t\,V^0_{DM}\bar{u} & S^0_{DM}t\,V^0_{DM}\bar{c} & S^0_{DM}t\,V^0_{DM}\bar{t} \\
\hline
V^0_{DM}u\,S^0_{DM}\bar{u} & V^0_{DM}u\,S^0_{DM}\bar{c} & V^0_{DM}u\,S^0_{DM}\bar{t} & V^0_{DM}u\,V^0_{DM}\bar{u} & V^0_{DM}u\,V^0_{DM}\bar{c} & V^0_{DM}u\,V^0_{DM}\bar{t} \\
V^0_{DM}c\,S^0_{DM}\bar{u} & V^0_{DM}c\,S^0_{DM}\bar{c} & V^0_{DM}c\,S^0_{DM}\bar{t} & V^0_{DM}c\,V^0_{DM}\bar{u} & V^0_{DM}c\,V^0_{DM}\bar{c} & V^0_{DM}c\,V^0_{DM}\bar{t} \\
V^0_{DM}t\,S^0_{DM}\bar{u} & V^0_{DM}t\,S^0_{DM}\bar{c} & V^0_{DM}t\,S^0_{DM}\bar{t} & V^0_{DM}t\,V^0_{DM}\bar{u} & V^0_{DM}t\,V^0_{DM}\bar{c} & V^0_{DM}t\,V^0_{DM}\bar{t}
\end{array}\right) \tag{3.6}
$$

To limit ourselves to representative and simple scenarios, we will focus on the diagonal terms of this matrix and analyse in detail XQs coupling either to first or third generation quarks (though the main results for couplings with second generation will also be

provided). Effects of large width are different depending on the kinematics of the process and by selecting representative scenarios it is always possible to reconstruct intermediate configurations (XQs interacting partly with heavy and partly with light SM generations).

This analysis is of phenomenological interest only for mass values for which the number of final events is (ideally) larger than 1. In Fig. 2.3 we show the number of events for different LHC luminosities for XQ pair production. The number of events in Fig. 2.3 has been computed considering a Next-to-Next-to-Leading Order (NNLO) cross section, as accurate guidance for observability. For our analysis, however, we will consider only LO cross sections, and defer the evaluation of higher orders effects to future studies. From Fig. 2.3, it is possible to see that the ideal practical validity of our results is limited to mass values of around 1500 GeV for LHC@8TeV, 2500 GeV (2700 GeV) for LHC@13TeV with 100/fb (300/fb) integrated luminosity. Of course, we are not considering here effects due to experimental acceptances and efficiencies: this study is only meant to assess the role of the complete signal with respect to the common approximations made in theoretical and experimental analyses.

3.3 Analysis tools and experimental searches

As intimated, herein, we want to study the ratio of cross sections $(\sigma_S - \sigma_X)/\sigma_X$ (where we recall that σ_S corresponds to the full signal and σ_X to the NWA) as well as understand which influence the width of the XQ, in turn triggering the contribution of the forementioned new topologies not present in pair production, can have on its mass bounds. To do so we consider an XQ top-partner belonging to the doublet representation $\Psi_{1/6} = (T\ B)^T$ (corresponding to pure left-handed couplings in Eqs.3.1 and 3.2) and scan over the parameters M_T, $M_{\rm DM}$ and Γ_T.

For our simulation we analyse in detail scenarios where the DM state has masses $M_{\rm DM}$ = 10 GeV, 500 GeV and 1000 GeV and with an XQ of mass $M_T > M_{\rm DM} + m_q$, with $q \in \{u, c, t\}$ (such that its on-shell decay is kinematically allowed) up to $M_T^{\rm max} = 2500$ GeV, which is the maximal value of a T mass so that it can be produced for LHC@13TeV with 100/fb integrated luminosity as shown in Fig. 2.3. We also consider values of the T width from $\Gamma_T/M_T \simeq 0\%$ (NWA) to 40% of the T mass.

Our numerical results at partonic level are obtained using MadGraph5 [157, 158] and a model we implemented in Feynrules [160] to obtain the UFO interface format. The model we used is the same as the one in the analysis of Ref.[176]. For the Monte Carlo simulation we use the PDF set cteq6l1 [161]. Events are then passed to Pythia 8 [177, 178], which takes care of the hadronisation and parton showering.

To analyse and compare the effects of a set of 13 TeV analyses considering final states compatible with our scenarios, we employ CheckMATE 2 [164], which uses

the DELPHES 3 [165] framework for the emulation of detector effects. In our simulations we include all the ATLAS and CMS (carried out at 13 TeV) analyses available within the CheckMATE database but we will only list here the most relevant ones for our study. These analysis are the following ATLAS searches:

- ATLAS 1604.07773 [179], a search for new phenomena in final states with an energetic jet and large missing transverse momentum,
- ATLAS 1605.03814 [180], a search for squarks and gluinos in final states containing hadronic jets, missing transverse momentum but no electrons or muons,
- ATLAS 1605.04285 [181], a search for gluinos in final states with one isolated lepton, jets and missing transverse momentum. This search is however sensitive only to a specific region of the parameter space we explored, *i.e.* very light T and DM masses and small T width.
- ATLAS-CONF-2016-050 [182], a search for the stop in final states with one isolated electron or muon, jets and missing transverse momentum.

3.4 Extra T quark interacting with Dark Matter and the SM top quark

In this section we will study the case of XQs coupling to third generation SM quarks only. The possible decay channels are therefore $t\bar{t} + \{S^0_{DM}S^0_{DM}, V^0_{DM}V^0_{DM}\}$, i.e. $t\bar{t} + E_T^{\text{miss}}$. We start from this channel because, from a theoretical point of view, the top quark is considered the most likely to be affected by new physics phenomena.

3.4.1 Large width effects at parton level

In Fig. 3.2 the relative differences between the full signal and the QCD pair production cross sections $(\sigma_S - \sigma_X)/\sigma_X$ are plotted for an LHC energy of 13 TeV. Notice that here and in the following we do not apply cuts on E_T^{miss} at parton level.

A number of conclusions can be derived from the observation of these results:

- As expected, and as a health check of our results, in the NWA limit ($\Gamma_T/M_T \to 0$) the QCD pair production channel is always an excellent approximation, as the off-shell and non-doubly-resonant contributions become negligible.
- The effects of increasing the width becomes quickly relevant, independently of the DM spin, eventually becoming very large near the kinematics limit ($M_T = M_{DM} + m_t$) and for high T masses, where the ratio can reach values above 100%

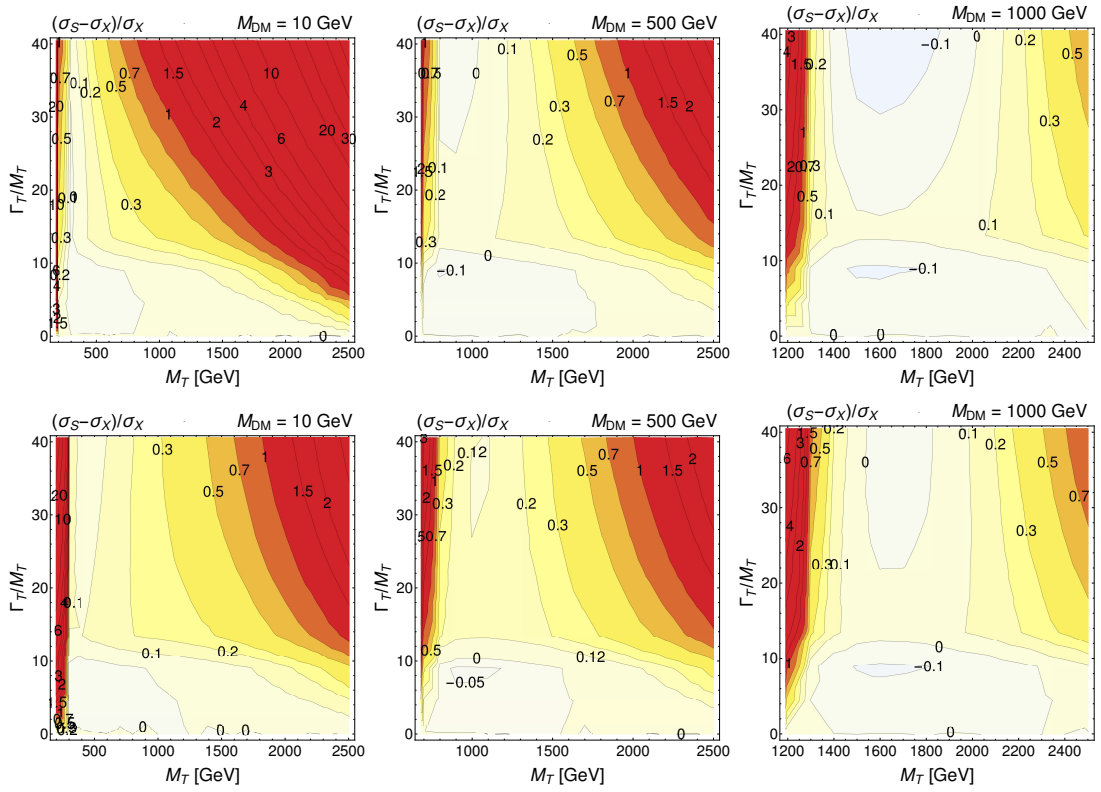

Figure 3.2: Relative difference between the full signal and the QCD pair production cross sections for a T coupling to a DM particle (coupling to third generation) of mass 10 GeV, 500 GeV and 1000 GeV. Top row: scalar DM; bottom row, vector DM.

(represented by red regions in Fig. 3.2). The increase near the kinematics limit can be explained by a non-trivial combination of factors, the most relevant being the fact that a larger width opens a larger phase space for the decay of the T, which is more limited (in the NWA) as the gap between the masses decreases. It is interesting to notice that the cross section for the full signal is large for values of M_T beyond those ideally accessible in the NWA (see Fig.2.3). Therefore, even if the T mass is too large to produce enough events in the NWA, if its width is sizeable it might still be possible to detect it, unless the experimental acceptances drop with a comparable rate with respect to the NWA values. In this respect, the performance of the aforementioned experimental searches will be discussed in the following section.

- For all channels, and in specific regions, a cancellation of effects takes place. Such cancellation makes the QCD pair production cross section similar to the cross section of the full signal even for large values of the width. The cancellation appears at different values of the T mass depending on the mass of the DM and of its spin and becomes stronger when the value of $M_{\rm DM}$ increases. Yet this cancellation does not mean that results in the NWA approximation are valid also for larger widths, as the cancellation is an accidental result due to the different scaling of the cross

sections in NWA and large width regime. The differences between NWA and large width results are clearer at differential level. In Fig. 3.3 we show the differential distributions of the missing transverse energy and of the transverse momentum of the top quark along the cancellation line for a scalar DM particle of mass 1000 GeV and for a vector DM particle of mass 10 GeV. A similar effect was already observed in [1], considering XQ decaying to SM particles instead of DM.

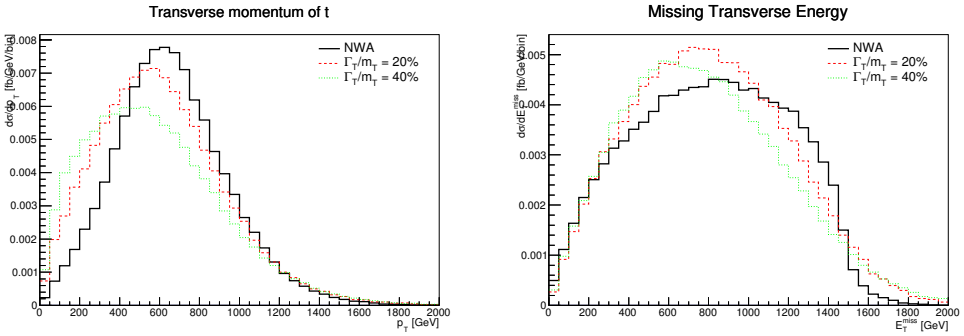

(a) Scalar DM: $M_{\mathrm{DM}} = 1$ TeV, $M_T = 2$ TeV

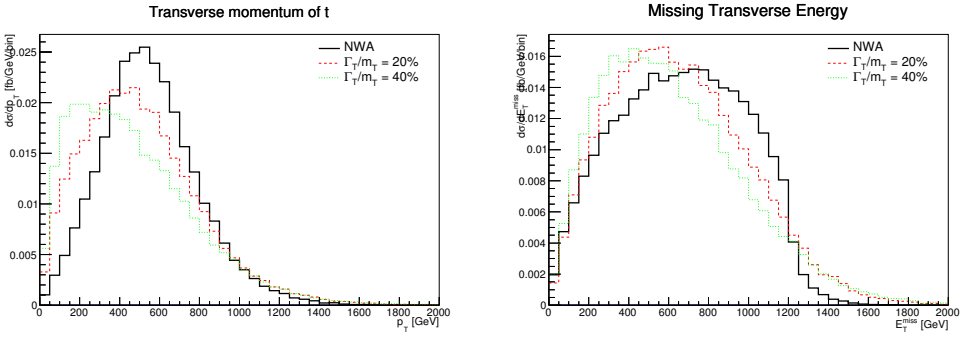

(b) Vector DM: $M_{\mathrm{DM}} = 10$ GeV, $M_T = 400$ GeV

Figure 3.3: Differential distributions of transverse momentum of the top quark and E_T^{miss} along the cancellation line for scalar and vector DM.

3.4.2 Large width effects at detector level

In this section we consider the effects of large widths on the exclusion limits for the T mass. We show in Fig 3.4 the exclusion limit, corresponding to $r_{\max}(\equiv \frac{S-1.96\Delta S}{S_{95}^{\exp}}) = 1$ as defined in [183], in the $(M_T, \Gamma_T/M_T)$ plane for both scalar and vector DM scenarios and for the same values of the DM mass previously considered. For each simulated point the best Signal Region (SR) is also shown using a color code.

The main conclusions which can be derived are the following:

- For all values of the DM mass the bounds for scalar and vector DM do not show sizeable differences. The most sensitive SR is almost always tN_high from the analysis ATLAS-CONF-2016-050, which is optimised for "high mass splitting,

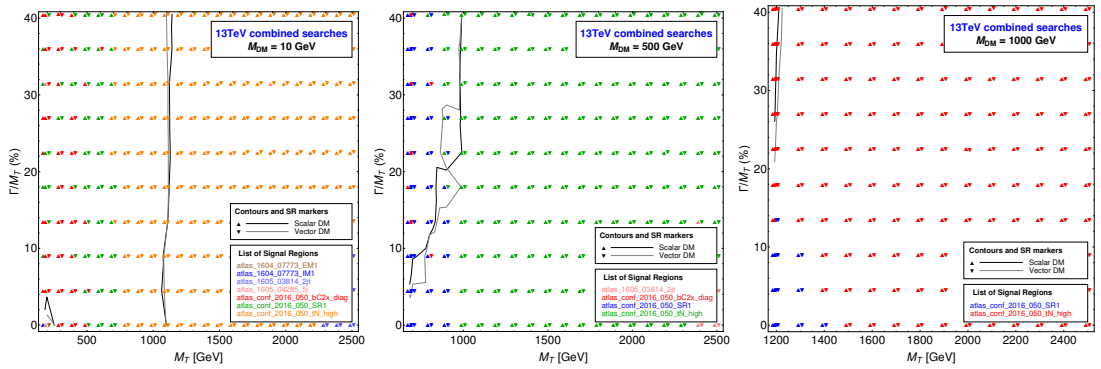

Figure 3.4: CheckMATE results for a T coupling to a DM particle (coupling to third generation) of mass 10 GeV, 500 GeV and 1500 GeV. The black (grey) line show which part of the parameter space is excluded for the scalar (vector) DM scenario.

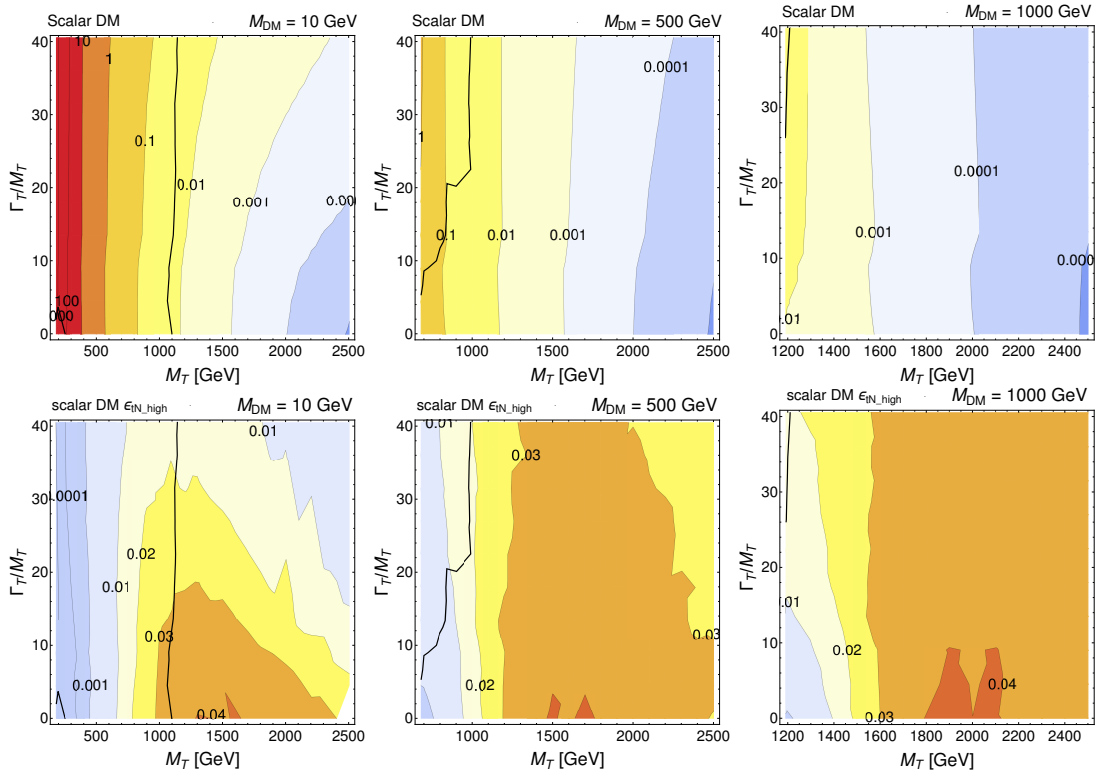

Figure 3.5: Top row: full signal cross sections for the scalar DM case. Bottom row: efficiencies of the SR tN_high from the analysis ATLAS-CONF-2016-050 [182] for different scalar DM masses.

leading to very boosted top quarks where the decay products are close-by and can be reconstructed within a single large-R jet" [182]. It is characterised by the requirement of at least 4 jets, at least 1 b-jet and E_T^{miss} larger than 450 GeV, and by further kinematical requirements on combination of variables, such as $E_{T,\perp}^{\text{miss}}$ for the definition of which we refer to [182], to optimise the signal-over-background ratio for boosted top quarks produced in association with E_T^{miss}, as is the case in both stops decaying to top and neutralino and T quarks decaying to top and

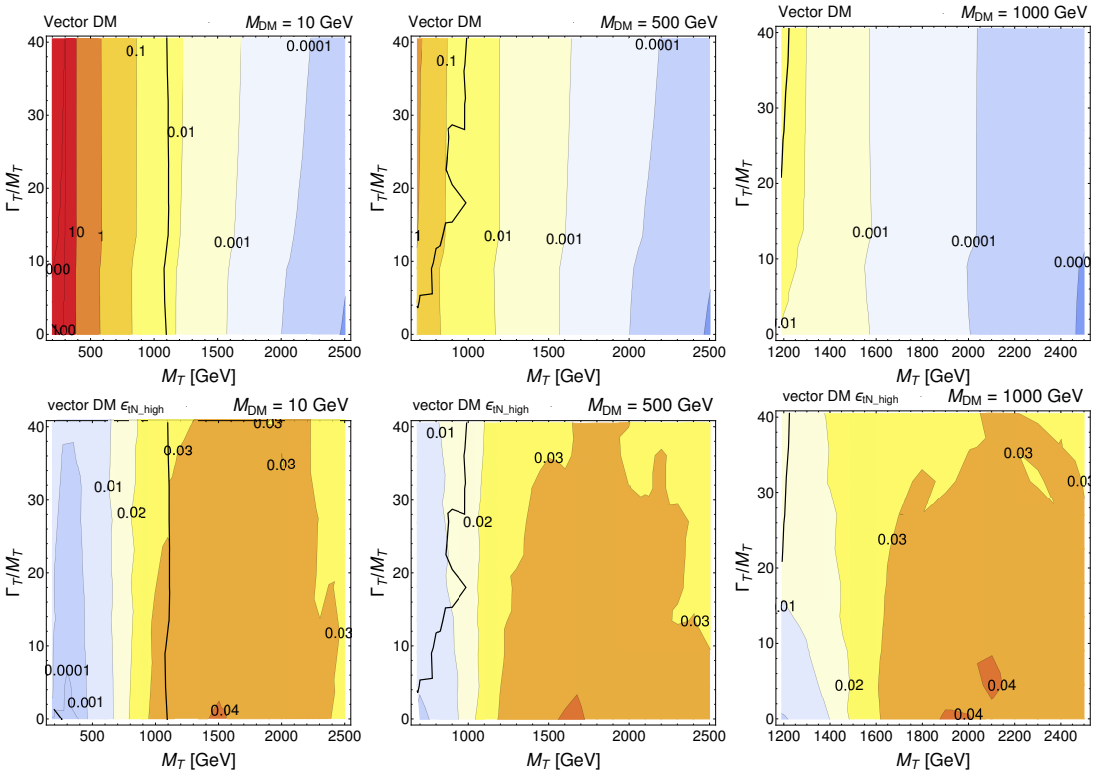

Figure 3.6: Top row: full signal cross sections for the vector DM case. Bottom row: efficiencies of the SR tN_high from the analysis ATLAS-CONF-2016-050 [182] for different vector DM masses.

bosonic DM candidates. Therefore, this SR is dominantly sensitive to topologies of resonant production, which depend weakly on the spin of the DM particle.

- For $M_{\rm DM} = 10$ GeV the exclusion bound is around $M_T = 1100$ GeV and has basically no width dependence. It is therefore instructive compare the width dependence of the full signal cross section and of the efficiency for the tN_high signal region, shown in Figs.3.5 and 3.6. Clearly, the increase in the cross section is compensated by an analogous decrease in the efficiency of this SR, and this compensation accounts for the fact that the bound is almost independent of the width. The reduction of the efficiency between small and large widths in the bound region is mostly due to the cuts on the $E_T^{\rm miss}$ and on the p_T of the 4 jets, respectively 450 GeV and {120,80,50,25} GeV in this SR [182]. In figure 3.7 we plot the distributions of these observables at detector level, where it is possible to see that cutting on these variables has a stronger effect for the large width scenarios. It is worth noticing that points where the T mass is close to the top mass and its width approaches the NWA are not excluded: in such region the top background hides the XQ signal and makes it undetectable.

- For $M_{\rm DM} = 500$ GeV and 1000 GeV the bound shows a slight dependence on the width: the larger the width, the stronger the exclusion. This could be understood looking again at the relation between the efficiencies of the most sensitive SR and

the full signal cross section. It's also worth noticing that for these DM masses the NWA region is never excluded, only XQ with a large width can be excluded, and only up to mass of $M_T \sim 1000$ (1200) GeV for $M_{\text{DM}} = 500$ (1000) GeV.

- For higher DM masses the exclusion contour is gradually pushed to the kinematics limit and above the maximum value of the width-over-mass ratio we have tested (40%), and eventually disappears due to the limited sensitivity of the detector for small mass splittings between T and DM.

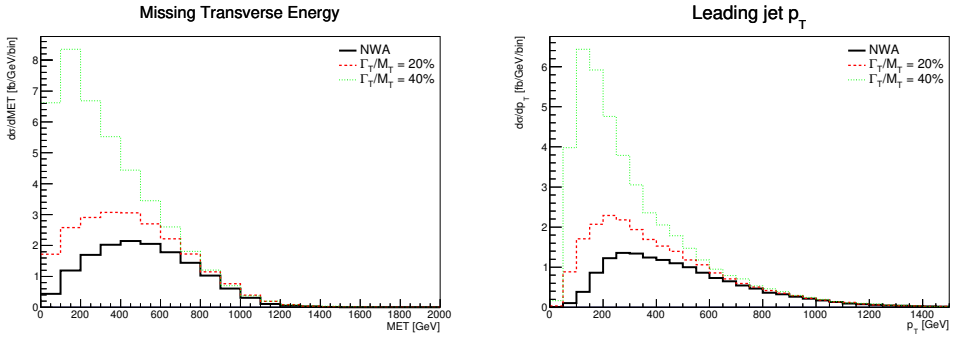

Figure 3.7: Differential distributions along the bound for a T with mass $M_T = 1100$ GeV coupling to the top quark and scalar DM with mass $M_{DM} = 10$ GeV.

3.4.3 Dependence on the chirality of the couplings

To conclude the analysis of XQs interacting with DM states and third generation SM quarks, we consider how the bounds change if the T quark is a VLQ singlet (pure right-handed couplings) or a ChQ (where we consider either pure scalar or pseudoscalar couplings if the DM is a scalar or pure vector or axial-vector couplings if the DM is a vector). In Fig. 3.8 the bounds are shown for all the aforementioned scenarios: keeping in mind that the uncertainty due to the use of a recasting tool is quite large, it is possible to see that with the set of experimental searches considered in this study, the differences between various chiralities are not significant for the vector DM scenario, while there are visible differences if the DM is scalar. The more pronounced effects for scalar DM with respect to vector DM can be due to the fact that the transverse components of vector DM are less sensitive to the coupling chiralities than its (pseudo)scalar one, and dilute the effects of different couplings. Therefore, with the set of cuts currently used to optimise the discovery of new physics in the $t\bar{t} + E_T^{\text{miss}}$ channels, a characterisation of the couplings of a T interacting with a vector DM and the top quark would be challenging even in the large width regime. If the DM is scalar there could be more room for a characterisation of the properties of the T. Designing signal regions optimised for the discrimination of different coupling hypotheses and for different Γ/M regimes would be advisable in case of discovery of a signal in this channel, but this goes beyond the scope of the present analysis and we defer this to a future study.

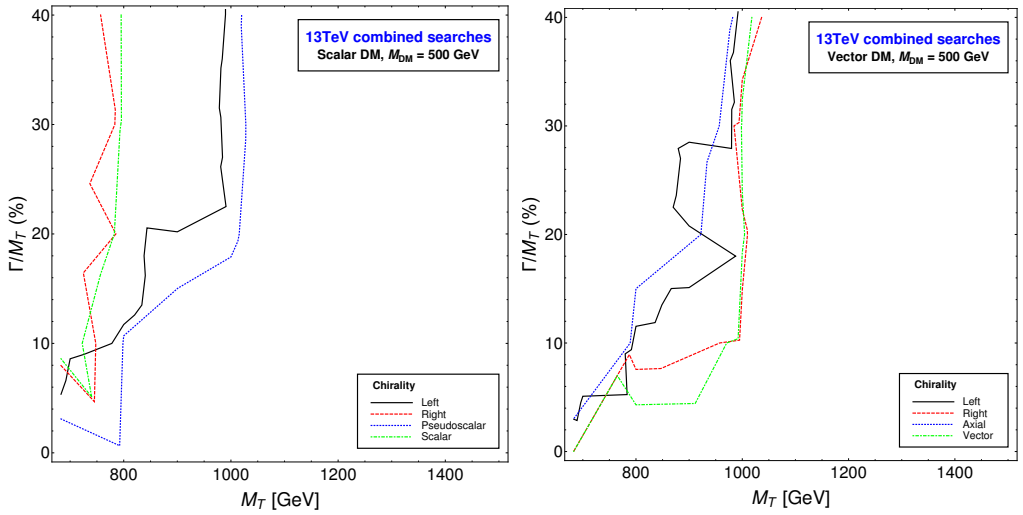

Figure 3.8: Exclusion bounds for a T interacting with the SM top quark and DM for different hypotheses on the chirality of the couplings: for a VLQ T pure left-handed and pure right-handed couplings, and for a ChQ T pure scalar (vector) or pseudoscalar (axial-vector) couplings if T interacts with scalar (vector) DM.

3.5 Extra T quark interacting with Dark Matter and the SM up quark

In this section we will study the case of XQs coupling to first generation SM quarks and a DM candidate. The possible final states are therefore $S^0_{DM}u\ S^0_{DM}\bar{u}$ and $V^0_{DM}u\ V^0_{DM}\bar{u}$.

3.5.1 Large width effects at parton level

When the T quark couples to quarks of the first generation, the $2 \to 4$ process contains topologies where the initial state partons interact directly with the T (examples are shown in Fig. 3.9) which are absent in the case of coupling to third generation.

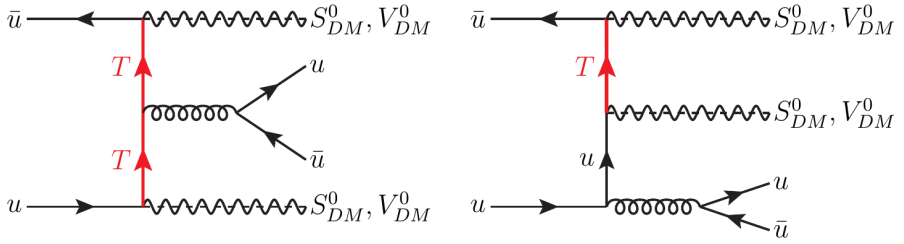

Figure 3.9: Examples of topologies which are peculiar to scenarios with heavy quarks coupling to first generation.

These topologies contain collinear divergences, due to the gluon splitting, which drastically enhance the full signal cross section with respect to QCD pair-production. In Fig. 3.10 the logarithm of the relative differences between the full signal cross section and the

QCD pair production cross section are plotted for an LHC energy of 13 TeV. Notice that to allow a consistent comparison with the NWA case no cuts have been applied on the light jet at parton level.

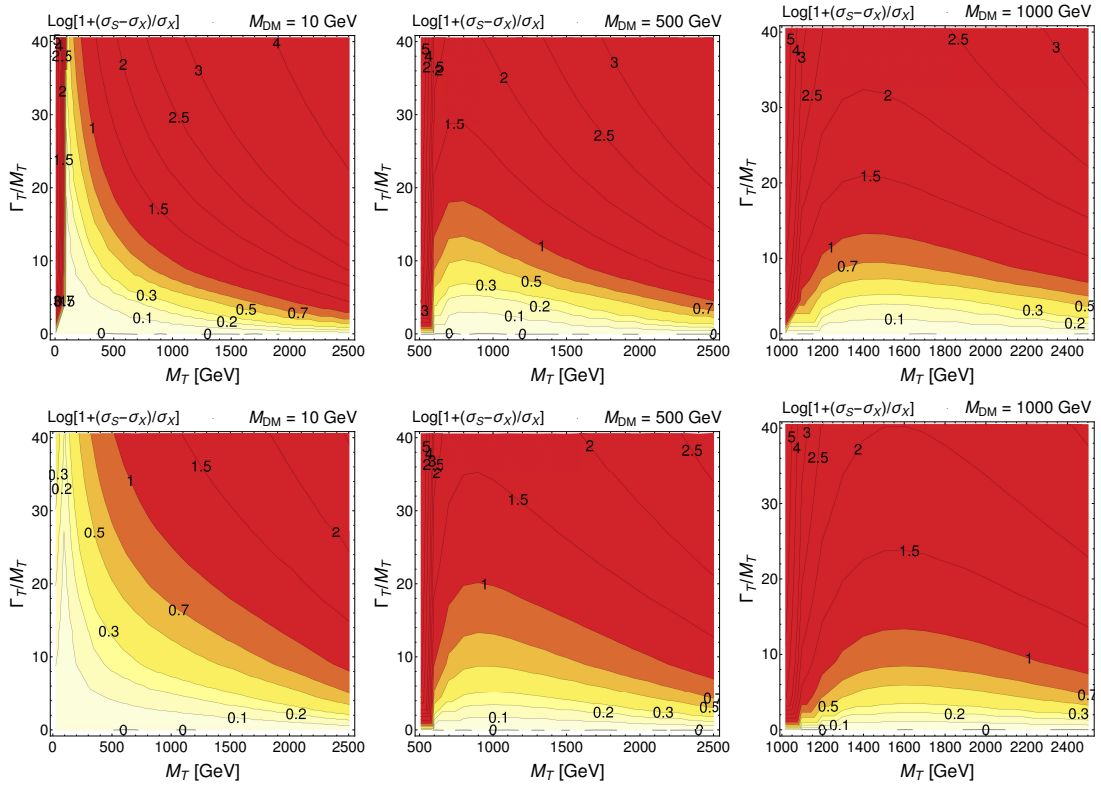

Figure 3.10: Relative difference between the full signal and the QCD pair production cross sections for a T coupling to a DM particle (coupling to first generation) of mass 10 GeV, 500 GeV and 1000 GeV. Due to the large differences between cross sections, the ratio is plotted as $\log[1 + (\sigma_S - \sigma_X)/\sigma_X]$ instead of $(\sigma_S - \sigma_X)/\sigma_X$. Notice that in that case the contours at 0.1, 0.2, 0.3, 0.5 and 1 respectively correspond to a value of $(\sigma_S - \sigma_X)/\sigma_X$ equal to 26%, 58%, 100%, 216% and 900%. Top row: scalar DM; bottom row, vector DM.

The main conclusions which can be derived from our results are the following:

- In the NWA the full signal and the QCD pair production topologies become equivalent, as expected. The latter topologies describe the process in an excellent way in the NWA, as subleading topologies and off-shell contributions are indeed negligible.

- The contributions of new topologies and of off-shell T become more and more relevant as the width of the T increases, quickly becoming extremely relevant for the determination of the cross section, especially when the mass of the XQ and of the DM particle are close.

- The cancellation of effects which makes the σ_S similar to σ_X as in the case of coupling to third generation is not observed in this case. However, a minimum of

the cross section ratio (for fixed Γ_T/M_T) appears for all value of the DM mass and spin in regions that are very similar to the cancellation region observed in section 3.4.1. This decrease is due again to a different scaling of the phase space in the NWA and large width regimes, but due to the additional diagrams in the case of coupling with first generation, the cancellation only lowers the cross section ratio and does not bring it to zero as it was the case for third generation coupling.

3.5.2 Large width effects at detector level

In Fig 3.11 the exclusion bound and the best SR are shown in the $(M_T, \Gamma_T/M_T)$ plane for both scalar and vector DM scenarios and for the same value of the DM mass considered in Fig.3.10. In Figs. 3.12 and 3.13 the exclusion bounds for scalar and vector DM respectively are shown together with the full signal cross sections and with the efficiencies of the most relevant signal regions for the two DM spin hypotheses.

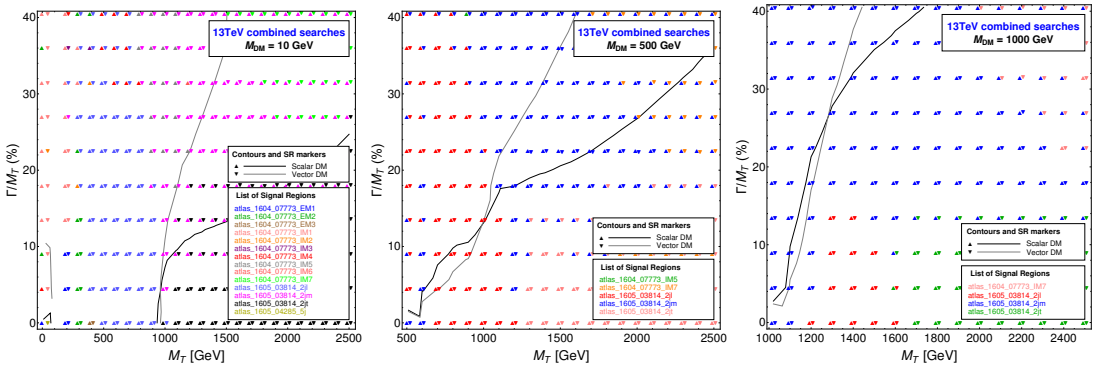

Figure 3.11: CheckMATE results for a T coupling to a DM particle (coupling to first generation) of mass 10 GeV, 500 GeV and 1000 GeV. The black (grey) line shows which part of the parameter space is excluded in the scalar (vector) DM scenario.

The main results for the case of T coupling to first generation quarks are the following.

- For DM masses below to the TeV the bounds have a qualitatively similar behaviour, the width dependence is always sizable, the bounds for small width are similar between scalar and vector DM and as the width increases the different DM spins exhibit different behaviours, where scalar DM scenarios show a stronger dependence on the T width.
- The most sensitive SRs for the determination of the bounds are almost always 2jl, 2jm or 2jt of the ATLAS search [180], which are optimised for signals with two jets and E_T^{miss} in the final state.
- For DM masses around the TeV or higher the width dependence of the bound is still present but the difference between the scalar and the vector DM scenarios

becomes weaker. Furthermore, the NWA region is never excluded. Analogously to the case of coupling with third generation, this is a consequence of a combination between larger phase space and width dependence of the experimental acceptances.

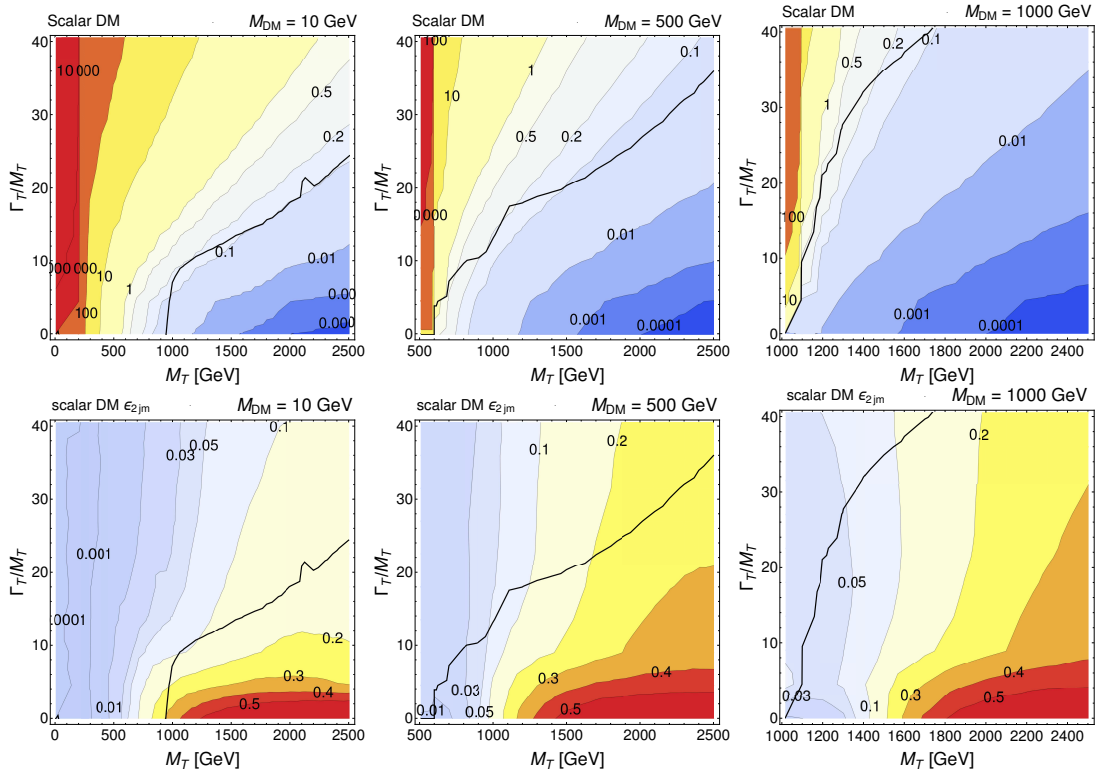

Figure 3.12: Top row: full signal cross sections for the scalar DM case. Bottom row: efficiencies of the SR 2jm from the ATLAS search [180] for different scalar DM masses.

3.5.3 Dependence on the chirality of the couplings

Analogously to the case of T coupling with third generation quarks, the analysis of the dependence of the limits on the chirality of the couplings (and therefore on the hypotheses about the properties and representations of T) is presented. In Fig. 3.14 the exclusion bounds for different couplings are shown. Once again even if the uncertainty due to the use of a recasting tool is quite large, we observe that the scenario with pure left-handed coupling exhibits a slightly stronger width dependence than the rest of the scenarios in the large width regime, especially for the scalar DM scenario. This can be due again to the milder dependence of the transverse components of vector DM on the chirality of the couplings, which is however not completely diluted, as scenarios with left-handed couplings and vector DM still exhibit a slight stronger width dependence. Even if the bounds are in the same regions, the most sensitive SRs of (the subset of) current searches could be in principle used to distinguish the scenario where the T is a VLQ doublet from the others, in case of discovery. We are not going, however, to explore this potentiality

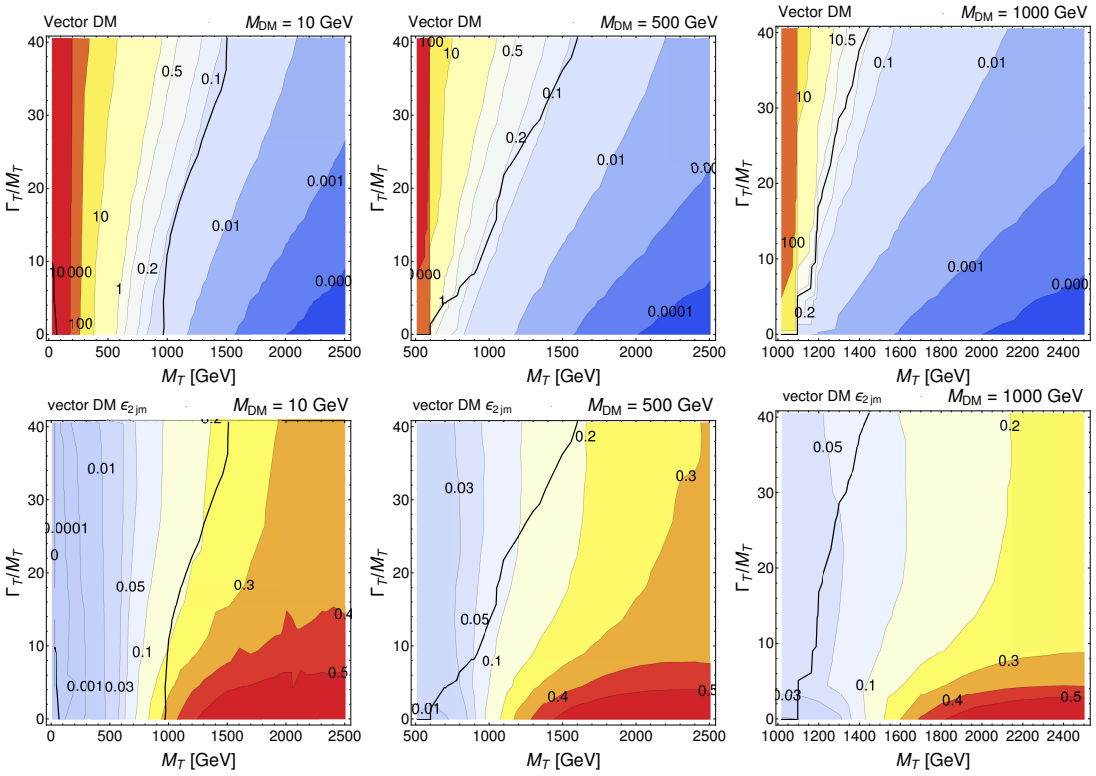

Figure 3.13: Top row: full signal cross sections for the vector DM case. Bottom row: efficiencies of the SR 2jm from the ATLAS search [180] for different scalar DM masses.

in the present study, as it goes beyond the scope of our analysis, and we defer it to a subsequent one.

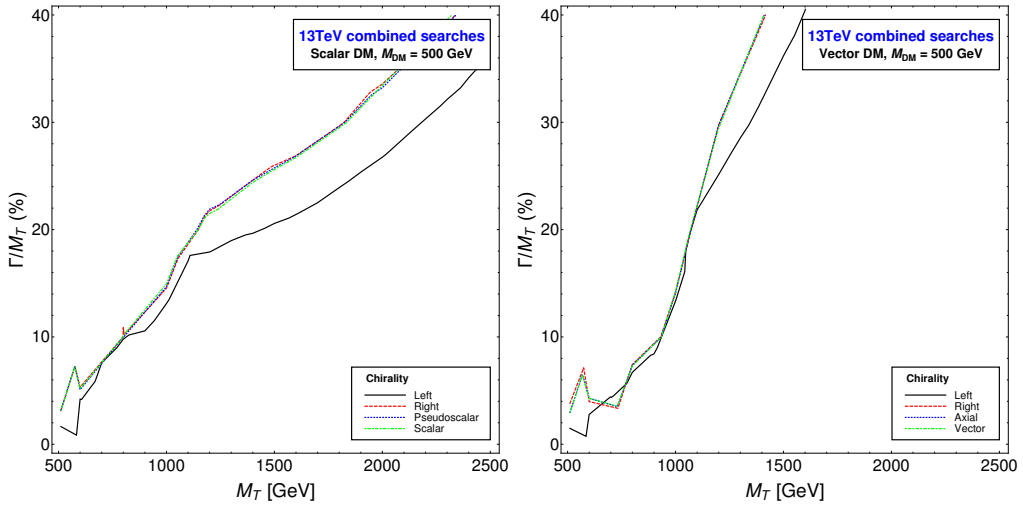

Figure 3.14: Exclusion bounds for a T interacting with the SM up quark and DM for different hypotheses on the chirality of the couplings: for a VLQ T pure left-handed and pure right-handed couplings, and for a ChQ T pure scalar (vector) or pseudoscalar (axial-vector) couplings if T interacts with scalar (vector) DM.

3.6 Exclusion limits in the $M_T - M_{DM}$ plane

The scenarios we are considering have three parameters: the mass of the T, the width of the T and the mass of the DM, with the only constraints given by the kinematical limit between the masses ($M_T > M_{\rm DM} + m_q$) and by the fact that the width should not really exceed 50% of the mass, otherwise the concept of resonant state is essentially lost. The exclusion bound at 2σ will therefore identify a 3D surface in the space defined by the three parameters (where the width is substituted by the Γ_T/M_T ratio) and therefore it is instructive to analyse the projections of this surface on the plane identified by the masses of T and DM for different values of the Γ_T/M_T ratio. Such representation is also useful to directly compare bounds on T and bosonic DM with analogous results in other models, such as SUSY. Indeed the exclusion limits of SUSY searches are often presented in the $(M_{\tilde{t}}, M_{\chi_0})$ plane. We show in Fig. 3.15 the bounds in the $(M_T, M_{\rm DM})$ plane for specific values of Γ_T/M_T: the NWA case, 20% and 40%. We included in this figure the results for a T quark coupling to DM and the charm quark.

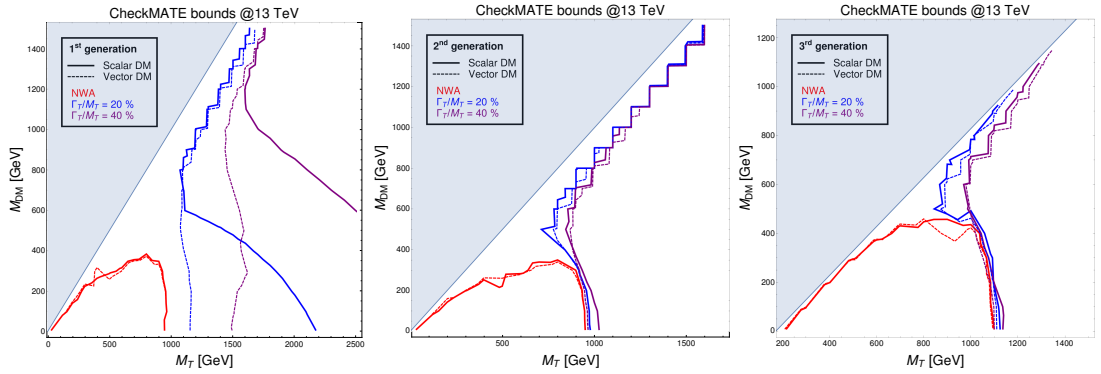

Figure 3.15: Bounds in the $(M_T, M_{\rm DM})$ plane for T quark coupling DM particle and first (left panel), second (center panel) and third (right panel) generations of SM quarks for different values of Γ_T/M_T.

The qualitative behaviours of the exclusion limits strongly depend on the assumption about which SM quark generation the T couples to.

- T **coupling to DM and up quark**: in the NWA the exclusion limits for scalar and vector DM are not distinguishable in practice (barring numerical fluctuations). When the width of the T increases, however, the bounds for scalar and vector exhibit a sizably different dependence on the T and DM masses. If the DM mass is below a width-dependent threshold, the scalar DM case excludes a much wider region of the parameter space. This behaviour can be understood by looking again at Figs. 3.12 and 3.13, which show that the full signal cross section has a largely different trend with changing width depending on the scalar or vector nature of the DM. For high enough DM masses, the dependence on the width is less pronounced and this erases the differences between the bounds above a certain value of the DM

mass. A further peculiarity of the large width regime, with respect to the NWA, is that the region where the mass gap between T and DM is small is always excluded.

- T **coupling to DM and charm quark**: in both NWA and large width regime it is not possible to distinguish scalar from vector scenarios. As the width increases, the region close to the kinematics limit ($M_T = M_{\rm DM} + m_c$) becomes excluded, while it would be allowed in the NWA. If the DM mass is below 300 GeV and far from the kinematics limit, the bound depends very weakly on the width.

- T **coupling to DM and top quark**: the mass bounds for scalar and vector DM are very similar in both the NWA and large width regime. The increase of the width modifies the bound (with respect to the NWA) if the mass of T is close enough to the kinematics limit ($M_{\rm DM} + m_t$): unlike in the NWA case, as the values of the T mass approaches the kinematics limit, they become more and more excluded by experimental data as the T width increases. Moreover, if the DM mass is below ~ 400 GeV and far from the kinematics limit, the bound on the T mass does not depend on the width. Designing new specific cuts could allow a more optimised exploration of the large width regime of XQs decaying into DM and third generation SM quarks, especially considering the fact that efficiencies for the most sensitive SRs exhibit a general decrease along the bound region as the width increases (as shown in Fig. 3.5).

To conclude this section, the bounds obtained under the NWA are less stringent than the bounds obtained when the NWA is relaxed and the width is allowed to have large values, relative to the T mass. This results can be intuitively expected when considering that larger widths correspond to larger cross sections and, unless the selection and cut efficiencies compensate the cross section enhancement, the number of signal events increases with respect to the NWA scenario. It is remarkable, though, that different assumptions about the couplings of T with different SM quark generations produce either negligible or sizeably different bounds if the DM is scalar or vector. This result could be exploited for the design of new experimental searches which are not only meant to discover new signals in channels with $E_T^{\rm miss}$ but also to characterise the signal.

3.7 Conclusions

Experimental analyses aimed at assessing current LHC limits on the possible existence of XQs, or else at establishing the machine potential in unravelling them, rely upon a NWA emulation of the signal yield, the latter being limited to the contribution of QCD induced pair production of such new states of matter. While this approach is essentially model-independent, as the XQ BRs are the only physics observables carrying the model dependence, and further offers one the possibility of eventually enabling the

interpretation of limits (or indeed evidences) in a variety of BSM scenarios, it suffers from the drawback that the accuracy of the ensuing results worsen considerably as the width of the XQ grows larger and/or all (gauge invariant) topologies relevant to the final state searched for (in addition to those pertaining to XQ pair production), all containing at least one XQ state (hence rightfully classifiable as signal), are accounted for. Conversely, the accurate emulation of such effects is necessarily model dependent, since the standard factorisation possible in NWA between QCD pair production topologies and decay BRs is no longer possible (i.e., model independent couplings now enter both the production and decay dynamics).

Herein, we have estimated such effects in a rather simple model with only one XQ decaying into DM and a SM quark. The XQ was taken to have electric charge $+2/3$, with either a VLQ or ChQ nature. The DM candidate was assumed to be either a scalar or a vector state. Hence, necessarily, the SM quark is a t-quark in the case the XQ only couples to a third generation SM quark or a $u(c)$-quark in case it does with a first(second) generation one instead. In all such cases, we looked at the differences, initially at the parton level and eventually at the detector one as well (including cuts in this case), between the complete XQ process and the one only including $T\bar{T}$ hadron-production at the LHC Run 1 and 2, in the final states $t\bar{t} + E_T^{\rm miss}$ and $jj + E_T^{\rm miss}$, respectively.

Upon choosing discrete values for the DM mass, of 10 GeV, 500 GeV, 1000 GeV and 1500 GeV, and an XQ of mass $M_T > M_{\rm DM} + m_q$, with $q \in \{u(c), t\}$ (such that its on-shell decay is kinematically allowed) up to $M_T^{\rm max} = 2500$ GeV (essentially the ideal kinematics reach of the 13 TeV LHC for quark pair production), we have ascertained the following, as a function of Γ_T/M_T taken between 0 and 40%. As a general result, we have concluded that the XQ nature, whether it be VLQ or ChQ, does not play a significant role in the phenomenology we have studied, primarily because one can be turned into the other by simply changing the left and right fermion couplings suitably and the observables normally adopted in experimental analyses do not resolve their relative size and/or sign. Furthermore, we have established that, for the same choice of $M_{\rm DM}$, there occur sizeable differences between the two aforementioned approaches (NWA versus full result) depending on whether one adopts the scalar or vector nature of the DM candidate, the more so the larger the value of Γ_T/M_T. However, are the coupling properties of the T state that are most responsible for the largest differences seen between the simplistic (model-independent) and realistic (model-dependent) approaches outlined. On the one hand, when coupling is allowed to the third generation only, the exclusion limits depend only slightly upon Γ_T/M_T, with a general trend pointing towards the cross section becoming larger when the width increases, yet with the additional contributions with respect to the NWA being generally suppressed by the cuts on missing transverse energy normally adopted in experimental searches. On the other hand, when coupling is allowed to the first(second) generation only, exclusion limits massively depend upon the width because the aforementioned additional topologies are not suppressed by such

cuts in missing transverse energy, the more so the larger both M_Q and Γ_Q/M_Q are. (In fact, differences between the DM nature are significantly more prominent in the case of coupling to first(second) generation than in the third generation one.) Clearly, a fully-fledged model incorporating coupling to any generation will fall in between these two extreme conditions, with further subtleties induced by the PDF behaviour, as one can already see by comparing our results for the first and second generation cases.

In conclusion then, results from LHC searches for any XQs, when decaying to DM (whether spin 0 or 1) and either a heavy or light SM quark, should be taken with caution, as they do not account for effects induced by either the large XQ width, the additional (to the pair production ones) topologies or both, which can be very large even in a simplified model with only one XQ. Hence, one should rescale the observed limits from established experimental analyses to the actual ones upon accounting for such effects (as we have done here) or else attempt deploying new ones adopting different selection strategies which minimise (in the case of exclusion) or indeed exalt (in the case of discovery) such effects (which will be the subject of a future publication). At any rate, the time-honoured assumption that the NWA is a reliable investigative approach applicable over most of the parameter space of the BSM scenarios dealt with here should be dismissed. In fact, we also have cautioned that, despite cancellations may exist between the various effects described here, which in the end might not change sizeably the inclusive cross section for certain values of Γ_Q/M_Q, these are only accidental and do not apply to the exclusive observables used in experimental searches, so that, again, limits obtained in the NWA would be inaccurate, owing to mis-estimated efficiencies.

Chapter 4

Single production of vector-like quarks with large width at the Large Hadron Collider

4.1 Introduction

In this chapter the focus is on work performed in [3] which like the previous two studies in this thesis, examines the effects of large width regions, but in this research the scenario of a singly produced VL-top mixing with either the third or light generations of the SM quarks is considered. All processes yielding single VLQ production proceed via model-dependent electro-weak interactions which enter already at the production level due to quark-antiquark induced topologies that connect the production rate to large width and interference effects.

In order to interpret the limits of an experimental search on a given range of cross-sections one must determine the size of the VLQ couplings which generate such cross-sections. If the couplings are large, finite width effect and/or interference effects may be not negligible, and it becomes imperative to take them into account in the experimental searches. The exact relation between the EW couplings and those effects is rather model-dependent, resulting on many possibilities for signal modelling.

In this research we will propose strategies for presenting the results of experimental analyses in a simple, though solid, model-independent framework, allowing a straightforward re-interpretation of experimental data. A similar approach has been already used in its simplest form in Refs. [4, 184]. Such strategy should limit the need of performing numerical recasting for the reinterpretation of results: the possibility of having ways to avoid numerical recasting (when possible) is becoming pressing as experimental searches rely more and more upon numerical frameworks which cannot be easily reproduced

in tools for phenomenological analyses, such as boosted decision trees or multi-variate analyses.

The plan of this chapter is as follows. In Section 4.2 we describe the analytical model-independent parameterisation and we discuss the issues induced by interference contributions. In Section 4.3 we perform the phenomenological analysis: first, in Section 4.3.1, we set up our framework, then, in Section 4.3.2, we undertake a numerical recasting of a CMS search to obtain bounds for VLQs with large width, finally, in Section 4.3.3, we adopt an analytical parameterisation and compare it to numerical results, also discussing how to treat interference in a specific benchmark. In the final section we draw our conclusions.

4.2 Model-independent parameterisation of the cross-section

Apart from the aforementioned small contamination due to EW interactions in the case of mixing with light quarks, in processes of VLQ pair production, the VLQs are produced through their QCD couplings to the SM gluons and subsequently decay to the SM quarks through couplings induced by their mixing which, together with the mass of the VLQs, are the free parameters of the Beyond the SM (BSM) physics scenario under consideration. The advantage, from a phenomenological point of view, of pair production processes is thus given by the fact that the production of VLQs is essentially only dependent upon their mass, as the QCD coupling is a SM parameter unmodified by new physics.

In processes of VLQ single production, in contrast, the same type of couplings which induce the VLQ decays also determine the production rate, i.e., the cross-section of single VLQ production processes depends on their couplings to SM quarks, irrespectively of their mixing patterns. The size of such couplings determines for which VLQ mass the cross-section of single production becomes dominant with respect to pair-production at a given collider energy. Moreover, such couplings also contribute to the partial width of the VLQ in their decay channels to SM states. In the case of a VLQ with large width, large couplings of VLQs with SM quarks are in general strongly constrained by oblique observables and Higgs couplings [185, 1, 169], but such constraints apply to minimal scenarios where the VLQ is the only BSM state. Scenarios with multiple VLQs can induce cancellations which allow to enlarge the couplings while evading current constraints [170]. The total width of the VLQ can also be increased by including further decay channels to other new physics states. To perform an analysis of single production of VLQs with large width it is therefore essential to separate the effects which are purely due to the large width from the dependence of the cross-section on the VLQ couplings. As we shall see, in the context of our analysis, such a goal can be achieved considering a suitable parameterisation which factors out the contributions of different couplings.

But let us now proceed to define the constituent processes of VLQ production in single mode. In essence, herein, we consider any topology leading to a three-particle final state made up by SM objects only which contains at least one VLQ propagator. A subtlety, however, arises when deciding upon the initial state. In fact, single production of VLQs can be studied either by considering the proton to be constituted of five quark flavours, the so-called 5-Flavour Scheme (5FS), or else assuming that bottom quarks are not in the initial state but can only appear from gluon splitting, i.e. the 4-Flavour Scheme (4FS). Any phenomenological difference between 4FS and 5FS would vanish if it was possible to describe the processes at all orders in QCD perturbation theory[1]. In our analysis we will work in the 5FS, for which the topologies are represented in Fig. 4.1. (Notice that some of these only exist in the Large Width (LW) regime, not in the NWA.) This choice is simply dictated by the preliminary results of Ref. [186], which show that, for a specific process and in the NWA, when kinematical distributions of final state objects computed at LO in the 5FS exhibit sizeable differences with respect to those computed at LO in the 4FS, the distributions obtained through a NLO description of the process are closer in shape to the LO results in the 5FS.

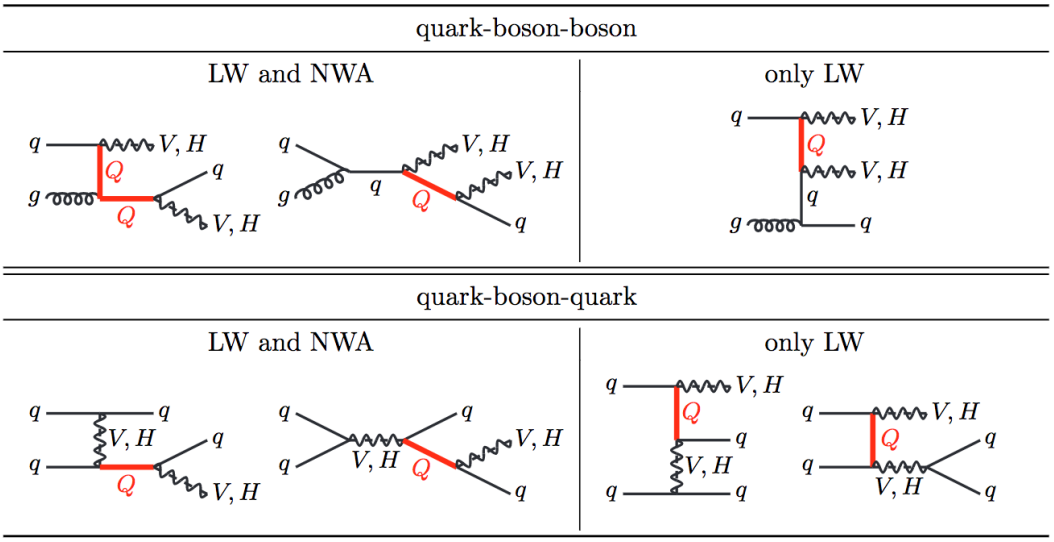

Figure 4.1: Complete list of the generic topologies for final states compatible with single VLQ production in the 5FS. Topologies on the left column can be described in both the NWA and LW regimes while topologies on the right column are neglected in the NWA approximation. Here, V represents the W and Z bosons of the SM.

The total cross-section (σ) can be parameterised by factorising the BSM couplings considering a *reduced* quantity, labelled as $\hat{\sigma}$, analogously to what was done in [137]. In the absence of any kind of interference between different topologies, the model-independent $\hat{\sigma}$ depends only on the mass and total width of the VLQ. The factorisation of the signal cross-section (labelled with the subscript S in the following) can be written

[1]For specific details we refer to the wide literature on this subject (see for example [143, 144, 145] for single top production).

as (see Fig. 4.1):

$$\sigma_S(C_1, C_2, M_Q, \Gamma_Q) = C_1^2\ C_2^2\ \hat{\sigma}_S(M_Q, \Gamma_Q), \tag{4.1}$$

where C_1 and C_2 are the couplings corresponding to the interactions at both sides of the Q propagator, and $\Gamma_Q = \Gamma(C_i, M_Q, m_{\text{decays}})$ is the total width of the VLQ, which depends on its mass, the masses of all its decay products and the couplings through which the VLQ interacts with all the particles it can decay to, including (but not exclusively) C_1 and C_2.

This parameterisation cannot be generalised if interference contributions amongst signal components that contain different coupling content and/or with SM background are non-negligible. In this case the cross-sections for the pure signal and its interference contributions with the irreducible background are written as σ_S and σ_{SB}^{int}, where the second represents the interferences amongst signal (S) topologies or with the SM background (B). In Fig. 4.2 it is shown an example for the Wtb final state: in this case $\sigma_S = \sigma_W + \sigma_Z + \sigma_{WZ}^{\text{int}}$ and $\sigma_{SB}^{\text{int}} = \sigma_{WB}^{\text{int}} + \sigma_{ZB}^{\text{int}}$ where the subscript of each term represents the bosons propagating in the corresponding topologies. The individual terms of the sum are not necessarily gauge invariant, while the *observable* quantities σ_S and σ_{SB}^{int} are. The only possible

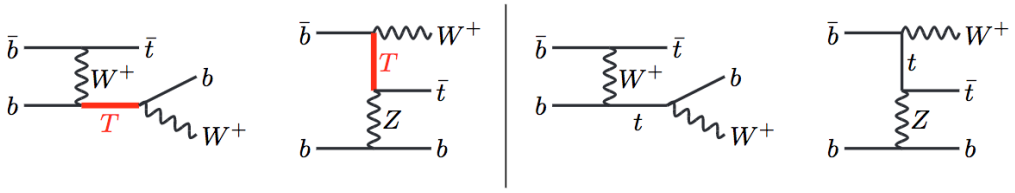

Figure 4.2: Example on the left of a subset of interfering topologies in the process $bb \to bW^+\bar{t}$ mediated by a T VLQ and different SM bosons. The diagrams on the right show analogous contributions from the SM background, which interferes with the signal.

factorisation in case interference terms are not negligible is:

$$\sigma_S(C_{1...}, C_2, M_Q, \Gamma_Q, \chi_Q) = C_2^2\ \hat{\sigma}_S(C_{1...}, M_Q, \Gamma_Q, \chi_Q),\ \sigma_{SB}^{\text{int}} = C_2\ \hat{\sigma}_{SB}^{\text{int}}(C_{1...}, M_Q, \Gamma_Q, \chi_Q) \tag{4.2}$$

where C_2 is the coupling corresponding to the interaction between Q and the boson in the final state, $C_{1...}$ are the couplings through which Q interacts with the different virtual bosons and χ_Q the dominant chirality of the VLQ couplings, which can be LH or RH depending on the VLQ representation and for total rates only plays a role in interference terms. As an example, a T singlet will decay through charged current to a bottom quark with a dominantly LH chirality [137, 185] whereas a T as part of a doublet will produce a dominantly RH bottom: the interference with the SM background, for which the bottom quark can only be produced with LH chirality through charged currents, will be different in the two scenarios.

In the limit of negligible interference between different signal topologies, the pure signal contribution can be approximated as:

$$\sigma_S(C_{1...}, C_2, M_Q, \Gamma_Q) \sim C_2^2 \sum_i C_{1i}^2 \, \hat{\sigma}_{Si}(M_Q, \Gamma_Q) \tag{4.3}$$

where the potentially gauge-dependent contribution is assumed to be negligible as well.

A further limit is represented by scenarios in which the VLQ interacts exclusively with one SM boson. In this case, besides recovering Eq. (4.1) for the cross-section of the pure signal contribution, the interference with SM background can be written as:

$$\sigma_{SB}^{\text{int}}(C_2, M_Q, \Gamma_Q, \chi_Q) = C_2^2 \, \hat{\sigma}_{SB}^{\text{int}}(M_Q, \Gamma_Q, \chi_Q). \tag{4.4}$$

Eqs. (4.1) to (4.4) are valid in all width regimes, though their range of applicability is different. The values of $\hat{\sigma}_S$ in the parameterisation of Eq. (4.1) can be computed for any possible final state and can be used for a model-independent reinterpretation of the results, under the assumption that the model for which the reinterpretation is made does not contain sizeable interference terms of any kind for the considered final state. Such parameterisation, when associated with a proper way to interpret experimental results, discussed below, represents a robust model-independent framework for testing any theoretical scenario predicting VLQs with small or large width against experimental limits in a given channel. This approach has been followed in two CMS analyses [4, 184], where $\hat{\sigma}$ was used for an interpretation of experimental results for single production of VLQs with large width. The values of $\hat{\sigma}_S$ and $\hat{\sigma}_{SB}^{\text{int}}$ in Eqs. (4.2) to (4.4), however, contain a further model-dependency, represented by the impossibility to factorise the $\{C_{1...}\}$ couplings in a gauge-invariant way. If interference terms are sizeable, this is an unavoidable consequence and the analysis would have in any case a limited reinterpretation applicability.

Both parameterisations can be easily generalised to compute cross-sections at NLO in QCD, as the factorisation of the EW couplings to derive the $\hat{\sigma}$'s is not affected by the contribution of radiative QCD effects. A NLO calculation of single production of VLQs with finite width is however beyond the scope of this paper.

4.3 Phenomenological analysis

In this section we will provide case studies for the reinterpretation of experimental results of searches for single production of VLQs with finite width, comparing the bounds obtained through a numerical recasting with the results obtained applying the analysis strategies of Sect. 4.2.

4.3.1 Benchmarks

Analogously to what has already been done in the CMS analyses [4, 184], we will consider specific and representative scenarios for the interactions of VLQs with the SM states. Couplings between VLQs and SM quarks and bosons are parameterised as:

$$c_Z = \frac{e}{2c_w s_w}\kappa_Z, \quad c_W = \frac{e}{\sqrt{2}s_w}\kappa_W \quad \text{and} \quad c_H = \frac{M_Q}{v}\kappa_H, \tag{4.5}$$

where $v = 246$ GeV is the Higgs Vacuum Expectation Value (VEV), c_w and s_w are the cosine and sine of the weak angle θ_w and $\kappa_{W,Z,H}$ are coupling strengths. In the limit where only one VLQ representation is present in Nature and the particles are narrow the κ parameters accurately approximate the sine of the mixing angle between VLQ and SM quark (for a relation between couplings and mixing angles see, e.g. Ref. [169]). In the NWA, if the VLQ is a singlet, the coupling parameters are related as $\kappa_Z \simeq \kappa_H \simeq \kappa_W \simeq \kappa$ while, if the VLQ is within a doublet (and assuming that the Yukawa coupling of the other element of the doublet is zero), the coupling parameters become $\kappa_Z \simeq \kappa_H \simeq \kappa$ and $\kappa_W \simeq 0$. These relations are not satisfied in the large width regime.

Minimal extensions of the SM with one unique VLQ representation where the VLQ has large couplings are excluded by other constraints (such as EW precision tests or corrections to SM couplings) [185, 1, 169]. In our case study the large width regime will be achieved by considering the total width as a free parameter but imposing for VLQ singlets and doublets identical relations between the κ parameters as in the NWA. We also consider more extreme scenarios where we assume 100% couplings of the VLQ with each of the SM bosons. A summary of the benchmarks we consider is reported in Tab. 4.1. Through this procedure the assumption of a minimal model is relaxed: new physics, in the form of mixings either in the quark or bosonic sectors due to additional representations of VLQs or new gauge bosons or scalar fields, must contribute to generate the relations between couplings.

100% W	100% Z	100% H	Singlet-like	Doublet-like
$\kappa_Z^q = \kappa_H^q = 0$	$\kappa_W^q = \kappa_H^q = 0$	$\kappa_W^q = \kappa_Z^q = 0$	$\kappa_W^q = \kappa_Z^q = \kappa_H^q$	$\kappa_W^q = 0$ and $\kappa_Z^q = \kappa_H^q$

Table 4.1: Benchmark points and corresponding coupling relations.

The event generation has been performed through MadGraph5_aMC@NLO [157, 158] using the NNPDF3.0 PDF set [187] at LO with $\alpha_S = 0.118$ and setting the QCD renormalisation and PDF factorisation scales to the mass of the VLQ. The generated events have been subsequently processed through Pythia 8 [177, 178] to include parton showering and hadronisation. Finally, the hadronised events have been analysed through MadAnalysis 5 [188], which uses Delphes 3 [165] for the emulation of detector effects.

The VLQ model used for the simulation was implemented in FEYNRULES [160] to obtain the `UFO` [189] model format to be used inside MADGRAPH5_aMC@NLO. This model is a slightly modified version of the public model described in [152] where each coupling of the VLQ has been assigned a different label in order to isolate individual interference contributions through the MADGRAPH5_aMC@NLO syntax COUPLING_ORDER_I^2==N in the process of diagram generation, where the I'th coupling order is counted N times in the squared amplitudes, making it possible to generate separately each term of Eq. (4.2).

It is not within the scope of this paper to investigate the impact on searches due to the choice of the proton scheme. However, as most of the experimental searches performed so far adopt the 4FS (including the one recast in this analysis) a more quantitative discussion about the choice of the flavour number scheme is in order. As an example, in Fig. 4.3, we show the p_T distribution of the leading b-jet comparing the 4FS and 5FS at LO for a B VLQ mixing with third generation, in different width regimes, for the processes $pp \to tWj$ and $pp \to bZj$. The dependence of the distributions on the width of the VLQ can be sizeable, thus potentially affecting the efficiency of experimental cuts. The final state b-quark is dominantly generated in the B decay and therefore is fairly central in both 5FS and 4FS in any width regime. The width-dependent differences in the shapes are generally of similar size in both 4FS and 5FS.

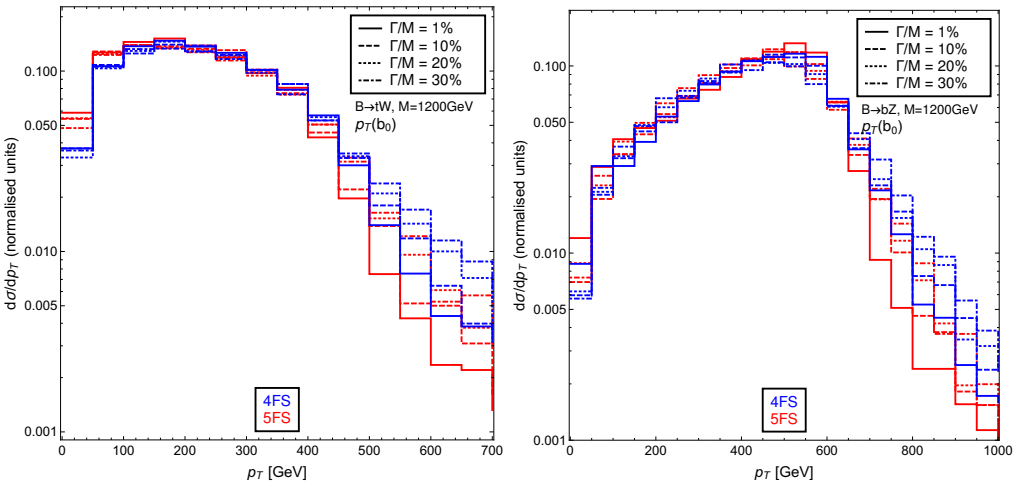

Figure 4.3: Distributions of the transverse momentum of the leading b-tagged jet for two processes. Left panel: $pp \to tWj$ (in the 5FS) or $pp \to tWjb$ (in the 4FS); right panel: $pp \to bZj$ (in the 5FS) or $pp \to bZjb$ (in the 4FS), with subsequent on-shell decays of the SM states in both cases. The comparison is made for a B mass of 1200 GeV and for different values of the width-over-mass ratio (Γ_Q/M_Q) of the VLQ.

The signal cross-sections are generally of similar size between 4FS and 5FS in the NWA at LO [186]. We had also checked that in all parameter space we probe the cross-sections calculated in the 4FS are always smaller than the ones calculated on the 5FS. Therefore, the interpretation of results in terms of number of events in the 4FS acts as a lower bound to the a more realistic exclusion bound.

4.3.2 Recasting and reinterpretation of experimental data

As a representative analysis for the recast of experimental data, the CMS search CMS-B2G-16-006 [190] has been chosen. This analysis specifically targets a heavy VLQ with charge $+2/3$ or $-4/3$ decaying into a b-quark and a W boson, which is produced singly in association with a light flavour quark and a b-quark. Thus, in the 4FS, the considered process is $pp \to T(\to W\,b)\,\bar{b}\,j$. The search selects events with one lepton (electron or muon in two different signal regions) and at least two jets, one central (b-tagged) and one forward. A set of kinematical cuts are also imposed, and we refer to [190] for all the relevant details. In the experimental analysis the limits are computed analyzing the shape of the mass of the heavy quark candidate, formed by the vectorial sum of the lepton, the leading central jet, and the neutrino candidate (where the neutrino candidate is reconstructed assuming its x,y-components to be the missing transverse momentum and that the invariant mass of it summed with the lepton is the W mass). In our case the limits are computed by a simple counting on the signal region. In table 4.2 we compare the efficiencies obtained by our recast implementation with the ones reported by [190] under the same signal assumptions of the experimental search. We stress that, for the purposes of this study, we are not interested in an overly precise reconstruction of the experimental results: our intent is to achieve a realistic analysis framework to demonstrate how to reinterpret experimental data in scenarios where the VLQs have a large width.

Channel	Electron	Muon	Total
Experimental efficiencies	1.3%	1.4%	2.7%
Recasting efficiencies	0.98%	1.31%	2.29%

Table 4.2: Comparison of the experimental and recasted efficiencies for the different signal regions for a $pp \to T(\to Wb)jb$ signal in the 4FS with $m_T = 1000$ GeV in the NWA.

We recast this analysis for the large width case by scanning the Γ_Q/M_Q from, e.g., 1% to 40% in steps of 5% and M_Q from 600 to 2000 GeV in steps of 100 GeV. Four processes will be considered: the original target of the search (a third generation T partner in the $pp \to W\,b\,q$ channel) but also a third generation B partner in the $pp \to W\,t\,t$ channel, and a light generation T and B partner on the $pp \to W\,\bar{q}\,q$ channel (notice that, as we consider the 5FS, a q may also be a b). For the sake of linearity, we first show the results of the recast in the $pp \to W\,b\,q$ channel. The values of the the largest allowed observed cross-section at 95% Confidence Level (CL) on the $(M_Q, \Gamma_Q/M_Q)$ plane that we obtain for this channel are shown in Fig. 4.4.

To interpret the results with the benchmarks of Tab. 4.1 we saturate the values of the VLQ couplings to obtain the needed size of the width for each point in the $(M_Q, \Gamma_Q/M_Q)$ grid of our scan. The total cross-section obtained by saturation is then compared to the experimental limits and it is verified to be excluded or not. In fact, the coupling

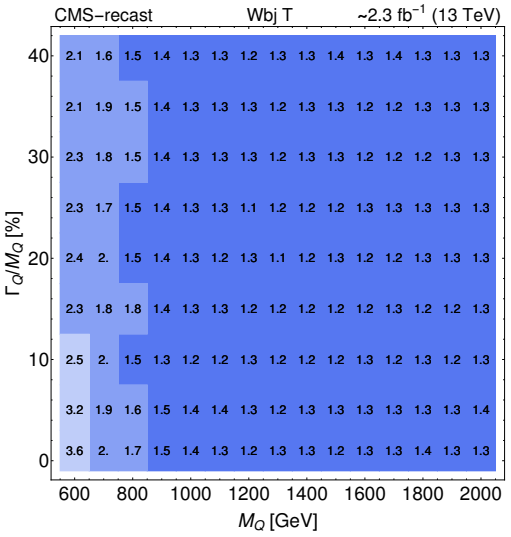

Figure 4.4: 95% CL largest allowed cross-sections (in pb) for the Wbj final state as a function of M_T and of Γ_T/M_T for a VLQ T coupling to the third SM quark generation and decaying 100% to bW.

necessary to fix Γ_Q/M_Q have an effect on the cross-section of the process and therefore on the region of exclusion on the $(M_Q, \Gamma_Q/M_Q)$ plane, using the same data. For instance, trivially, the value of the VLQ couplings will be larger for benchmark points where they interact 100% in a specific channel than for the singlet- or doublet-like benchmarks, given the contribution from other decay channel(s) in the latter case.

This done in Fig. 4.5, where we show the value of the Wbj signal cross-section as a function of the VLQ mass and of its Γ_Q/M_Q ratio, together with the 95% exclusion line for the Wbj final state. It is possible to notice that the NWA region is not excluded while the exclusion range appears as Γ_Q/M_Q increases, thus highlighting the phenomenological impact of the LW regime. The shape of the exclusion boundary is a balance between how the theory cross-section grows on the $(M_Q, \Gamma_Q/M_Q)$ plane and the behaviour of the signal kinematics. In Fig. 4.5 we see that the exclusion bounds roughly track the variation of the cross-section, with the exclusion line in the region where the cross-section is slightly larger than 1 pb. Such behaviour is related to the fact that, for the considered CMS search, selection cuts are designed in such a way that the signal efficiencies vary only moderately in the whole plane. In the light of this result, in the following, we will only show results for VLQ coupling which are 100% to a specific SM boson, the results for singlet- and doublet-like cases being qualitatively analogous to a simple rescaling of the cross-section.

In Fig. 4.6 we show the values of the the largest allowed cross-section at 95% CL, together with the exclusion bound, for each point of the grid in the $(M, \Gamma_Q/M_Q)$ plane for a VLQ T (top row) or B (bottom row) coupling to the first (top and bottom-left panels) or third (bottom-right panel) SM quark generations. For the scenario where the B couples with the third SM quark generation (bottom-right) the value of the the largest allowed

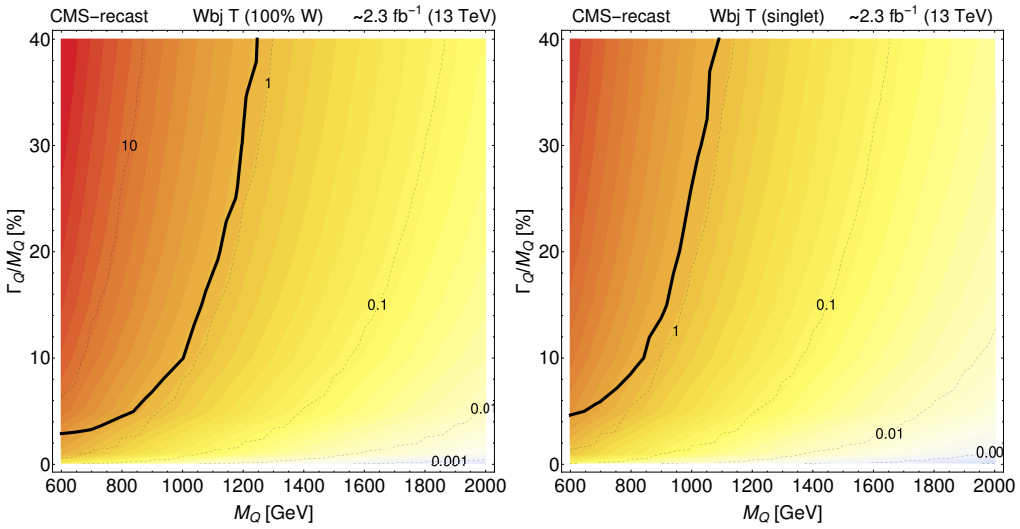

Figure 4.5: Cross section (in pb) for the Wbj final state as a function of M_T and of Γ_T/M_T and 95% exclusion line (in black) for a VLQ T decaying 100% to bW (left panel) or singlet-like (right panel).

cross-section is rather large in comparison with the other benchmarks we consider and therefore no exclusion can be made[2]. In contrast, we do find exclusion regions for the Wjj channel mediated by a light generation T or B partner.

Analogously to the Wbj case, the exclusion lines in both the Wjj scenarios basically follow the increase of the cross-section due to the increase of the coupling. However, as the search is not optimised for Wjj final states, the largest allowed cross-section is much larger than for the Wbj case[3] The fact that we still get a similar exclusion for these final states is due to the higher cross-section for the light generation VLQs: PDF effects makes the b-initiated processes less likely that the u- and d-initiated ones, leading to a much larger cross-section for the Wjj final states. Between the two Wjj plot results, we observe a stronger exclusion in the case of the propagation of a B VLQ, rather than a T VLQ, due to the fact that the cross-section is larger while the efficiencies are similar in the whole parameter space.

In all the channels we consider the largest allowed cross-section decreases when the mass increases but, except for small masses (less than 1 TeV), this search is not really sensitive to the width variation. The effect of the width on the excluded cross-section is larger for $M_Q \simeq 600$ GeV where it can increase by a factor 4 with Γ_Q/M_Q increasing from the NWA to $\simeq 40\%$. The overall weak dependence of the results on the VLQ width is related to the fact that the kinematic distributions of the final states are also often

[2]This can be explained by a combination of two factors: the final state Wtt is heavier than the other ones we consider, leading to a much smaller cross-section and, since the search is not targeting this specific final state, the signal efficiencies are smaller than for the other channels.

[3]For instance, the search we are recasting requires a b quark in the final state, which can only come from the accompanying jet when the VLQ only decays to light quarks.

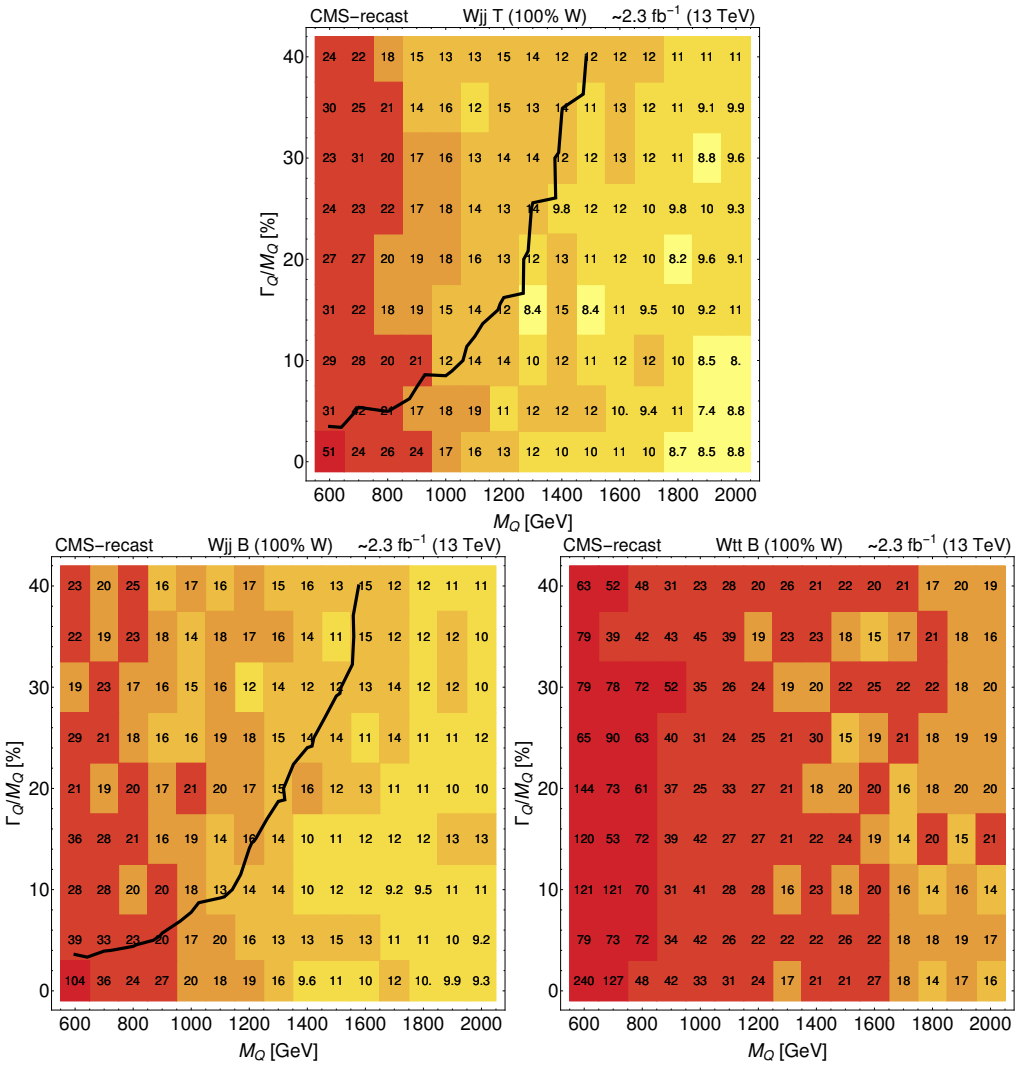

Figure 4.6: 95% CL excluded cross-sections (in pb) and exclusion bound (black line) as a function of M_Q and Γ_Q/M_Q for a VLQ T (top row) and B (bottom row) coupling to the first (top and bottom-left panels) or third (bottom-right panel) SM quark generation.

weakly affected. The same weak dependence was found in the two CMS single production searches exploring the large VLQ width regime [4, 184].

4.3.3 Reinterpretation through the reduced cross-section $\hat{\sigma}$

In this section we provide an example of how to interpret experimental data only using the reduced cross-section $\hat{\sigma}$ described in Sect. 4.2 for a model featuring a VLQ interaction with SM bosons with given couplings, mass and total width. The procedure can be generalised for any search of BSM states which can decay into SM final states, for which the width of the resonance can be considered as a further degree of freedom, complementary to the mass of the BSM state, for the determination of the maximum excluded cross-section.

If the interference terms are negligible for the signal topologies, and likewise for the interference between signal and SM background, then the cross-section for any process $pp \to V\ q\ q$, where V is any SM boson and q any SM quark, can be obtained from the $\hat{\sigma}$ cross-sections, rescaled with appropriate couplings. By comparing it to the excluded cross-sections (minding the model-dependent relation between the couplings and Γ_Q/M_Q) it is possible to determine whether a specific scenario is excluded by the experimental search without the need of performing a dedicated recast (as it was done to construct Fig. 4.4). This is possible provided the results of the searches are presented in the $(M_Q, \Gamma_Q/M_Q)$ plane, as it has been done in the last section and in Refs. [4, 184].

In Fig. 4.7 the $\hat{\sigma}$'s for the process $pp \to bWj$ mediated by a T interacting exclusively through charged current are shown on the left panel while on the right panel we report a comparison between the limit obtained through a numerical recasting and the limit obtained by rescaling the $\hat{\sigma}$ values with the coupling needed to obtain the corresponding width of the T in this benchmark scenario. The results are qualitatively very close and allow to identify with good accuracy the excluded region of this benchmark scenario.

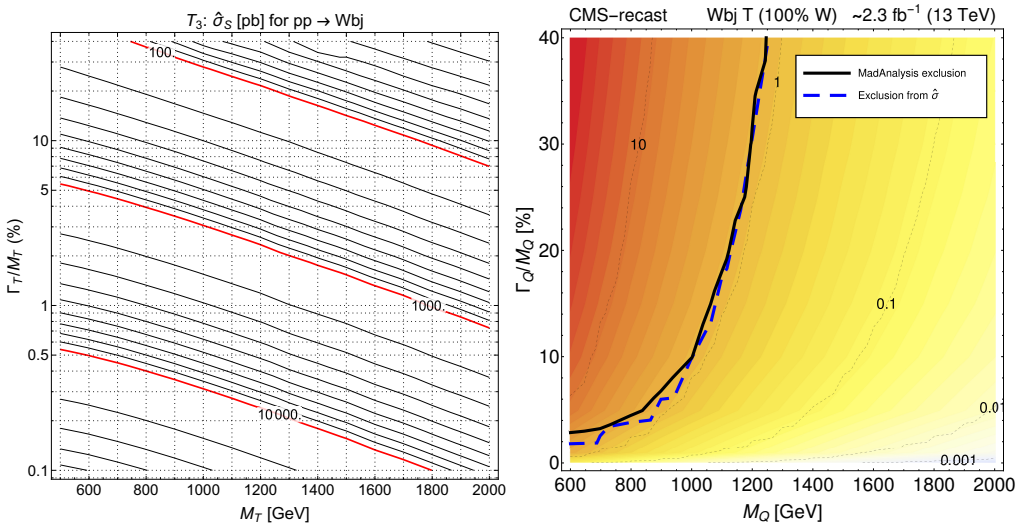

Figure 4.7: The 13 TeV $\hat{\sigma}$ values (left) and the signal cross-section (right), both given in pb, as a function of M_Q and Γ_Q/M_Q for a VLQ T coupling to the third generation shown together with the exclusions line obtained using the $\hat{\sigma}$ data (in dashed blue) and with the original exclusion line (in black, same as Fig. 4.5), assuming negligible interference contributions from any source.

4.3.3.1 Including interference terms for $pp \to Wbj$ via T

Finally, we consider the role of interference between signal and background for the $pp \to bWj$ channel with propagation of a T VLQ. This scenario is studied under two hypotheses: 1) T mixing with third SM quark generation and coupling only through charged current, such that new physics allowing for large width can be achieved only by requiring mixing with other new states in the VLQ sector; 2) T can only decay to Wb in

the SM, but other BSM decay channels (which do not play a role as interference within signal itself) are open, such as, e.g., $T \to St$ for a (generic) new BSM scalar S. Such assumptions allow us to study the scenario through the parameterisation of Eqs. (4.1) and (4.4). To perform the analysis for both cases, we start from the fact that, for any specific point, characterised by the mass and Γ_Q/M_Q ratio of the VLQ, the total number of events is composed by different contributions:

$$S + B = L(\sigma_S \epsilon_S + \sigma^{\text{int}}_{SB_{\text{irr}}} \epsilon^{\text{int}}_{SB_{\text{irr}}}) + B_{\text{irr+red}} \equiv L\sigma_{\text{eff}} + B, \tag{4.6}$$

where L is the integrated luminosity, B_{irr} and B_{red} are the number of events for the irreducible and reducible background terms respectively (which sum to the total number of background events B) and $\sigma_{\text{eff}} \equiv \sigma_{S,\text{eff}} + \sigma^{\text{int}}_{SB_{\text{irr}},\text{eff}}$ is the fiducial cross-section that is accessed by the experiment. The latter can be described by folding the experimental efficiencies of each contribution in the expression of $\hat{\sigma}$ of Eqs. (4.1) and (4.4) as:

$$\begin{aligned} \sigma_{\text{eff}}(C_2, M_Q, \Gamma_Q; \chi_Q) &= C_2^4\ \hat{\sigma}_S(M_Q, \Gamma_Q)\ \epsilon_S(M_Q, \Gamma_Q) + C_2^2\ \hat{\sigma}^{\text{int}}_{SB_{\text{irr}}}(M_Q, \Gamma_Q, \chi_Q)\ \epsilon^{\text{int}}_{SB_{\text{irr}}}(M_Q, \Gamma_Q, \chi_Q) \\ &\equiv C_2^4\ \hat{\sigma}_{S,\text{eff}}(M_Q, \Gamma_Q) + C_2^2\ \hat{\sigma}^{\text{int}}_{SB_{\text{irr}},\text{eff}}(M_Q, \Gamma_Q, \chi_Q). \end{aligned} \tag{4.7}$$

The $\hat{\sigma}^{\text{int}}_{SB_{\text{irr}}}$ plots for the interference between signal and SM background are provided in Fig. 4.8. Notice the different behaviour in the case of dominantly LH or RH coupling chirality of the T and that, as expected, the scenario with dominant LH chirality produces larger interference contributions as the T mass approaches the top mass region.

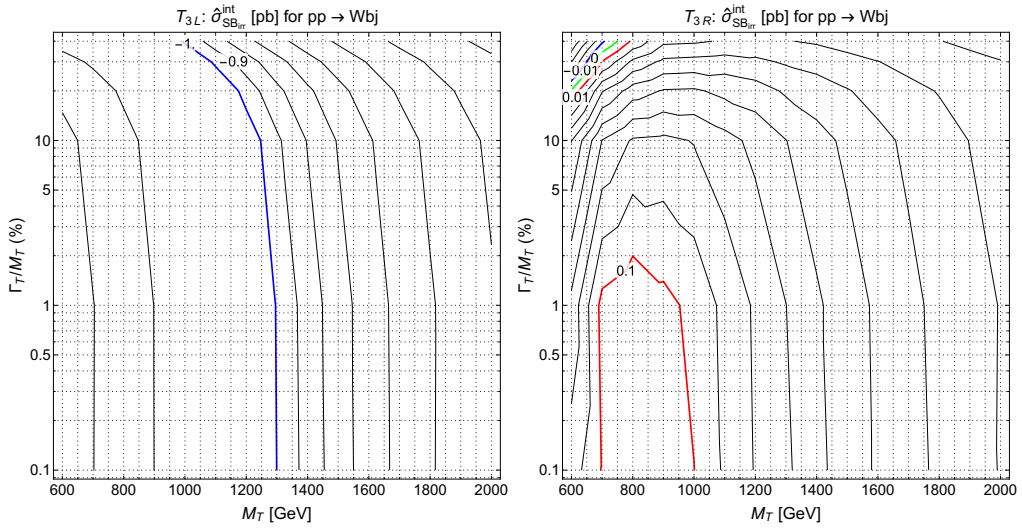

Figure 4.8: $\hat{\sigma}^{\text{int}}_{SB_{\text{irr}}}$ values at 13 TeV (in pb) for the process $pp \to bWj$ mediated by a T interacting with third generation SM quarks exclusively through charged current, for the interference between signal and SM background with dominant LH (RH) coupling chirality of the T in the left (right) panel.

In Fig. 4.9 the values of $\hat{\sigma}_{S,\text{eff}}$ and $\hat{\sigma}^{\text{int}}_{SB_{\text{irr}},\text{eff}}$ are provided for the signal and for the interference term in the case of dominant LH chirality, considering the signal region targeting final states with an electron in the CMS search [190]. With such information and with the knowledge of the total background B (from experimental data), it is possible to

reconstruct the number of events for $S + B$ for each point in the $(M_Q, \Gamma_Q/M_Q)$ plane through Eqs. (4.6) and (4.7).

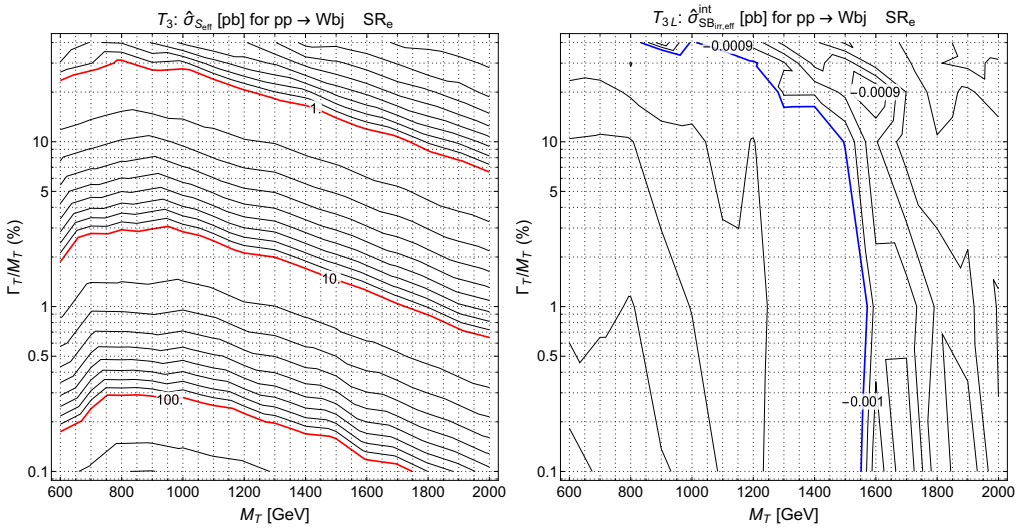

Figure 4.9: $\hat{\sigma}_{S,\text{eff}}$ and $\hat{\sigma}^{\text{int}}_{SB_{\text{irr}},\text{eff}}$ values at 13 TeV (in pb) for the process $pp \to bWj$ mediated by a T interacting with third generation SM quarks exclusively through charged current, for the pure signal (left panel) and for the interference between signal and SM background with dominant LH coupling chirality of the T (right panel). The signal region corresponding to the efficiencies is the single electron from the CMS search [190].

To study the two scenarios described at the beginning of this section, the value of the TWb coupling c_W is modified while keeping the Γ_Q/M_Q ratio fixed, from a maximum value which corresponds to having $BR(T \to Wb) = 100\%$, to smaller values which imply the existence of other decay channels. As a practical example, we consider the point with $M_T = 600$ GeV and $\Gamma_T/M_T = 10\%$. The values of σ_{eff} and the relative contribution of the interference term are plotted as function of the $C_2 \equiv c_W$ coupling in Fig. 4.10, considering c_W in a range for which σ_{eff} is larger than 10^{-1} fb up to when the partial width becomes equivalent to 60 GeV, (i.e., 10% of the mass). As it can also be inferred from Eq. (4.7), the contribution of the interference term becomes more and more relevant as the C_2 coupling decreases, eventually becoming dominant with respect to the pure signal, but the fiducial cross-section σ_{eff} decreases as well. It is now straightforward to apply a CL analysis to determine the significance for exclusion or non-exclusion of the tested point. The reported numbers of background and observed events in the electron signal region by [190] are 95 ± 17 and 78 respectively with a luminosity of 2.3 fb^{-1}, which imply that the quantity $\sigma_{\text{eff}} * L \simeq 30$ is excluded a 95% CL, or that σ_{eff} has to be less than 13 fb. Such value places an upper bound on the T coupling $c_W \lesssim 0.27$, in a region for which the interference contribution to the signal is around -1.7%.

The relative importance of the interference contributions becomes larger as the luminosity increases. Rescaling the number of background events for the nominal highest luminosity

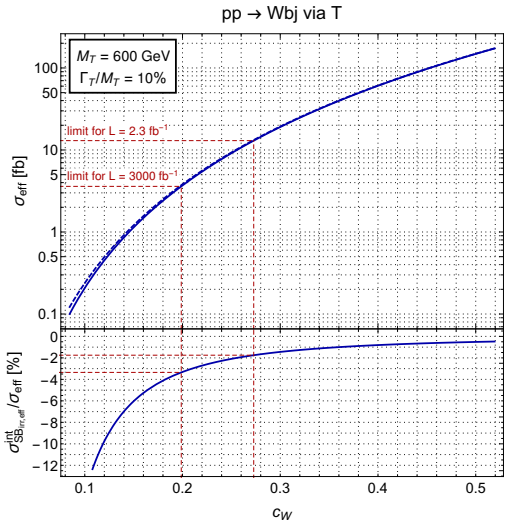

Figure 4.10: Upper panel: values of σ_{eff} with (solid line) and without (dashed line) interference contribution. Lower panel: relative contribution of the interference term to it (lower panel) at 13 TeV as function of the c_W coupling. The process is $pp \to bWj$ mediated by a T with $M_T = 600$ GeV and $\Gamma_T/M_T = 10\%$ interacting with third generation SM quarks exclusively through charged current. The maximum value of c_W in the plot corresponds to a partial width equivalent to 10% of the mass. Limits at two different LHC luminosities are also shown (see text for details).

for the LHC, 3 ab^{-1}, we obtain $B = 105556$. With such value, and assuming a systematic uncertainty for the background of 5%, the maximum expected value of σ_{eff} for 95% CL exclusion is 3.6 fb, corresponding to $c_W \lesssim 0.2$, in a region for which the interference contribution to the signal is around -3.4%.

We stress that this example represents an ideal situation in which the signal and interference contributions can be factorised in a simple and gauge-invariant way. More complex scenarios, in which the VLQ can couple through neutral currents and/or other BSM states, in such a way that other interference terms are non-negligible, cannot be reinterpreted analogously to the example of this section.

4.4 Conclusions

We have studied in a model-independent way processes of single production of VLQs with non-negligible width at the LHC, exploiting a simple, yet robust, framework for the presentation of experimental results and for their subsequent reinterpretation in terms of any scenario of new physics beyond the SM which predict VLQs of generic masses, couplings and total width which can decay into SM final states. Such framework can be generalised also for different BSM scenarios or for analyses of single VLQ production where QCD NLO effects are considered.

We have assessed the role of the total width in the determination of kinematic distributions of the final state finding that, in some cases, the shapes of such distributions can significantly be deformed depending on the Γ_Q/M_Q ratio. We have numerically recast a CMS search to determine how bounds in the plane $(M_Q, \Gamma_Q/M_Q)$ change and, finally, we have compared the results of the numerical recasting in one of the considered scenarios to those from the model-independent procedure, obtaining an excellent agreement. Finally we have discussed the role of interference terms, usually neglected in experimental analysis, described issues related to the reinterpretation of results if such terms are not negligible and applied a procedure for reinterpretation in an ideal scenario in which such terms can be easily factorised.

The possibility to interpret observed data in terms of exclusion regions in the parameter space of models of new physics is a crucial step for any phenomenological analysis of BSM scenarios. Nevertheless, in some cases, the experimental analysis techniques cannot be easily recast through phenomenological tools. In this case, for interpretations to be reliable, experimental results should provide all the essential information, so that a minimal, but complete, set of information can profitably be used for the characterisation of VLQs with generic assumptions on their mass, couplings and total width. In particular, the procedure adopted here allows for the possibility to perform a reinterpretation without the need of dedicated tools, thus growing the possibilities to test scenarios of new physics predicting VLQs.

Chapter 5

Conclusions

The LHC is best known for the discovery of the Higgs boson. However it has also made incredibly precise measurements of the SM, which helps in our understanding of the low scale universe we can currently explore but could also lead to discoveries of new physics.

Most of the experimental searches for VLQs at the LHC in the last couple of years have been for pair production channels of VLQs in simplified models. The increasingly strong mass bounds being set have led to interest in searches for single production of VLQs which do not suffer from the same suppression effects as pair production at higher VLQ masses. It is important to note that most of these searches performed at the LHC involve the addition of either a VL-top or VL-bottom or both. It is important to note a fact that is considered in [98], that more complex VLQ scenarios might not be excluded by current VLQ mass bounds.

The research reported in chapter 2 highlighted non-negligible LW effects that are not included in experimental searches for pair production of VLQs using simplified models with the NWA assumption. In chapter 3 an investigation of LW effects for VLQs decaying into DM is presented. In some channels there were considerable contributions at LW, even allowing to possibly differentiate between scalar and vector DM scenarios. The final piece of research performed and reported in chapter 4 considered single production of VLQs which is now more favoured experimentally due to the fact that a larger range of the VLQ mass parameter space can be explored. Contributions (in the form of Table 1.4) were also made to the experimental CMS collaboration paper [4] which compared mass bounds for the $T \to Zt$ single production channel from simplified models to more complex models that can describe LW effects, finding a similar mass bound (as expected for the channel considered in [4] from research performed in [3]).

The thesis was organised by initially describing the LHC due to the fact that the analyses performed are focused on its data. This is followed by a description of some aspects of the SM that are related to mass generation through the coupling of SM quarks to the Higgs

boson. A detailed account was then given of phenomena that the SM cannot account for, in addition to describing some BSM theories that attempt to solve some of these issues and why VLQs are of phenomenological interest for these BSM theories. A model framework [137, 132] was then described which was used in our studies [1, 2, 3], detailing the mixing allowed and the modified couplings to bosons required in the presence of VLQs, depending on the chosen representation of the VLQs. The Lagrangian for the model [137] was then described for the commonly experimentally investigated scenario of adding only one VL-top. The NWA was presented as it is a key assumption used in experimental searches and is the main topic of our studies in which we study the implication of this approximation for both single and pair production of VLQs. These production methods were then also described. Finally it was also useful to discuss the current state of experimental searches for VLQs at CMS and ATLAS.

The conclusions of the main studies of this thesis are:

In chapter 2 the study of off-shell contributions when considering LW effects for pair production of VL-tops, highlighted leading order contributions arising in channels involving final state b quarks and especially for when light generation quarks are in the final state. These contributions arise from collinear and soft effects when a gluon splits into either two bottom quarks in the final state for a a VL-top mixing with the third generation of SM quarks or u, d final state quarks for the first generation SM quarks mixing with a VL-top. These large contributions are not suppressed by PDFs and so can be of phenomenological relevance when comparing the use of more complex LW scenarios to that of a simplified approach which uses the NWA. This is apparent when considering the effect these contributions have on the mass bound due to the large size of the cross-section in the LW scenario, specifically when considering first generation SM quarks in the final state, though this effect is small in the case of a final state top quark. The mass bound in the NWA for pair produced VLQs cannot then simply be rescaled to LW scenarios, making it important to have experimental signal regions that investigate large width scenarios. This research also examined interference effects with the SM background, determining that such effects are mostly negligible and can be ignored.

The next topic explored in chapter 3 was on the production of VLQs decaying into DM in large width scenarios. It was concluded that the choice of the DM particles mass M_{DM} can create a large difference between the NWA compared to full signal depending also upon the nature of the DM particle explored (scalar or vector). The factor responsible for the largest difference seen between the simplistic (model-independent) and realistic (model-dependent) approaches outlined, was dependent on the coupling properties of the T state. When the coupling was to the third generation only, the exclusion limits then showed only slight dependence on Γ_T/M_T with increasing cross section as the width increases, in this case the contributions to the NWA were suppressed by cuts on missing transverse energy commonly adopted in experimental searches. When the coupling is allowed to the first (second) generation only, a massive dependence on the

exclusion limits from the width was found. This is due to the earlier discussed topologies not being suppressed by the same cuts in missing transverse energy, with increasing importance as M_T and Γ_T/M_T become large. It can then be seen that a fully-fledged model incorporating coupling to any generation will fall in between these two extreme conditions, with further subtleties induced by the PDF behaviour, as one can already see by comparing the results for the first and second generation cases shown in chapter 3. The main conclusion to be drawn from these results is that analyses from LHC searches for any VLQs, when decaying to DM (whether spin 0 or 1) and either a heavy or light SM quark, should be taken with caution, as they do not account for effects induced by either the large VLQ width or for the pair production topologies (nor the additional topologies). These effects can be very large even in a simplified model with only one VLQ. Hence, one should rescale the observed mass exclusion limits from established experimental analyses to the actual limits upon accounting for such effects or else attempt deploying new limits adopting different selection strategies which minimise these effects when setting exclusion limits. With these results the time-honoured assumption that the NWA is a reliable investigative approach applicable over most of the parameter space of the BSM scenarios dealt with here should be dismissed.

Finally in chapter 4 an investigation was made into single VLQ production methods which are becoming more and more relevant. This is due to the fact that the single production and decay processes of VLQs have larger cross section values when considering a higher VLQ mass range, as it does not suffer from the same PDF suppression effects as pair production. This work provided a simple yet robust framework for interpreting and presenting experimental results with the intention of subsequent reinterpretation in terms of any scenario of new physics BSM which predict VLQs of generic masses, couplings and total width which can decay into SM final states. The role of the total width was assessed in the determination of kinematic distributions of the final state finding that, in some cases, the shapes of such distributions can significantly be deformed depending on the Γ_T/M_T ratio. A numerical recast was performed on a CMS search to determine how bounds in the plane $(M_T, \Gamma_T/M_T)$ change and, finally, the results of the numerical recasting in one of the scenarios considered were compared to those from the model-independent procedure, obtaining excellent agreement. Finally the role of interference terms which are usually neglected in experimental analysis was discussed. Issues related to the reinterpretation of results if such terms are not negligible were identified and a procedure was applied for reinterpretation in an ideal scenario in which such terms can be easily factorised.

This thesis concludes with a positive outlook for VLQ phenomenology, with the need to develop and implement many search strategies for the many possible VLQ scenarios, while also being aware of the importance and the effects of the assumptions made. It is important when considering the present mass exclusion limits to take into account that

these limits strongly depend on the new particle content along with the assumptions made when performing an experimental search for VLQs.

References

[1] Stefano Moretti, Dermot O'Brien, Luca Panizzi, and Hugo Prager. Production of extra quarks at the Large Hadron Collider beyond the Narrow Width Approximation. *Phys. Rev.*, D96(7):075035, 2017.

[2] Stefano Moretti, Dermot O'Brien, Luca Panizzi, and Hugo Prager. Production of extra quarks decaying to Dark Matter beyond the Narrow Width Approximation at the LHC. *Phys. Rev.*, D96(3):035033, 2017.

[3] Alexandra Carvalho, Stefano Moretti, Dermot O'Brien, Luca Panizzi, and Hugo Prager. Single production of vectorlike quarks with large width at the Large Hadron Collider. *Phys. Rev.*, D98(1):015029, 2018.

[4] A. M. Sirunyan et al. Search for single production of a vector-like T quark decaying to a Z boson and a top quark in proton-proton collisions at $\sqrt{s} = 13$ TeV. *Phys. Lett.*, B781:574–600, 2018.

[5] Steven Weinberg. A model of leptons. *Phys. Rev. Lett.*, 19:1264–1266, Nov 1967.

[6] Mary K. Gaillard, Paul D. Grannis, and Frank J. Sciulli. The Standard model of particle physics. *Rev. Mod. Phys.*, 71:S96–S111, 1999.

[7] J. Alcaraz et al. A Combination of preliminary electroweak measurements and constraints on the standard model. 2006.

[8] John Ellis, Verónica Sanz, and Tevong You. The effective standard model after lhc run i. *Journal of High Energy Physics*, 2015(3):157, Mar 2015.

[9] V. Blobel, H. Fesefeldt, H. Franz, B. Hellwig, U. Idschok, J.W. Lamsa, D. MÃČÂűnkemeyer, H.F. Neumann, D. Roedel, W. Schrankel, B. Schwarz, F. Selonke, and P. SÃČÂűding. Observation of vector meson production in inclusive pp reactions. *Physics Letters B*, 48(1):73 – 76, 1974.

[10] G. W. Brandenburg, R. K. Carnegie, R. J. Cashmore, M. Davier, W. M. Dunwoodie, T. A. Lasinski, D. W. G. S. Leith, J. A. J. Matthews, P. Walden, S. H. Williams, and F. C. Winkelmann. Observation of two strangeness-one axial-vector mesons. *Phys. Rev. Lett.*, 36:703–706, Mar 1976.

[11] Martin L. Perl. *The Discovery of The Tau Lepton*, pages 277–302. Springer US, Boston, MA, 1996.

[12] Jonathan Richard Ellis, Mary Katherin Gaillard, Dimitri V Nanopoulos, and S Rudaz. The phenomenology of the next left-handed quarks. *Nucl. Phys. B*, 131(CERN-TH-2346. 2-3):285–307, 1977.

[13] H. Fritzsch. Weak-interaction mixing in the six-quark theory. *Physics Letters B*, 73(3):317 – 322, 1978.

[14] D. P. Barber et al. Discovery of Three Jet Events and a Test of Quantum Chromodynamics at PETRA Energies. *Phys. Rev. Lett.*, 43:830, 1979.

[15] A Astbury. Found: W and z. *Physics Bulletin*, 34(10):434, 1983.

[16] R. Cashmore, L. Maiani, J.P. Revol, and European Organization for Nuclear Research. *Prestigious Discoveries at CERN: 1973 Neutral Currents. 1983 W & Z Bosons*. Springer, 2004.

[17] Bill Carithers and P. Grannis. Discovery of the top quark. *SLAC Beam Line*, 25N3:4–16, 1995. [SLAC Beam Line25,4(1995)].

[18] The ATLAS Collaboration. Observation of a new particle in the search for the standard model higgs boson with the atlas detector at the lhc. *Physics Letters B*, 716(1):1 – 29, 2012.

[19] Parul Aggarwal et al. Measuring the electric dipole moment of the electron in BaF. 2018.

[20] Vardan Khachatryan et al. Precise determination of the mass of the Higgs boson and tests of compatibility of its couplings with the standard model predictions using proton collisions at 7 and 8 TeV. *Eur. Phys. J.*, C75(5):212, 2015.

[21] The Integrated Luminosity recorded at CMS from 2010 to 2018 the cms collaboration. https://cms-service-lumi.web.cern.ch/cms-service-lumi/publicplots/int_lumi_cumulative_pp_2.pdf. Accessed: 24-08-2018.

[22] The Exotica summary plots for BSM theories presented at ICHEP 2016 the cms collaboration. https://twiki.cern.ch/twiki/pub/CMSPublic/PhysicsResultsCombined/exo-limits_ICHEP_2016.pdf. Accessed: 24-08-2018.

[23] The Standard Model, Particle Physics Theory research group, University of Edinburgh, 2014 dr. peter a boyle. https://www2.ph.ed.ac.uk/~paboyle/Teaching/StandardModel/SM_2014.pdf. Accessed: 24-08-2018.

[24] Part III lecture course The Standard Model, the Department of Applied Mathematics and Theoretical Physics, University of Cambridge during Lent Term 2018 dr. christopher e. thomas. http://www.damtp.cam.ac.uk/user/cet34/teaching/SM/stdmodel.pdf. Accessed: 24-08-2018.

[25] Steven Weinberg. *The Quantum theory of fields. Vol. 1: Foundations*. Cambridge University Press, 2005.

[26] Matthew D. Schwartz. *Quantum Field Theory and the Standard Model*. Cambridge University Press, 2014.

[27] Keith A Olive, Particle Data Group, et al. Review of particle physics. *Chinese Physics C*, 38(9):090001, 2014.

[28] C. L. Bennett, A. Banday, K. M. Gorski, G. Hinshaw, P. Jackson, P. Keegstra, A. Kogut, George F. Smoot, D. T. Wilkinson, and E. L. Wright. Four year COBE DMR cosmic microwave background observations: Maps and basic results. *Astrophys. J.*, 464:L1–L4, 1996.

[29] Y. Akrami et al. Planck 2018 results. I. Overview and the cosmological legacy of Planck. 2018.

[30] George R. Blumenthal, S. M. Faber, Joel R. Primack, and Martin J. Rees. Formation of Galaxies and Large Scale Structure with Cold Dark Matter. *Nature*, 311:517–525, 1984. [,96(1984)].

[31] Yoshiaki Sofue and Vera Rubin. Rotation curves of spiral galaxies. *Ann. Rev. Astron. Astrophys.*, 39:137–174, 2001.

[32] J. H. Oort. Problems of Galactic Structure. , 116:233, September 1952.

[33] V. C. Rubin and W. K. Ford, Jr. Rotation of the Andromeda Nebula from a Spectroscopic Survey of Emission Regions. , 159:379, February 1970.

[34] D. Merritt. The distribution of dark matter in the coma cluster. , 313:121–135, February 1987.

[35] T. Arlen et al. Constraints on Cosmic Rays, Magnetic Fields, and Dark Matter from Gamma-Ray Observations of the Coma Cluster of Galaxies with VERITAS and Fermi. *Astrophys. J.*, 757:123, 2012.

[36] E. Hubble. No. 324. Extra-galactic nebulae. *Contributions from the Mount Wilson Observatory / Carnegie Institution of Washington*, 324:1–49, 1926.

[37] W. L. Freedman et al. Final results from the Hubble Space Telescope key project to measure the Hubble constant. *Astrophys. J.*, 553:47–72, 2001.

[38] A. Udalski, M. Szymanski, J. Kaluzny, M. Kubiak, W. Krzeminski, M. Mateo, G. W. Preston, and B. Paczynski. The optical gravitational lensing experiment. Discovery of the first candidate microlensing event in the direction of the Galactic Bulge. , 43:289–294, July 1993.

[39] Nick Kaiser, Gordon Squires, and Thomas J. Broadhurst. A Method for weak lensing observations. *Astrophys. J.*, 449:460–475, 1995.

[40] Albert Einstein. Lens-like action of a star by the deviation of light in the gravitational field. *Science*, 84(2188):506–507, 1936.

[41] Douglas Clowe, Marusa Bradac, Anthony H. Gonzalez, Maxim Markevitch, Scott W. Randall, Christine Jones, and Dennis Zaritsky. A direct empirical proof of the existence of dark matter. *Astrophys. J.*, 648:L109–L113, 2006.

[42] J. R. Brownstein and J. W. Moffat. The Bullet Cluster 1E0657-558 evidence shows Modified Gravity in the absence of Dark Matter. *Mon. Not. Roy. Astron. Soc.*, 382:29–47, 2007.

[43] Image of Bullet Cluster 1E0657-558 the chandra x-ray observatory. http://chandra.harvard.edu/photo/2006/1e0657/. Accessed: 24-08-2018.

[44] Jianglai Liu, Xun Chen, and Xiangdong Ji. Current status of direct dark matter detection experiments. *Nature Phys.*, 13(3):212–216, 2017.

[45] E. Aprile et al. Dark Matter Search Results from a One Tonne×Year Exposure of XENON1T. 2018.

[46] BjÃűrn Penning. The pursuit of dark matter at collidersâĂŤan overview. *J. Phys.*, G45(6):063001, 2018.

[47] M. C. Gonzalez-Garcia and Michele Maltoni. Phenomenology with Massive Neutrinos. *Phys. Rept.*, 460:1–129, 2008.

[48] H. AlmazÃąn et al. Sterile neutrino exclusion from the STEREO experiment with 66 days of reactor-on data. 2018.

[49] M. G. Aartsen et al. IceCube-Gen2: A Vision for the Future of Neutrino Astronomy in Antarctica. 2014.

[50] T. Araki et al. Measurement of neutrino oscillation with KamLAND: Evidence of spectral distortion. *Phys. Rev. Lett.*, 94:081801, 2005.

[51] T. K. Gaisser, Todor Stanev, and Giles Barr. Cosmic-ray neutrinos in the atmosphere. *Phys. Rev. D*, 38:85–95, Jul 1988.

[52] P. Padovani, P. Giommi, E. Resconi, T. Glauch, B. Arsioli, N. Sahakyan, and M. Huber. Dissecting the region around IceCube-170922A: the blazar TXS 0506+056 as the first cosmic neutrino source. *Mon. Not. Roy. Astron. Soc.*, 480:192, 2018.

[53] Ankur Nath and Ng K. Francis. Detection techniques and investigation of different neutrino experiments. 2018.

[54] Michael Dine and Alexander Kusenko. The Origin of the matter - antimatter asymmetry. *Rev. Mod. Phys.*, 76:1, 2003.

[55] Laurent Canetti, Marco Drewes, and Mikhail Shaposhnikov. Matter and antimatter in the universe. *New Journal of Physics*, 14(9):095012, 2012.

[56] A. D. Dolgov. Baryogenesis, 30 years after. In *Surveys in high-energy physics. Proceedings, 25th ITEP Winter School, Snegiri, Russia, February, 1997*, 1997.

[57] Antonio Riotto. Theories of baryogenesis. In *Proceedings, Summer School in High-energy physics and cosmology: Trieste, Italy, June 29-July 17, 1998*, pages 326–436, 1998.

[58] Mark Trodden. Electroweak baryogenesis. *Rev. Mod. Phys.*, 71:1463–1500, 1999.

[59] C. A. Baker et al. An Improved experimental limit on the electric dipole moment of the neutron. *Phys. Rev. Lett.*, 97:131801, 2006.

[60] Michael Dine. TASI lectures on the strong CP problem. In *Flavor physics for the millennium. Proceedings, Theoretical Advanced Study Institute in elementary particle physics, TASI 2000, Boulder, USA, June 4-30, 2000*, pages 349–369, 2000.

[61] J. L. DÃŋaz-Cruz, W. G. Hollik, and U. J. SaldaÃśa-Salazar. A bottom-up approach to the strong CP problem. *Int. J. Mod. Phys.*, A33(14n15):1850088, 2018.

[62] V.A. Rubakov, M.V. Sazhin, and A.V. Veryaskin. Graviton creation in the inflationary universe and the grand unification scale. *Physics Letters B*, 115(3):189 – 192, 1982.

[63] Clifford M. Will. Bounding the mass of the graviton using gravitational-wave observations of inspiralling compact binaries. *Phys. Rev. D*, 57:2061–2068, Feb 1998.

[64] Priscila de Aquino, Kaoru Hagiwara, Qiang Li, and Fabio Maltoni. Simulating graviton production at hadron colliders. *JHEP*, 06:132, 2011.

[65] Chao-Qiang Geng, Da Huang, and Kimiko Yamashita. LHC Searches for Top-philic Kaluza-Klein Graviton. 2018.

[66] Carlo Rovelli. Loop quantum gravity. *Living Reviews in Relativity*, 11(1):5, Jul 2008.

[67] Guido Walter Pettinari. *The Standard Model of Cosmology*, pages 9–52. Springer International Publishing, Cham, 2016.

[68] Sergei Odintsov. Unifying the early-time inflationary era with late-time dark epoch universe: The case of modified gravity. *Proceedings*, 2(1), 2018.

[69] S. D. Odintsov, V. K. Oikonomou, and S. Banerjee. Dynamics of Inflation and Dark Energy from $F(R, \mathcal{G})$ Gravity. 2018.

[70] Ryan Scranton et al. Physical evidence for dark energy. 2003.

[71] Blake D. Sherwin et al. Evidence for dark energy from the cosmic microwave background alone using the Atacama Cosmology Telescope lensing measurements. *Phys. Rev. Lett.*, 107:021302, 2011.

[72] Varun Sahni, Arman Shafieloo, and Alexei A. Starobinsky. Model independent evidence for dark energy evolution from Baryon Acoustic Oscillations. *Astrophys. J.*, 793(2):L40, 2014.

[73] Heng-Yu Chen, Ilia Gogoladze, Shan Hu, Tianjun Li, and Lina Wu. The minimal gut with inflaton and dark matter unification. *The European Physical Journal C*, 78(1):26, Jan 2018.

[74] Blake D. Sherwin et al. Evidence for dark energy from the cosmic microwave background alone using the Atacama Cosmology Telescope lensing measurements. *Phys. Rev. Lett.*, 107:021302, 2011.

[75] S. Dodelson et al. Working Group Report: Dark Energy and CMB. In *Proceedings, 2013 Community Summer Study on the Future of U.S. Particle Physics: Snowmass on the Mississippi (CSS2013): Minneapolis, MN, USA, July 29-August 6, 2013*, 2013.

[76] P. de Bernardis et al. A Flat universe from high resolution maps of the cosmic microwave background radiation. *Nature*, 404:955–959, 2000.

[77] M. Bartelmann, M. Doran, and C. Wetterich. Non-linear structure formation in cosmologies with early dark energy. , 454:27–36, July 2006.

[78] Tomi Koivisto and David F. Mota. Dark energy anisotropic stress and large scale structure formation. *Phys. Rev.*, D73:083502, 2006.

[79] Margherita Grossi and Volker Springel. The impact of early dark energy on non-linear structure formation. *Monthly Notices of the Royal Astronomical Society*, 394(3):1559–1574, 2009.

[80] C. Wetterich. Inflation, quintessence, and the origin of mass. *Nucl. Phys.*, B897:111–178, 2015.

[81] J. A. Peacock. Large–scale structure and matter in the universe. *Philosophical Transactions of the Royal Society of London A: Mathematical, Physical and Engineering Sciences*, 361(1812):2479–2495, 2003.

[82] Luca Amendola. Linear and nonlinear perturbations in dark energy models. *Phys. Rev. D*, 69:103524, May 2004.

[83] Shinji Tsujikawa. Observational signatures of $f(r)$ dark energy models that satisfy cosmological and local gravity constraints. *Phys. Rev. D*, 77:023507, Jan 2008.

[84] S. Nesseris and L. Perivolaropoulos. Comparison of the legacy and gold type ia supernovae dataset constraints on dark energy models. *Phys. Rev. D*, 72:123519, Dec 2005.

[85] M. Baak, M. Goebel, J. Haller, A. Hoecker, D. Kennedy, R. Kogler, K. Moenig, M. Schott, and J. Stelzer. The Electroweak Fit of the Standard Model after the Discovery of a New Boson at the LHC. *Eur. Phys. J.*, C72:2205, 2012.

[86] Dean Carmi, Adam Falkowski, Eric Kuflik, Tomer Volansky, and Jure Zupan. Higgs After the Discovery: A Status Report. *JHEP*, 10:196, 2012.

[87] B. C. Allanach. Multiple solutions in supersymmetry and the Higgs. *Phil. Trans. Roy. Soc. Lond.*, A373(2032):0035, 2014.

[88] Pieter Maris, Craig D. Roberts, and Peter C. Tandy. Pion mass and decay constant. *Physics Letters B*, 420(3):267 – 273, 1998.

[89] Avik Banerjee, Gautam Bhattacharyya, Nilanjana Kumar, and Tirtha Sankar Ray. Constraining composite higgs models using lhc data. *Journal of High Energy Physics*, 2018(3):62, Mar 2018.

[90] David Marzocca, Marco Serone, and Jing Shu. General composite higgs models. *Journal of High Energy Physics*, 2012(8):13, Aug 2012.

[91] Wolfgang Bock, Christoph Frick, Jan Smit, and Jeroen C. Vink. Can the couplings in the fermion Higgs sector of the Standard Model be strong? *Nucl. Phys.*, B400:309–346, 1993.

[92] Dipankar Das, Anirban Kundu, and Ipsita Saha. Higgs data does not rule out a sequential fourth generation with an extended scalar sector. *Phys. Rev. D*, 97:011701, Jan 2018.

[93] Georges Aad et al. Measurements of the Higgs boson production and decay rates and constraints on its couplings from a combined ATLAS and CMS analysis of the LHC pp collision data at $\sqrt{s} = 7$ and 8 TeV. *JHEP*, 08:045, 2016.

[94] M. Aaboud et al. Search for pair production of heavy vector-like quarks decaying to high-p_T W bosons and b quarks in the lepton-plus-jets final state in pp collisions at $\sqrt{s} = 13$ TeV with the ATLAS detector. *JHEP*, 10:141, 2017.

[95] Search for pair-produced vectorlike b quarks in proton-proton collisions at $\sqrt{s} =$ 8 TeV. *Phys. Rev. D*, 93:112009, Jun 2016.

[96] C. Patrignani et al. Review of Particle Physics. *Chin. Phys.*, C40(10):100001, 2016.

[97] Kunal Kumar, Roberto Vega-Morales, and Felix Yu. Effects from New Colored States and the Higgs Portal on Gluon Fusion and Higgs Decays. *Phys. Rev.*, D86:113002, 2012. [Erratum: Phys. Rev.D87,no.11,119903(2013)].

[98] Bogdan A. Dobrescu and Felix Yu. Exotic Signals of Vectorlike Quarks. 2016.

[99] Nima Arkani-Hamed, Andrew G. Cohen, Emanuel Katz, Ann E. Nelson, Thomas Gregoire, and Jacob G. Wacker. The minimal moose for a little higgs. *Journal of High Energy Physics*, 2002(08):021, 2002.

[100] Maxim Perelstein, Michael E. Peskin, and Aaron Pierce. Top quarks and electroweak symmetry breaking in little Higgs models. *Phys.Rev.*, D69:075002, 2004.

[101] Tao Han, Heather E. Logan, Bob McElrath, and Lian-Tao Wang. Phenomenology of the little Higgs model. *Phys.Rev.*, D67:095004, 2003.

[102] Martin Schmaltz and David Tucker-Smith. Little Higgs review. *Ann.Rev.Nucl.Part.Sci.*, 55:229–270, 2005.

[103] Marcela Carena, Jay Hubisz, Maxim Perelstein, and Patrice Verdier. Collider signature of T-quarks. *Phys. Rev.*, D75:091701, 2007.

[104] Shigeki Matsumoto, Takeo Moroi, and Kazuhiro Tobe. Testing the Littlest Higgs Model with T-parity at the Large Hadron Collider. *Phys. Rev.*, D78:055018, 2008.

[105] N. Arkani-Hamed, A.G. Cohen, E. Katz, and A.E. Nelson. The Littlest Higgs. *JHEP*, 0207:034, 2002.

[106] Peter W. Graham, Ahmed Ismail, Surjeet Rajendran, and Prashant Saraswat. A Little Solution to the Little Hierarchy Problem: A Vector-like Generation. *Phys. Rev.*, D81:055016, 2010.

[107] R. Sekhar Chivukula, Bogdan A. Dobrescu, Howard Georgi, and Christopher T. Hill. Top quark seesaw theory of electroweak symmetry breaking. *Phys.Rev.*, D59:075003, 1999.

[108] Hael Collins, Aaron K. Grant, and Howard Georgi. The Phenomenology of a top quark seesaw model. *Phys.Rev.*, D61:055002, 2000.

[109] Hong-Jian He, Christopher T. Hill, and Timothy M.P. Tait. Top quark seesaw, vacuum structure and electroweak precision constraints. *Phys.Rev.*, D65:055006, 2002.

[110] Roberto Contino, Leandro Da Rold, and Alex Pomarol. Light custodians in natural composite Higgs models. *Phys.Rev.*, D75:055014, 2007.

[111] R. Nevzorov and A. W. Thomas. E_6 inspired composite Higgs model. *Phys. Rev.*, D92:075007, 2015.

[112] Kyoungchul Kong, Mathew McCaskey, and Graham W. Wilson. Multi-lepton signals from the top-prime quark at the LHC. *JHEP*, 04:079, 2012.

[113] Adrian Carmona, Mikael Chala, and Jose Santiago. New Higgs Production Mechanism in Composite Higgs Models. *JHEP*, 1207:049, 2012.

[114] M. Gillioz, R. Grober, C. Grojean, M. Muhlleitner, and E. Salvioni. Higgs Low-Energy Theorem (and its corrections) in Composite Models. *JHEP*, 10:004, 2012.

[115] Giacomo Cacciapaglia, Haiying Cai, Alexandra Carvalho, Aldo Deandrea, Thomas Flacke, Benjamin Fuks, Devdatta Majumder, and Hua-Sheng Shao. Probing vector-like quark models with Higgs-boson pair production. *JHEP*, 07(7):005, 2017.

[116] Natascia Vignaroli. Top Signatures From Composite Higgs Theories. In *Proceedings, 9th International Workshop on Top Quark Physics (TOP 2016): Olomouc, Czech Republic, September 19-23, 2016*, 2016.

[117] Christopher T. Hill and Elizabeth H. Simmons. Strong dynamics and electroweak symmetry breaking. *Phys.Rept.*, 381:235–402, 2003.

[118] Giacomo Cacciapaglia and Alberto Parolini. Light ÃćÂĂÂŹt Hooft top partners. *Phys. Rev.*, D93(7):071701, 2016.

[119] Charalampos Anastasiou, Elisabetta Furlan, and Jose Santiago. Realistic Composite Higgs Models. *Phys.Rev.*, D79:075003, 2009.

[120] Bogdan A. Dobrescu and Christopher T. Hill. Electroweak symmetry breaking via top condensation seesaw. *Phys.Rev.Lett.*, 81:2634–2637, 1998.

[121] Pieter Maris, Craig D. Roberts, and Peter C. Tandy. Pion mass and decay constant. *Phys. Lett.*, B420:267–273, 1998.

[122] Gilles Couture, Mariana Frank, Cherif Hamzaoui, and Manuel Toharia. Top and bottom partners, Higgs boson on the brane, and the tth signal. *Phys. Rev.*, D95(9):095038, 2017.

[123] Yutaka Hosotani, Shusaku Noda, and Kazunori Takenaga. Dynamical gauge-Higgs unification in the electroweak theory. *Phys. Lett.*, B607:276–285, 2005.

[124] Ignatios Antoniadis, K. Benakli, and M. Quiros. Finite Higgs mass without supersymmetry. *New J. Phys.*, 3:20, 2001.

[125] Kaustubh Agashe, Roberto Contino, and Alex Pomarol. The Minimal composite Higgs model. *Nucl.Phys.*, B719:165–187, 2005.

[126] Takeo Moroi and Yasuhiro Okada. Upper bound of the lightest neutral Higgs mass in extended supersymmetric Standard Models. *Phys. Lett.*, B295:73–78, 1992.

[127] Takeo Moroi and Yasuhiro Okada. Radiative corrections to Higgs masses in the supersymmetric model with an extra family and antifamily. *Mod. Phys. Lett.*, A7:187–200, 1992.

[128] Stephen P. Martin. Extra vector-like matter and the lightest Higgs scalar boson mass in low-energy supersymmetry. *Phys. Rev.*, D81:035004, 2010.

[129] K. S. Babu, Ilia Gogoladze, Mansoor Ur Rehman, and Qaisar Shafi. Higgs Boson Mass, Sparticle Spectrum and Little Hierarchy Problem in Extended MSSM. *Phys. Rev.*, D78:055017, 2008.

[130] Martin Hirsch, Manuel E. Krauss, Toby Opferkuch, Werner Porod, and Florian Staub. A constrained supersymmetric left-right model. *JHEP*, 03:009, 2016.

[131] Stephen P. Martin. Raising the Higgs mass with Yukawa couplings for isotriplets in vector-like extensions of minimal supersymmetry. *Phys. Rev.*, D82:055019, 2010.

[132] Yasuhiro Okada and Luca Panizzi. LHC signatures of vector-like quarks. *Adv.High Energy Phys.*, 2013:364936, 2013.

[133] G. Barenboim, F. J. Botella, and O. Vives. Constraining Models with Vector - Like Fermions from FCNC in K and B Physics. *Nucl. Phys.*, B613:285–305, 2001.

[134] Jae Yong Lee. A Vector-like heavy quark in the Littlest Higgs model. *JHEP*, 12:065, 2004.

[135] Giacomo Cacciapaglia, Aldo Deandrea, Luca Panizzi, Naveen Gaur, Daisuke Harada, et al. Heavy Vector-like Top Partners at the LHC and flavour constraints. *JHEP*, 1203:070, 2012.

[136] Joshua Berger, Jay Hubisz, and Maxim Perelstein. A Fermionic Top Partner: Naturalness and the LHC. *JHEP*, 1207:016, 2012.

[137] Mathieu Buchkremer, Giacomo Cacciapaglia, Aldo Deandrea, and Luca Panizzi. Model Independent Framework for Searches of Top Partners. *Nucl.Phys.*, B876:376–417, 2013.

[138] Giacomo Cacciapaglia, Aldo Deandrea, Daisuke Harada, and Yasuhiro Okada. Bounds and Decays of New Heavy Vector-like Top Partners. *JHEP*, 1011:159, 2010.

[139] Neil D. Christensen and Claude Duhr. FeynRules - Feynman rules made easy. *Comput.Phys.Commun.*, 180:1614–1641, 2009.

[140] Pdflatex instructions.

[141] M. Bondarenko, A. Belyaev, L. Basso, E. Boos, V. Bunichev, et al. High Energy Physics Model Database : Towards decoding of the underlying theory (within Les Houches 2011: Physics at TeV Colliders New Physics Working Group Report). https://hepmdb.soton.ac.uk/, arXiv:1203.1488, 2012.

[142] Daniele Barducci, Alexander Belyaev, Jacob Blamey, Stefano Moretti, Luca Panizzi, and Hugo Prager. Towards model-independent approach to the analysis of interference effects in pair production of new heavy quarks. *JHEP*, 07:142, 2014.

[143] John M. Campbell, Rikkert Frederix, Fabio Maltoni, and Francesco Tramontano. Next-to-Leading-Order Predictions for t-Channel Single-Top Production at Hadron Colliders. *Phys. Rev. Lett.*, 102:182003, 2009.

[144] Rikkert Frederix, Emanuele Re, and Paolo Torrielli. Single-top t-channel hadroproduction in the four-flavour scheme with POWHEG and aMC@NLO. *JHEP*, 09:130, 2012.

[145] Enrico Bothmann, Frank Krauss, and Marek SchÃűnherr. Single top-quark production with SHERPA. *Eur. Phys. J.*, C78(3):220, 2018.

[146] The ATLAS collaboration. Combination of the searches for pair-produced vector-like partners of the third generation quarks at $\sqrt{s} = 13$ TeV with the ATLAS detector. 2018.

[147] J.A. Aguilar-Saavedra. Identifying top partners at LHC. *JHEP*, 0911:030, 2009.

[148] Michal Czakon and Alexander Mitov. Top++: A Program for the Calculation of the Top-Pair Cross-Section at Hadron Colliders. *Comput. Phys. Commun.*, 185:2930, 2014.

[149] Morad Aaboud et al. Search for pair- and single-production of vector-like quarks in final states with at least one Z boson decaying into a pair of electrons or muons in pp collision data collected with the ATLAS detector at $\sqrt{s} = 13$ TeV. 2018.

[150] Oleksii Matsedonskyi, Giuliano Panico, and Andrea Wulzer. On the Interpretation of Top Partners Searches. *JHEP*, 12:097, 2014.

[151] Albert M Sirunyan et al. Search for vector-like T and B quark pairs in final states with leptons at $\sqrt{s} = 13$ TeV. 2018.

[152] Benjamin Fuks and Hua-Sheng Shao. QCD next-to-leading-order predictions matched to parton showers for vector-like quark models. *Eur. Phys. J.*, C77(2):135, 2017.

[153] Alexandra Oliveira. Gravity particles from Warped Extra Dimensions, predictions for LHC. 2014.

[154] N. Kauer and D. Zeppenfeld. Finite width effects in top quark production at hadron colliders. *Phys. Rev.*, D65:014021, 2002.

[155] CMS Collaboration. Search for single production of vector-like quarks decaying to a Z boson and a top or a bottom quark in proton-proton collisions at 13 TeV. 2017.

[156] CMS Collaboration. Search for a singly produced vector-like quark B decaying to a b quark and a Higgs boson in a fully hadronic final state using boosted topologies. 2017.

[157] Johan Alwall, Michel Herquet, Fabio Maltoni, Olivier Mattelaer, and Tim Stelzer. MadGraph 5 : Going Beyond. *JHEP*, 1106:128, 2011.

[158] J. Alwall, R. Frederix, S. Frixione, V. Hirschi, F. Maltoni, O. Mattelaer, H. S. Shao, T. Stelzer, P. Torrielli, and M. Zaro. The automated computation of tree-level and next-to-leading order differential cross sections, and their matching to parton shower simulations. *JHEP*, 07:079, 2014.

[159] VLQ FeynRules model. http://feynrules.irmp.ucl.ac.be/wiki/VLQ.

[160] Adam Alloul, Neil D. Christensen, CÃČÂľline Degrande, Claude Duhr, and Benjamin Fuks. FeynRules 2.0 - A complete toolbox for tree-level phenomenology. *Comput.Phys.Commun.*, 185:2250–2300, 2014.

[161] J. Pumplin, D.R. Stump, J. Huston, H.L. Lai, Pavel M. Nadolsky, et al. New generation of parton distributions with uncertainties from global QCD analysis. *JHEP*, 0207:012, 2002.

[162] TorbjÃĆÂŽrn SjÃĆÂŽstrand, Stefan Ask, Jesper R. Christiansen, Richard Corke, Nishita Desai, Philip Ilten, Stephen Mrenna, Stefan Prestel, Christine O. Rasmussen, and Peter Z. Skands. An Introduction to PYTHIA 8.2. *Comput. Phys. Commun.*, 191:159–177, 2015.

[163] The ATLAS collaboration. Search for production of vector-like top quark pairs and of four top quarks in the lepton-plus-jets final state in pp collisions at $\sqrt{s} = 13$ TeV with the ATLAS detector. 2016.

[164] Daniel Dercks, Nishita Desai, Jong Soo Kim, Krzysztof Rolbiecki, Jamie Tattersall, and Torsten Weber. CheckMATE 2: From the model to the limit. 2016.

[165] J. de Favereau et al. DELPHES 3, A modular framework for fast simulation of a generic collider experiment. *JHEP*, 1402:057, 2014.

[166] F. del Aguila, M. Perez-Victoria, and Jose Santiago. Observable contributions of new exotic quarks to quark mixing. *JHEP*, 0009:011, 2000.

[167] M. Aliev, H. Lacker, U. Langenfeld, S. Moch, P. Uwer, and M. Wiedermann. HATHOR: HAdronic Top and Heavy quarks crOss section calculatoR. *Comput. Phys. Commun.*, 182:1034–1046, 2011.

[168] A. D. Martin, W. J. Stirling, R. S. Thorne, and G. Watt. Uncertainties on alpha(S) in global PDF analyses and implications for predicted hadronic cross sections. *Eur. Phys. J.*, C64:653–680, 2009.

[169] Chien-Yi Chen, S. Dawson, and Elisabetta Furlan. Vector-like Fermions and Higgs Effective Field Theory Revisited. 2017.

[170] Giacomo Cacciapaglia, Aldo Deandrea, Naveen Gaur, Daisuke Harada, Yasuhiro Okada, and Luca Panizzi. Interplay of vector-like top partner multiplets in a realistic mixing set-up. *JHEP*, 09:012, 2015.

[171] Giacomo Cacciapaglia, Aldo Deandrea, Naveen Gaur, Daisuke Harada, Yasuhiro Okada, and Luca Panizzi. The LHC potential of Vector-like quark doublets. 2018.

[172] Georges Aad et al. Search for top squark pair production in final states with one isolated lepton, jets, and missing transverse momentum in $\sqrt{s}$ =8 TeV pp collisions with the ATLAS detector. *JHEP*, 11:118, 2014.

[173] Georges Aad et al. Search for squarks and gluinos with the ATLAS detector in final states with jets and missing transverse momentum using $\sqrt{s} = 8$ TeV proton–proton collision data. *JHEP*, 09:176, 2014.

[174] D. Barducci, A. Belyaev, M. Buchkremer, G. Cacciapaglia, A. Deandrea, et al. Model Independent Framework for Analysis of Scenarios with Multiple Heavy Extra Quarks. 2014.

[175] D. Barducci, A. Belyaev, M. Buchkremer, J. Marrouche, S. Moretti, and L. Panizzi. XQCAT: eXtra Quark Combined Analysis Tool. 2014.

[176] Sabine Kraml, Ursula Laa, Luca Panizzi, and Hugo Prager. Scalar versus fermionic top partner interpretations of $t\bar{t} + E_T^{\text{miss}}$ searches at the LHC. *JHEP*, 11:107, 2016.

[177] Torbjorn Sjostrand, Stephen Mrenna, and Peter Z. Skands. A Brief Introduction to PYTHIA 8.1. *Comput. Phys. Commun.*, 178:852–867, 2008.

[178] Torbjorn Sjostrand, Stephen Mrenna, and Peter Z. Skands. PYTHIA 6.4 Physics and Manual. *JHEP*, 0605:026, 2006.

[179] Morad Aaboud et al. Search for new phenomena in final states with an energetic jet and large missing transverse momentum in pp collisions at $\sqrt{s} = 13$ TeV using the ATLAS detector. *Phys. Rev.*, D94(3):032005, 2016.

[180] Morad Aaboud et al. Search for squarks and gluinos in final states with jets and missing transverse momentum at $\sqrt{s} = 13$ TeV with the ATLAS detector. *Eur. Phys. J.*, C76(7):392, 2016.

[181] Georges Aad et al. Search for gluinos in events with an isolated lepton, jets and missing transverse momentum at $\sqrt{s} = 13$ Te V with the ATLAS detector. *Eur. Phys. J.*, C76(10):565, 2016.

[182] Search for top squarks in final states with one isolated lepton, jets, and missing transverse momentum in $\sqrt{s} = 13$ TeV pp collisions with the ATLAS detector. http://cds.cern.ch/record/2206132, Aug 2016.

[183] Manuel Drees, Herbi Dreiner, Daniel Schmeier, Jamie Tattersall, and Jong Soo Kim. CheckMATE: Confronting your Favourite New Physics Model with LHC Data. *Comput.Phys.Commun.*, 187:227–265, 2014.

[184] Albert M Sirunyan et al. Search for single production of vector-like quarks decaying to a b quark and a Higgs boson. 2018.

[185] J. A. Aguilar-Saavedra, R. Benbrik, S. Heinemeyer, and M. PÃČÂĭrez-Victoria. Handbook of vectorlike quarks: Mixing and single production. *Phys. Rev.*, D88(9):094010, 2013.

[186] G. Brooijmans et al. Les Houches 2017: Physics at TeV Colliders New Physics Working Group Report. In *10th Les Houches Workshop on Physics at TeV Colliders (PhysTeV 2017) Les Houches, France, June 5-23, 2017*, 2018.

[187] Richard D. Ball et al. Parton distributions for the LHC Run II. *JHEP*, 04:040, 2015.

[188] Eric Conte, BÃČÂĭranger Dumont, Benjamin Fuks, and Chris Wymant. Designing and recasting LHC analyses with MadAnalysis 5. *Eur.Phys.J.*, C74(10):3103, 2014.

[189] Celine Degrande, Claude Duhr, Benjamin Fuks, David Grellscheid, Olivier Mattelaer, et al. UFO - The Universal FeynRules Output. *Comput.Phys.Commun.*, 183:1201–1214, 2012.

[190] Albert M Sirunyan et al. Search for single production of vector-like quarks decaying into a b quark and a W boson in proton-proton collisions at $\sqrt{s} = 13$ TeV. *Phys. Lett.*, B772:634–656, 2017.